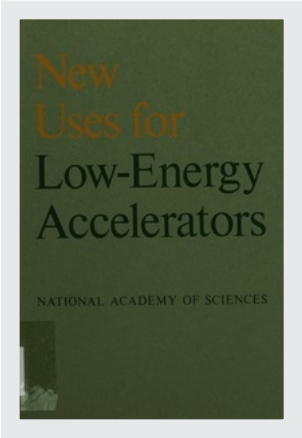

New Uses for Low-Energy Accelerators

DETAILS

184 pages | 5 x 9 | PAPERBACK
ISBN 978-0-309-35960-3 | DOI 10.17226/21292

AUTHORS

Ad Hoc Panel on New Uses for Low-Energy Accelerators; Committee on Nuclear Science; National Research Council

New Uses for Low-Energy Accelerators

PREPARED BY
THE AD HOC PANEL ON
NEW USES FOR LOW-ENERGY ACCELERATORS
OF THE COMMITTEE ON NUCLEAR SCIENCE
NATIONAL RESEARCH COUNCIL

National Academy of Sciences
Washington, D.C.
1968

This is a report of work under Contract NSF-C310 T.O.47 between the National Science Foundation and the National Academy of Sciences. A limited number of copies of this report are available from the Physics Section, Division of Mathematical and Physical Sciences, National Science Foundation, 1800 G Street, N.W., Washington, D.C. 20550.

Foreword

The world of science is a world of ever-widening horizons. New discoveries and new concepts continually extend the breadth and depth of scientific knowledge and insight. In experimental science, new tools become available and new uses are found for well-used tools which can readily be adapted to meet advances in technical requirements and applications.

Low-energy particle accelerators have produced a great part of our current knowledge of nuclear physics, are producing new fundamental knowledge at the present time, and can be expected to continue to do so. In this report we address ourselves to the recently developed applications of these accelerators to problems in three distinctly different areas: nuclear astrophysics, atomic physics, and solid-state physics. In doing so, we respond to the request by the Committee on Nuclear Science of the National Research Council, made early in November 1967, to examine the extended use of low-energy accelerators in the field of nuclear astrophysics. After discussions with Professor D. A. Bromley, Chairman of the Committee on Nuclear Science, and with several representatives of government agencies interested in the problem, it was decided to include new applications of the accelerators in atomic and solid-state physics as well as in nuclear astrophysics. We wish to emphasize that this extension of the techniques and apparatus of low-energy nuclear physics in no way implies a decrease in the importance of those facilities to nuclear structure work itself.

At an early stage, it was decided to limit consideration to accelerators with maximum singly charged particle energies of 6 MeV. This meant, for example, the exclusion of medium- and high-energy physics from nuclear astrophysics but yielded a clear-cut delineation of the major

problem area. Even with this limitation, it was ascertained that there exist at least 112 low-energy accelerators in universities and colleges in the United States, 53 in government laboratories, and 64 in industrial laboratories. Of these, approximately 80 percent are electrostatic accelerators. In universities and colleges, it was determined that in round numbers there are at least 320 faculty members and research associates and 250 graduate students engaged in research with low-energy facilities. It was estimated that a comparable number of individuals are similarly engaged in government and industrial laboratories. It was thus felt that this report will be of specific interest to a substantial number of physicists and chemists and to the institutions in which they work, as well as of general interest to the scientific community at large.

It is realized that a redirection in the use of an accelerator or any other type of instrument must be primarily motivated by a change in the goals and aspirations of the user. New fields and new concepts must be explored, and new techniques must be learned. Special devotion and dedication are required in a major reorientation of effort. This poses a clear-cut challenge, and it is in full knowledge of this challenge and its consequences that this report must be read. The rewards measured in terms of real and significant contributions to frontier fields speak for themselves.

Basic to this report is the firm belief that great discoveries in science can be made with small means In spelling this out in practical terms, some discussion of instrumentation costs has been incorporated where relevant. References have been given to specific manufacturers or to specific publications that exemplify particular instruments or techniques. These references are *not* intended to be complete, and the choice of referenced manufacturers and publications does *not* represent the result of a careful, comparative evaluation; in most cases these are simply examples which happen to be conveniently accessible or familiar to the authors of this report. The references to industrial organizations are included, because these organizations undoubtedly constitute a primary resource of knowledge and sophistication concerning the instruments under discussion and their uses, existing and potential. The specific organizations referenced are not always necessarily the single best, or even the only, sources of sound experience and information. Undoubtedly, there are many of equal competence not named simply because of the constitution of the Panel and its experience.

This foreword does not attempt a general introduction to the report. Each major part of the text—I. Nuclear Astrophysics, II. Atomic Physics, and III. Solid-State Physics—includes introductory material outlining

the scope and contents of that part. These three introductory sections might well be read first before a complete reading of the report.

The Panel that authored this report decided to operate in a "no nonsense" fashion. At its first and only meeting in late April 1968, introductory presentations in the three disciplinary areas were made, and the nature and scope of the report decided upon. Specific assignments were made to individual panel members for both preparation of text and coordination of activities in the three main areas. It was agreed that drafts would be sent to all panel members working in the specific area involved, as fast as prepared, and that communication between panel members would be maintained at a high level. Deadlines were set and met which required that the report be prepared during the summer of 1968 and finalized by early fall.

Although the report is the considered consensus of the entire Panel, it is well to note those who undertook primary responsibility for the actual writing of specific parts or sections of the report: thermonuclear reactions, Donald D. Clayton; practical considerations in experimental nuclear astrophysics, Peter D. Parker; beam-foil spectroscopy, Stanley Bashkin; atomic lifetime measurements, Ward Whaling; penetration, energy loss, and application of channeling, John A. Davies; ion implantation, James W. Mayer and Walter L. Brown; interactions of nuclear moments, David Fossan; materials analysis, Eligius A. Wolicki. Those unsung worked no less hard!

At the organization meeting of the Panel, the following representatives of government agencies were present: Paul F. Donovan, National Science Foundation; George A. Kolstad, Atomic Energy Commission; Doran W. Padgett, Office of Naval Research; William S. Rodney, National Science Foundation; George L. Rogosa, Atomic Energy Commission. The Panel gratefully acknowledges the initial guidance and wise counsel provided by these gentlemen. We also acknowledge a careful reading of the manuscript by William S. Rodney and his helpful and constructive suggestions.

Charles K. Reed, Executive Secretary of the Committee on Nuclear Science, served in a similar capacity for the Panel. He surveyed accelerator facilities and personnel for the Panel, he coordinated many of the activities of the Panel during its working period, and he undertook supervision of the final editing and publication of the report. To him the Panel is immensely grateful. As a final acknowledgment we express our appreciation for funding by the National Science Foundation.

In this time of increasing demands for other purposes on the government purse, scientific budgets are shrinking and the prospects of obtaining

major new equipment are dim. We must weather the storm and find innovative uses for what we have. In making do for now, but at the same time widening the horizons of science in spite of budgetary limitations, we will have done what we can to assure a more generous support of our aims and efforts for science and society in the future.

Contents

Part I NUCLEAR ASTROPHYSICS

Part II ATOMIC PHYSICS

Part III. SOLID-STATE PHYSICS

Part I

NUCLEAR ASTROPHYSICS

The application of nuclear physics to problems in astrophysics consists of ascertaining which nuclear reactions are of importance and of measuring the relevant nuclear data—primarily cross sections. General astrophysical theory can delineate the potential importance of specific reactions, but painstaking laboratory experiments are required to establish quantitatively their significance within the astrophysical scheme. A potential investigator in laboratory nuclear astrophysics should confront squarely the nature of the problem he is to encounter. The desired cross sections are among the smallest measured in the low-energy nuclear laboratory. Long integration times and careful attention to background counts are common necessities. From a purely nuclear point of view, moreover, the reactions studied are often of comparatively little interest. The intellectual stimulation is more to be found in wresting from nature a hard-won number that she herself has presumably used and in evaluating its astrophysical consequences. An investigator not sharing this interest will be little amused by his task. The nuclear physicist interested in astrophysics, on the other hand, will find many advantages to this type of research: it is an excellent vehicle for entering an exciting field of research on a learn-as-you-go basis; it requires an assimilation of basic laboratory technique with the associated benefit of student training; and it can be relatively inexpensive for those having access to a low-energy accelerator. The clarification of these advantages is a major objective of this report.

The discussion of nuclear astrophysics will be presented in three chapters. In Chapter 1, the general problem of thermonuclear reaction rates, what they are and how they are determined, will be described and illustrated by examples. The examples will be chosen from the existing literature of laboratory nuclear astrophysics and accordingly represent problems that are, for the most part, solved. There is no simple recipe for determining thermonuclear reaction rates, so our hope is that the

classic examples will illustrate both the spirit of the research problems and some already established means of overcoming technical obstacles. In Chapter 2, we survey the basic apparatus of the nuclear astrophysics experiment. Inasmuch as the equipment and experimental arrangements are very similar to those of the usual studies of nuclear reactions, we have attempted to point out many features that are especially useful in studies of astrophysical interest. In these chapters we have attempted to be understood by all prospective readers and thus make no apologies to the experienced researcher for describing subjects already familiar to him. In Chapter 3, we present a list of reactions of importance in nuclear astrophysics, along with a selected bibliography of papers relevant to each reaction or its astrophysical application.

We have not attempted a critical assessment of the relative importance of the reactions listed in Chapter 3 or a list of priorities for the reader. This information is either clearly stated in the papers referred to or is sufficiently unclear that our present opinions may be outdated in two years' time. Nuclear astrophysics shares the property of all expanding fields of science that the numerical results obtained in the laboratory modify the evaluation of the studies needed next. By the same token, we have not attempted an exhaustive review of the present adequacy of nuclear knowledge for each of the major thermonuclear epochs to be encountered in the course of stellar evolution. Such an evaluation would not only have been unduly lengthy but would be quickly dated. Several laboratories have already followed the lead of the California Institute of Technology in this field, and so some of today's urgent needs may have been answered by the time a new researcher is ready to produce results. The number of useful and exciting studies seems nearly inexhaustible, however, and the few laboratories working in this area can only scratch the surface. We believe that it is the independent study of the prospective investigator that must determine his ability to use the specific equipment at his disposal to increase the available information on a given thermonuclear reaction.

From the above introductory remarks it will be clear that we do not intend to give a detailed discussion of the various thermonuclear epochs of stellar evolution. In Table 1, which will be referred to from time to time, these epochs are listed for charged-particle reactions primarily to serve as background for the typical reactions described in the table. To this list should be added two neutron capture processes, one on a slow time scale called the *s*-process and one on a rapid time scale called the *r*-process. The astrophysical literature abounds with references to these epochs and processes, and a comprehensive analysis of the major nuclear burning stages in stellar evolution also exists in a recently published textbook.[1]

CHAPTER 1

Thermonuclear Reactions

Nuclear astrophysics requires measurements over the full range of energies available to the experimental nuclear physicist. For example, accurate measurements of nuclear cross sections at high energy are needed to provide spallation yields from the interactions of cosmic rays and of flare-accelerated particles in stellar atmospheres, in the interstellar medium, in the surfaces of planets and satellites, and in meteorites.[2] These and other high-energy aspects of nuclear astrophysics will be omitted from this discussion, since we are concerned here with investigations employing low-energy accelerators having energies of not more than ~6 MeV for singly charged particles.

It is in the evaluation of thermonuclear reaction rates that low-energy accelerators play a major role. The object of the experimental and theoretical research on these rates can best be appreciated by first considering the physical setting for thermonuclear reactions. It is assumed that the distribution functions in velocity space are thermalized and that for almost all circumstances of practical interest the nuclei are completely ionized and constitute an ideal nonrelativistic Maxwellian gas. In a gas composed of distinct species of ions, each of which is described by a Maxwell-Boltzmann population of particle states, the velocity distribution in the center-of-mass system of colliding particles is also Maxwellian. The probability that the relative velocity between any pair of particles has the magnitude v in the interval dv is given by

$$\varphi(v,T)dv=\left(\frac{M}{2\pi kT}\right)^{\frac{3}{2}}\exp\left(-\frac{Mv^2}{2kT}\right)4\pi v^2 dv, \qquad (1)$$

where T is the temperature and M is the reduced mass of the pair; $M=M_1M_2/(M_1+M_2)$. The relative velocity distribution is normalized

such that $\int_0^\infty \varphi(v,T)dv=1$. The reaction rate per unit volume is then*

$$r(T)=N_1N_2\int_0^\infty \sigma(v)v\varphi(v,T)dv, \tag{2}$$

where N is the number density of the species and $\sigma(v)$ is the cross section for the reaction between species 1 and 2 when their relative velocity is equal to v. This product is often written

$$r(T)=N_1N_2\langle\sigma v\rangle, \tag{3}$$

where the bracketed quantity $\langle\sigma v\rangle$ represents the average over the velocity distribution $\varphi(v,T)$ of the product of cross section times relative velocity.

The problem is that of determining sufficient information in the nuclear laboratory for the calculation of $\langle\sigma v\rangle$. Because of the average over the thermal spectrum, the cross section must be known as a function of energy—albeit over a rather limited energy region. For neutron reactions, the important energy region is the peak in the thermal-energy distribution, but reactions between charged particles are restricted by Coulomb repulsion to pairs having center-of-mass energies far out on the high-energy tail of the thermal distribution. The four following sections illustrate the essential aspects of several types of problems.

Nonresonant Charged-Particle Reactions

In addition to the effects of intrinsic nuclear properties, reactions between two charged particles are determined at low energy by two highly energy-dependent factors. The factor $\pi\lambda\!\!\!^{-2}$ involving the square of the reduced de Broglie wavelength introduces a $1/E$ dependence on energy. Because thermal energies are far below the Coulomb barrier, the barrier penetrability introduces a factor $\exp(-2\pi Z_1Z_2e^2/\hbar v)$ into low-energy cross sections. Both factors are very energy-dependent as $E=Mv^2/2\rightarrow 0$, so it is convenient to factor them explicitly from the cross section by writing

$$\sigma(E)=\frac{S(E)}{E}\exp(-2\pi Z_1Z_2e^2/\hbar v). \tag{4}$$

This definition of $S(E)$ is useful in that if the intrinsic nuclear factors are slowly varying over the thermal energy region, $S(E)$ itself may be nearly equal to a constant over that same energy region. Thermonuclear reactions for which $S(E)$ is nearly constant over the important energy region are conventionally designated as "nonresonant," although the

* We ignore the quite straightforward modifications which are necessary if particles 1 and 2 are identical. For example, in this case, the right-hand sides of Eqs. (2) and (3) should be multiplied by ½, and later on the right-hand side of Eq. (10) should be multiplied by 2.

value of $S(E)$ may be determined by the wings of distant compound nuclear resonances. The provisional assumption of constant $S(E)$ allows determination of the energies that are expected to contribute most to the reaction rate. From Eq. (2), the reaction rate per pair of particles is

$$\langle \sigma v \rangle = \left(\frac{8}{\pi MkT}\right)^{\frac{1}{2}} \int_0^\infty S(E) \exp\left(-\frac{E}{kT} - \frac{b}{\sqrt{E}}\right)\frac{dE}{kT}, \tag{5}$$

where the factor b coming from the barrier penetrability has the convenient numerical value $b = 31.28\ Z_1Z_2A^{\frac{1}{2}}\ \text{keV}^{\frac{1}{2}} = 0.989\ Z_1Z_2A^{\frac{1}{2}}\ \text{MeV}^{\frac{1}{2}}$, and $A = A_1A_2/(A_1+A_2)$ is the reduced atomic mass. The exponential factor within the integrand vanishes at high energy because the number of thermal pairs of high energy vanishes, and it vanishes at low energy due to the Coulomb barrier. The maximum in the integrand is easily seen to occur at

$$E_0 = \left(\frac{bkT}{2}\right)^{\frac{2}{3}} \begin{matrix} = 1.220(Z_1^2Z_2^2AT_6^2)^{\frac{1}{3}}\ \text{keV} \\ = 0.122(Z_1^2Z_2^2AT_9^2)^{\frac{1}{3}}\ \text{MeV} \end{matrix}, \tag{6}$$

where T_6 is the temperature in millions of degrees Kelvin and T_9 is in billions of degrees Kelvin. Thermal energy is only $kT = 0.0862T_6$ keV, so the Coulomb barrier forces reactions to occur near energy E_0, which is much greater than kT. If, as is justifiable[3] for slowly varying $S(E)$, the sharply peaked integrand is approximated by a Gaussian

$$\exp\left(-\frac{E}{kT} - \frac{b}{\sqrt{E}}\right) \simeq C \exp -\left(\frac{E-E_0}{\Delta/2}\right)^2, \tag{7}$$

the full width of the effective energy distribution at $1/e$ times maximum is given by

$$\Delta = \frac{4}{\sqrt{3}}(E_0kT)^{\frac{1}{2}} \begin{matrix} = 0.749(Z_1^2Z_2^2AT_6^5)^{\frac{1}{6}}\ \text{keV} \\ = 0.237(Z_1^2Z_2^2AT_9^5)^{\frac{1}{6}}\ \text{MeV} \end{matrix}, \tag{8}$$

and the energy band over which the cross section is important is

$$E_0 - \Delta \lesssim E \lesssim E_0 + \Delta. \tag{9}$$

The basic features of the energy dependence are illustrated in Figure 1.

The major problem in nuclear astrophysics results from the fact that the favored energy band near E_0 is generally at energies too low for direct measurement of the cross section, so that indirect determinations of the value of the cross section are required. The standard solution to this problem is to measure S and dS/dE at the lowest energies possible and then to determine by independent arguments whether that value of S can be extrapolated downward in energy to E_0 by using dS/dE. The procedure would seem to be a very good one if the mechanism for the reaction at energy E_0 is the same as it is at the measured energies and if

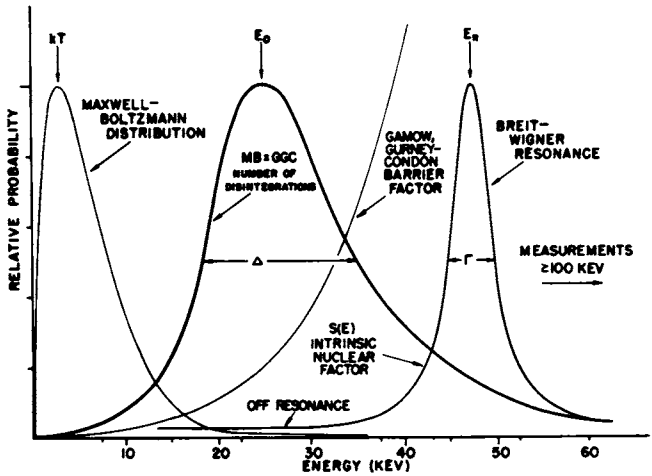

FIGURE 1. The dominant energy-dependent factors in the thermonuclear reactions between charged particles. The necessity of penetrating the Coulomb barrier introduces the Gamow-Gurney-Condon barrier factor $\exp(-bE^{-\frac{1}{2}})$, which vanishes so strongly at very low energy that the reactions are forced to occur in the high-energy tail of the Maxwell-Boltzmann energy distribution. The product of these factors results in a peak near an energy designated by E_0, which is generally much larger than kT. If the nuclear interaction in question is only weakly dependent upon the energy, the reaction rate will be proportional to the value of that product. If, on the other hand, a nuclear resonance at energy E_R is sufficiently near E_0, the reaction rate into the main peak of that resonance may, in spite of the small number of particles having that energy, exceed the reaction rate in the peak at E_0. In nuclear astrophysics, reactions are called nonresonant or resonant according to whether the reaction rate is dominated by the off-resonance reactions in the peak at E_0 or by the reactions in the main peak of the resonance at E_R.

dS/dE can be determined as accurately as can S. It frequently happens that a good theoretical model of the reaction is necessary in order to determine the behavior of $S(E)$ at energies lower than the lowest energy at which it can be accurately measured.

The basic idea can be seen most clearly in the relatively simple case of the reaction* $^{12}C(p,\gamma)^{13}N$, for which $E_0 = 3.93T_6^{\frac{2}{3}}$ keV and $\Delta = 1.34T_6^{\frac{2}{3}}$ keV. Near the center of an upper-main-sequence star, therefore, where $T_6 \simeq 25$, the favored reaction energies are $E \simeq 34 \pm 20$ keV. Figure 2 displays the measured[4] cross section for this reaction as a function of laboratory proton energy. The cross section was measurable down to energies near 100 keV, but an extrapolation downward to 34 keV or

* We use the standard reaction notation with projectile and observed particle incorporated within the parentheses with the notation $p = {}^1H$, $d = {}^2D$, $t = {}^3T$, $\tau = {}^3He$, $\alpha = {}^4He$. Target and residual nuclei are placed outside the parentheses.

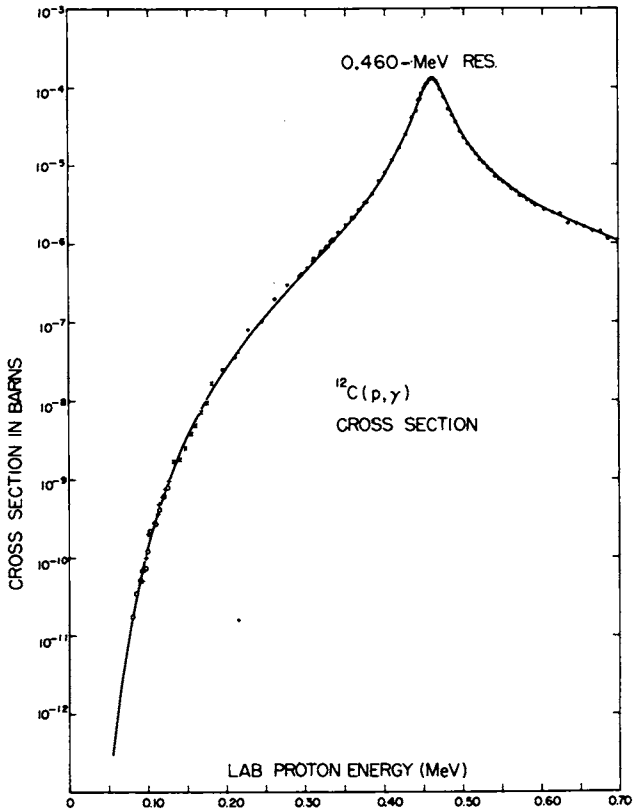

FIGURE 2. The measured cross section for the reaction $^{12}C(p,\gamma)^{13}N$ as a function of laboratory proton energy. A five-parameter theoretical curve has been fitted to the measured points.[4] Without the theoretical understanding of this reaction, an extrapolation to $E_p = 0.025$ MeV, which is the interesting energy for this reaction in astrophysics, appears treacherous.

so appears treacherous, because the measured cross section is changing by an order of magnitude each 25 keV near 100 keV and is getting steeper as the energy decreases. That this behavior is largely due to the penetration factor can be clearly seen in Figure 3, where the cross-section factor $S(E)$ has been plotted. It is a much more gently varying quantity which is observed to decrease by only about 10 percent in 25 keV near 100 keV. A reliable estimate of the cross section near E_0 can be obtained by extrapolating $S(E)$ as long as the reaction mechanism does not change over this small energy region. In this particular case, the extrapolation can be made even more plausible by understanding the nature of the reaction. The curve through the points of Figure 3 is the

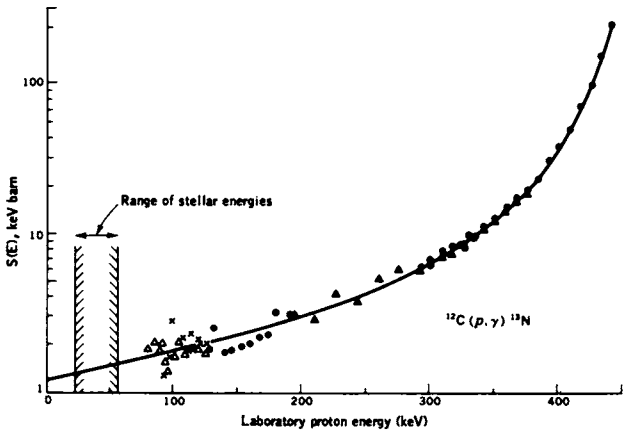

FIGURE 3. The cross-section factor $S(E)$ for the radiative capture of protons by ^{12}C. The differing data points represent measurements by different investigators.[4] The smooth curve shown is much more readily extrapolated than the one in Figure 2, especially if the reaction mechanism is imperfectly understood so that a simple graphical extrapolation is required. (From D. D. Clayton, *Principles of Stellar Evolution and Nucleosynthesis,* McGraw-Hill Book Company, Inc., New York, 1968. Used by permission.)

result[4] of fitting to the data a four-parameter formula for a Breit-Wigner single-level resonance interfering with a weak continuum component which introduces one additional free parameter. The good fit indicates that between 100 and 600 keV the reaction proceeds via the formation of a compound nucleus by the *s*-wave capture of a proton primarily into the broad *s*-wave state near $E(\text{lab}) = 460$ keV. The extrapolation downward to E_0 seems in this case secure provided the *s*-wave strength of that level has not decreased to near the value of the average distributed *s*-wave strength, with which it interferes in the *s*-wave compound nuclear formation, and provided that no other nuclear mechanism becomes competitive near E_0. In the latter regard, it was especially important to determine that there exist no narrow ^{13}N states near $E_0 \pm \Delta$ that could have provided narrow but important resonances in $^{12}C+p$. Possible states had to be eliminated by studies of other reactions since $^{12}C+p$ could not itself be measured to sufficiently low energy.

An example of a similar case is shown in Figure 4, in which the reaction $^{15}N(\tau,a)^{14}N$ was performed specifically to locate any states near 7.6 MeV in ^{14}N which could have served as narrow resonances in the reaction $^{13}C(p,\gamma)^{14}N$. The quantitative effect of such narrow resonances will be considered further in the next section. In this case, a suggested level at an excitation near 7.6 MeV in ^{14}N could have caused such a large

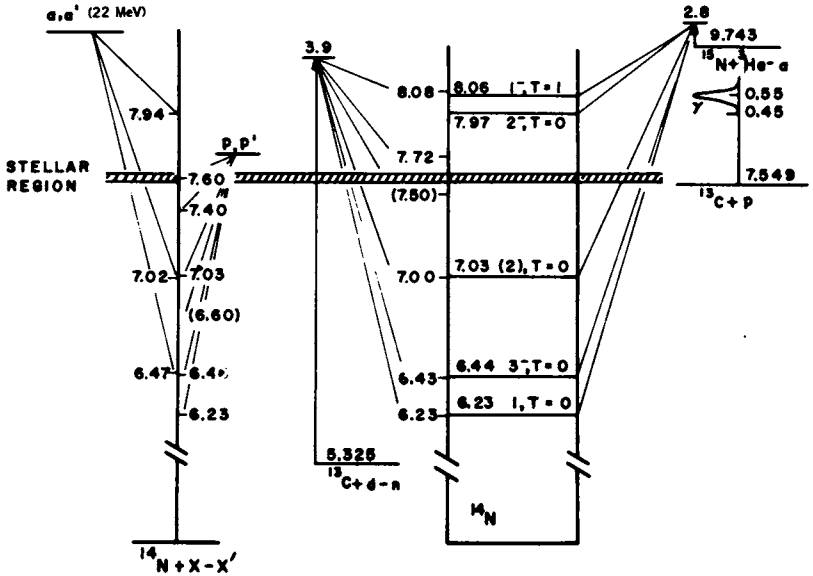

FIGURE 4. Energy level diagram of ^{14}N, which serves as the compound nucleus for the reaction $^{13}C(p,\gamma)^{14}N$. Historically it was necessary to perform the reaction $^{15}N(\tau,\alpha)^{14}N$ to see whether the ^{14}N nucleus possessed undetected states near the mass-energy equivalent of $^{13}C + p$, which would provide resonances near the effective stellar energy for the radiative capture reaction. The existence of such states had erroneously been suggested by inelastic scattering experiments and by the reaction $^{13}C(d,n)^{14}N$, as shown on the left. Decisive laboratory experiments, capable of settling the existence or nonexistence of nuclear energy levels, play an essential role in the determination of thermonuclear reaction rates.

cross section for the $^{13}C(p,\gamma)^{14}N$ reaction[5] that only very small concentrations of ^{13}C could survive during the CN cycle in a hot proton bath. In stars, ratios as large as $^{13}C:^{12}C = 1:4$ have been observed,[6] and this value is precisely the one to be expected during the CN cycle if both $^{12}C(p,\gamma)$ and $^{13}C(p,\gamma)$ are nonresonant. Had the resonance in $^{13}C(p,\gamma)$ existed, the source of such a large ^{13}C abundance would be a major mystery. Fortunately, the existence of the level was not confirmed.[5]

The reaction $^{3}He(\tau,2p)^{4}He$ is a good example of a reaction mechanism changing for a nonresonant reason. The cross-section factor measured[7,8] by several experiments is shown in Figure 5. Above 1 MeV it is found that $S(E)$ decreases slowly as the energy is decreased, but an extrapolation of those results to $E_0 \simeq 25$ keV would have been incorrect. The recent experiments show that, below 1 MeV, $S(E)$ begins to increase with decreasing energy and that, at the same time, the intermediate state $^{5}Li + p$, which moderates the reaction above 1 MeV, becomes less

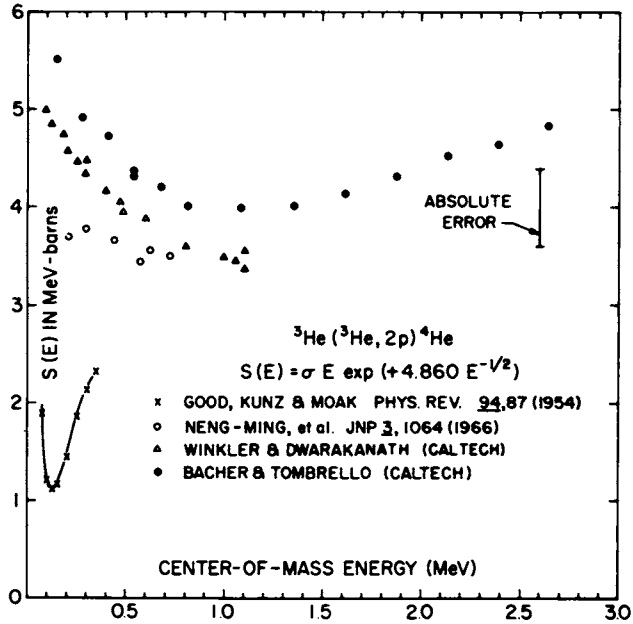

FIGURE 5. Cross-section factor for the reaction ^{3}He(τ,2p)^{4}He as measured by several experiments[7,8]; confident knowledge of the stellar reaction rate near 20 keV requires a good theoretical understanding of the upward rise of $S(E)$ indicated by the recent measurements.

important.[7] It appears likely that a transition occurs near 1 MeV between two different three-body direct reaction mechanisms, and a confident extrapolation to E_0 cannot be made without an understanding of that transition. May and Clayton[9] have suggested that the low-energy mechanism is the direct tunneling of a neutron from one ^{3}He to another and have estimated the low-energy dependence upon energy as a guide for the extrapolation. The situation is still somewhat unclear, but not so much so as a few years ago when the uncertainty in this cross section was the major nuclear uncertainty in the estimation of the solar-^{8}B-neutrino flux.[10]

For heavier particles and high temperatures, it frequently happens that there are many resonances arising from energy levels in all relevant energy regions of the compound nucleus. The concept of the most effective stellar energy, $E_0 \pm \Delta$, is useful in these cases as well, because it shows which resonances are *a priori* most important. In Table 1, several characteristic energies are listed for some specific reactions of importance in the natural sequence of thermonuclear epochs in stars.[11] These reactions will be discussed in subsequent material as examples of

TABLE 1. Characteristic Charged-Particle Reactions

THERMONUCLEAR EPOCH	TYPICAL REACTION	TYPICAL TEMPERATURE (K)	E_0 (keV)	Δ (keV)	MINIMUM EXPERIMENTAL E (CENTER-OF-MASS) (keV)
Proton–proton chain	$^{1}H,(p,e^{+}\nu)^{2}D$	15×10^{6}	5.9	6.4	unmeasurable
Proton–proton chain	$^{3}He(\tau,2p)^{4}He$	15×10^{6}	21	12	150
Carbon–nitrogen cycle	$^{12}C(p,\gamma)^{13}N$	25×10^{6}	34	20	85
Helium burning	$^{12}C(\alpha,\gamma)^{16}O$	10^{8}	200	96	2100
Carbon burning	$^{12}C(^{12}C,\alpha)^{20}Ne$	10^{9}	2410	1060	3500
	$^{12}C(p,\gamma)^{13}N$	10^{9}	393	425	85
	$^{12}C(\alpha,\gamma)^{16}O$	10^{9}	923	650	2100
Oxygen burning	$^{16}O(^{16}O,\alpha)^{28}Si$	2×10^{9}	6200	2400	
	$^{28}Si(\alpha,\gamma)^{32}S$	2×10^{9}	2710	1580	
Silicon burning	$^{28}Si(\gamma,p)^{27}Al$	4×10^{9}	1680	1760	1060
	$^{16}O(\gamma,\alpha)^{12}C$	4×10^{9}	2320	2070	2100
	$^{44}Ti(\alpha,p)^{47}V$	4×10^{9}	3720	2620	
Explosions from very high density	$^{4}He(d,\gamma)^{6}Li$	10^{9}–10^{10}	$186T_9^{\frac{1}{3}}$		
	$^{18}O(p,\alpha)^{15}N$	10^{9}–10^{10}	$480T_9^{\frac{1}{3}}$		

relatively well-studied cases of importance during these various epochs. For example, the reaction $^3He(\tau,2p)^4He$ is important in the proton–proton chains of hydrogen burning, which occurs near $T_6=15$ in the center of the sun. In these circumstances $E_0=21$ keV and $\Delta=12$ keV, but the lowest energy for which the cross section has been measured accurately is about 150 keV, center-of-mass, or 300 keV, laboratory bombarding energy. It will be noted that in the later stages of stellar evolution, when the temperature is high, the value of E_0 becomes large enough for some reactions that the cross section can be measured directly. It can also be noticed that some reactions are of importance in more than one stage of thermonuclear evolution. The physics required to understand the cross section for $^{12}C(\alpha,\gamma)^{16}O$, for example, is much different in helium burning than it is in carbon burning and silicon burning. It is for just such reasons as this that some knowledge of astrophysics is helpful in ascertaining the detailed nuclear problems that must be solved to obtain a relevant reaction rate.[11]

Resonant Reactions and Associated Studies of Nuclear Energy Levels

Figure 4 illustrated a search via the $^{15}N(\tau,a)^{14}N$ reaction for ^{14}N states having excitation near 7.60 MeV, where they could serve as stellar resonances in the $^{13}C(p,\gamma)^{14}N$ reaction and yet be undetectable in the laboratory by the direct study of that reaction. Such resonances will usually be very narrow unless they involve a neutron channel with $E>\sim 10$ keV or a high-energy charged-particle channel with E comparable to or greater than the Coulomb barrier height. For a narrow resonance of spin J_r the small partial widths Γ_{12} and Γ_{34} in the single-level resonant cross section $1+2\rightarrow 3+4$,

$$\sigma=\frac{2J_r+1}{(2J_1+1)(2J_2+1)}\pi\lambda\!\!\!^{-2}\frac{\Gamma_{12}\Gamma_{34}}{(E-E_r)^2+(\Gamma/2)^2} \tag{10}$$

will be essentially constant over the resonance width $\Gamma=\Sigma\Gamma_{ij}$, which is in turn frequently smaller than kT. Then the factors $v\varphi(v,T)$ in Eq. (2) can be evaluated at the resonance energy E_r so that[12]

$$\langle\sigma v\rangle_{res}=[v\varphi(v,T)]_{E=E_r}\int_0^\infty\sigma(v)dv$$

$$=\hbar^2\left(\frac{2\pi}{MkT}\right)^{\frac{3}{2}}\frac{2J_r+1}{(2J_1+1)(2J_2+1)}\frac{\Gamma_{12}\Gamma_{34}}{\Gamma}\exp\left(-\frac{E_r}{kT}\right). \tag{11}$$

This equation applies to any narrow resonance involving neutrons or charged particles. Although the contribution of the resonance to $\langle\sigma v\rangle$

may not be measurable directly it is seen to be calculable if E_r, J_r, and the widths are known. It frequently happens that only a single width need be determined—specifically when there are only two channels and when one of the two widths is much smaller than the other. For example, in a low-energy (p,γ) reaction it frequently happens that those are the only two channels open and that because of the Coulomb barrier $\Gamma_p \ll \Gamma_\gamma \approx \Gamma$, where to avoid cumbersome notation we designate the partial widths such as $\Gamma_{^{13}\mathrm{C_p}}$ and $\Gamma_{^{14}\mathrm{N}\gamma}$ by Γ_p and Γ_γ, respectively. In that case, a reaction occurs each time a proton forms the resonant state, and the rate depends only on the proton width; viz., $\Gamma_p\Gamma_\gamma/\Gamma \rightarrow \Gamma_p$. The barrier effects on Γ_p are calculable so that the major data needed to calculate the effects of resonances are frequently the resonance energy E_r and spin J_r and an estimate of the reduced proton width. If, on the other hand, the resonance energy is not so low it frequently happens that $\Gamma_p \gg \Gamma_\gamma$. In that case, the reaction rate due to the resonance requires the determination of J_r and Γ_γ. Measurement of the appropriate quantities frequently demands nuclear studies that bear only subtle connections to the reaction of interest. Some examples follow.

The formation of ^{12}C in a helium gas occurs by way of an (α,γ) reaction on unstable ^{8}Be, which exists in the gas in small concentrations by virtue of the equilibrium $^{4}\mathrm{He}+{}^{4}\mathrm{He} \rightleftarrows {}^{8}\mathrm{Be}$. The establishment of the process by study of the reverse sequence $^{12}\mathrm{C}^*(7.65\ \mathrm{MeV}) \rightarrow {}^{8}\mathrm{Be}+{}^{4}\mathrm{He} \rightarrow 3\,{}^{4}\mathrm{He}$ is described by Cook *et al.*[13] The energy-level diagram is shown in Figure 6. Because the 7.65-MeV state decays overwhelmingly by alpha emission, the rate of formation of ^{12}C is independent of $\Gamma_\alpha(7.65)$. In fact,

$$r(3\alpha \rightarrow {}^{12}\mathrm{C}) \propto \Gamma_\gamma(7.65)\ \exp(-Q/kT),$$

where $\Gamma_\gamma(7.65)$ is the radiative decay width of the state and Q is the energy difference between the mass of $^{12}\mathrm{C}^*(7.65)$ and the mass of three alpha particles. The radiative width has not been directly measurable, and Seeger and Kavanagh[14] describe the way in which the measurement of several ratios of widths can be combined with the measurement by inelastic electron scattering of the absolute monopole matrix element for decay to the ground state to obtain Γ_γ. This story provides a fascinating example of the way in which nuclear astrophysics must draw upon many facets of nuclear knowledge.

This reaction also provides an example of the care with which energetics must be treated in nuclear astrophysics. Because the 3α reaction occurs in stars near 10^8 K, or $kT = 8.62$ keV, an uncertainty of 10 keV in Q amounts to an uncertainty of a factor 3 in the reaction rate. The favorite ways of measuring the mass of $^{12}\mathrm{C}^*(7.65)$, namely by

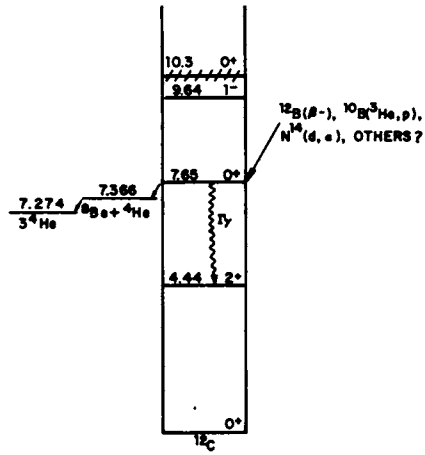

FIGURE 6. The energy level diagram of ^{12}C. The fusion of alpha particles into ^{12}C in a dense helium gas proceeds through the reverse steps of the decay of the 7.65-MeV state into three alpha particles. Calculation of the rate of fusion requires the radiative width Γ_γ of the 7.65-MeV state and an accurate measure of the mass of that state minus the mass of three alpha particles. The mass of the state, as measured by the three reactions displayed on the right, is still not known with the desired accuracy.

$^{12}B(e^-\bar{\nu})^{12}C^*(\alpha)^8Be$, by $^{10}B(\tau,p)^{12}C^*$, and by $^{14}N(d,\alpha)^{12}C^*$, lead to values of Q that differ by as much as 10 keV,[15] so additional high-resolution studies of these reactions, especially the first, would be valuable if the investigator is confident that he can locate the state to a few keV. There exist, moreover, many reactions for which accurate energetics are required—whenever a resonance dominates an important reaction rate and whenever two nuclear species come into statistical equilibrium with the compound nucleus.

Another example of the importance of low-lying resonances to stellar reaction rates can be found in the reaction $^{14}N(p,\gamma)^{15}O$, the slowest and thus the rate-determining reaction in Bethe's carbon–nitrogen cycle. A comparison with the states in the mirror nucleus, ^{15}N, as shown in Figure 7, suggests that all the ^{15}O states in the energy region near $^{14}N+p$ are now known. A precise measurement of the excitation energy of states near the mass of $^{14}N+p$ was needed to clarify their astrophysical importance. That need is obvious enough for states above $^{14}N+p$, but the exact location is important even if the state is located in the negative-energy domain, because such a state may, due to its natural width, provide a resonant wing in the positive-energy domain; alternatively, if the radiative capture is direct, the binding energy of the proton determines

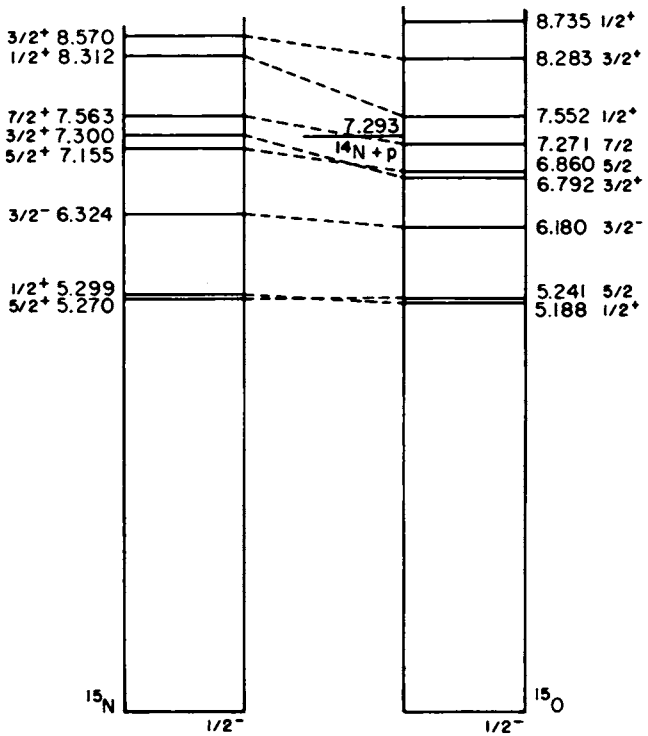

FIGURE 7. Energy level diagrams of ^{15}O, the compound and final nucleus for the reaction $^{14}N(p,\gamma)^{15}O$, and of its mirror nucleus, ^{15}N. Comparison of these energy-level diagrams suggests that all states in this energy region have now been detected.

the extranuclear size of the state, which is an important quantity for that process.[16] Recent high-resolution studies,[17,18] such as the one in Figure 8, have shown that the state in ^{15}O closest to the mass-energy equivalent of $^{14}N+p$ is actually 17 to 22 keV below it. In addition, Hensley[17] was also able to show that the state has $J^\pi = 7/2^+$, in which case it can be formed as a compound nucleus only by the capture of d-wave protons by ^{14}N. The strong centrifugal suppression at low positive energies therefore makes that process of negligible importance for the CN cycle. [The $^{12}C(\alpha,\gamma)^{16}O$ reaction, to be discussed below, is an example of a negative energy state contributing to $\langle\sigma v\rangle$.]

The precise location and properties of this potential resonance for $^{14}N(p,\gamma)^{15}O$ is of great astronomical importance. If it had been placed at such an energy and had such properties that it contributed more strongly to the thermal cross section than does the nonresonant con-

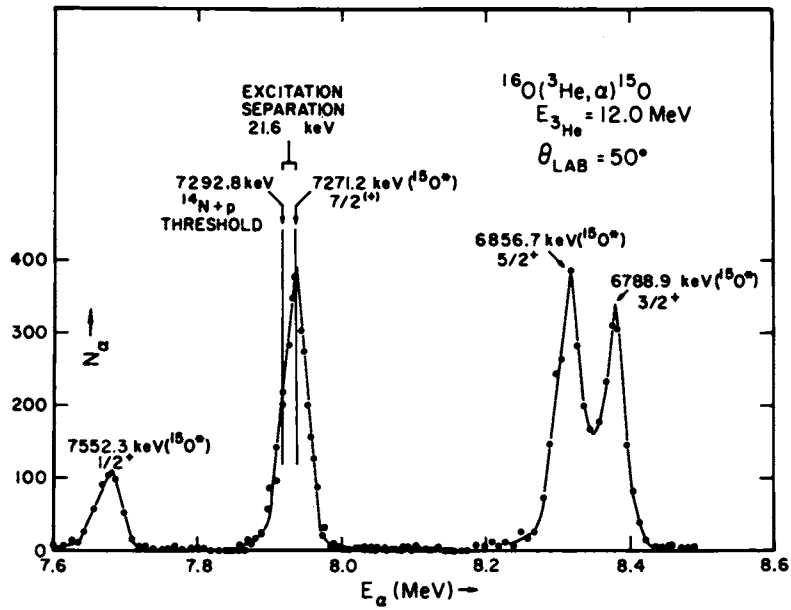

FIGURE 8. Energy spectrum of the alpha particles from $^{16}O(\tau,\alpha)^{15}O^*$ at 12.0-MeV laboratory bombarding energy and 50° laboratory angle with the incident beam.[17] The high-energy resolution was obtained by analyzing the emerging alpha particles with a 61-cm-radius, double-focusing magnetic spectrometer.

tinuum measured at bombarding energies higher than the stellar energy E_0, it would then have been difficult to understand a star in which nitrogen is observed[19] to be more abundant than carbon. If $^{14}N(p,\gamma)$ had been much faster, $^{12}C(p,\gamma)$ would have been the rate-determining reaction in the CN cycle and the resulting hundredfold increase in the rate would, moreover, have increased its importance in energy generation within the sun to the point that the solar neutrinos from the CN cycle would have exceeded the upper limit measured by Davis *et al.*[20] Of such importance is 30 keV or so in the nuclear laboratory!

The chains of reactions which convert hydrogen into helium[11] are the most thoroughly studied set in nuclear astrophysics.[21,22] However, the field is still not closed, and a number of problems remain open. Of these, undoubtedly the most serious one involves the lack of high-energy solar neutrinos[20] with observed flux $\leq 2\times10^6/cm^2/sec$ at the earth and the predicted flux[23] $\approx 5\times10^6/cm^2/sec$. The predicted neutrinos come predominantly from the beta decay of ^8B to ^8Be after the ^8B has been formed as part of the proton–proton chain,

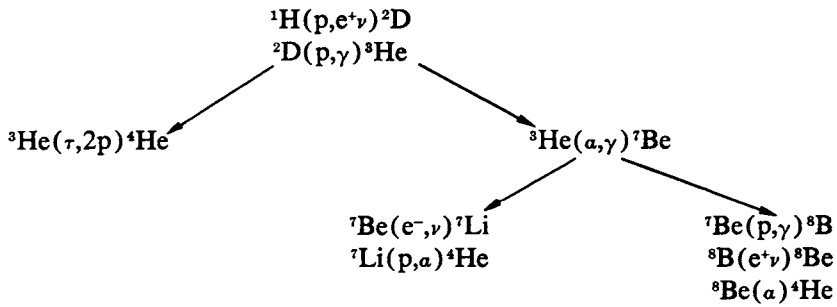

The rates of essentially all the important nuclear reactions involved directly in this problem have been measured "reliably" and independently checked with fair to good agreement, e.g.,

$^{3}He(\tau,2p)^{4}He$	Winkler and Dwarakanath[8] and Bacher and Tombrello[7]
$^{3}He(\alpha,\gamma)^{7}Be$	Parker and Kavanagh[24] and Nagatani *et al.*[25]
$^{7}Be(p,\gamma)^{8}B$	Parker[26] and Vaughn *et al.*[27]

However, particularly in this case involving the solar neutrino problem, further checks on these reactions would be very valuable, especially checks incorporating different approaches or novel techniques.

In addition, more work should be done on the spectrum of the delayed alphas from ^{8}B and its weak beta-decay branches to the highly excited states of ^{8}Be, since the strength of these branches will influence the expected neutrino spectrum. The $^{7}Li(d,p)^{8}Li$ 770-keV resonance [to which all the $^{7}Be(p,\gamma)^{8}B$ data are normalized] requires at least one more precise, absolute cross-section measurement to resolve the difference between the measurements of Kavanagh[28] and Parker,[26] 176 ± 15 mb and 211 ± 15 mb, respectively. Furthermore, the cross sections obtained by Imhof *et al.*[29] for the $^{7}Li(n,\gamma)^{8}Li$ reaction [the mirror of the $^{7}Be(p,\gamma)^{8}B$ reaction] should also be checked, since these $^{7}Li(n,\gamma)^{8}Li$ cross sections formed the basis of a calculation of the $^{7}Be(p,\gamma)^{8}B$ cross sections by Tombrello,[30] which yields results approximately a factor of 3 lower than the observed $^{7}Be(p,\gamma)^{8}B$ cross sections.

Other specific problems related to hydrogen burning by the CNO bi-cycle include (a) further study of the 5.60- and 5.66-MeV levels in ^{18}F and their influence as low-lying resonances on the $^{17}O(p,\alpha)^{14}N$ reaction as part of the CNO bi-cycle[31] and (b) essentially a wide open field in the Ne-Na cycle.[32–34]

It is believed that the reaction $^{12}C(\alpha,\gamma)^{16}O$, which is of great importance during helium burning, occurs primarily by the formation of a compound nuclear intermediate state that is the positive-energy tail of a

state bound by 46 keV. The situation is illustrated in Figure 9. The 7.115-MeV state of ^{16}O with $J^{\pi}=1^-$ has a natural width $\Gamma_\gamma=0.066$ eV. This width gives the state a finite amplitude in the positive energy region where it may be formed by p-wave alpha capture by ^{12}C. A calculation of the reaction rate via this mechanism depends upon the reduced alpha-particle width of the 7.115-MeV state of ^{16}O. The quantity is clearly unmeasurable by a direct technique, so indirect evidence that can be measured must be used. One of the clever possibilities is shown in Figure 10, where a direct alpha-particle transfer mechanism for the reaction $^6Li(^{12}C,d)^{16}O$ is illustrated. The deuteron spectrum obtained with a bombarding energy of 7-MeV ^{12}C ions is shown in Figure 11, and

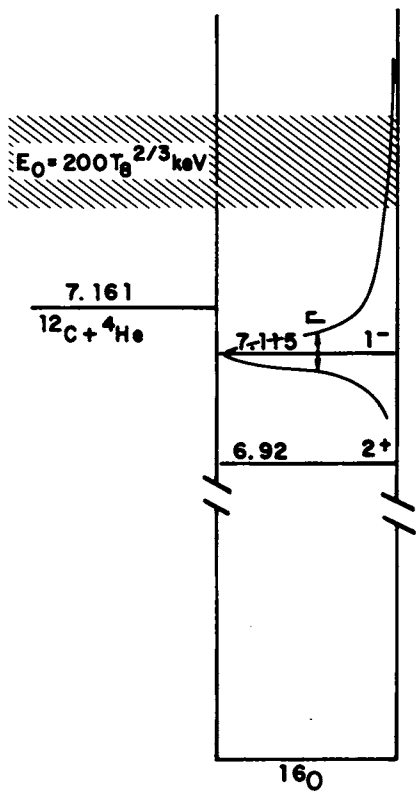

FIGURE 9. Energy level diagram of ^{16}O near 7-MeV excitation. The reaction $^{12}C(\alpha,\gamma)^{16}O$ via the formation of a $J^{\pi}=1^-$ compound nuclear state is dominated at alpha energies near E_0 by the wing of the state at 7.115 MeV. This reaction has not been directly measurable because at alpha energies of 2 MeV or so, where the cross section is large enough to measure, the formation of the compound nucleus is dominated by other states.

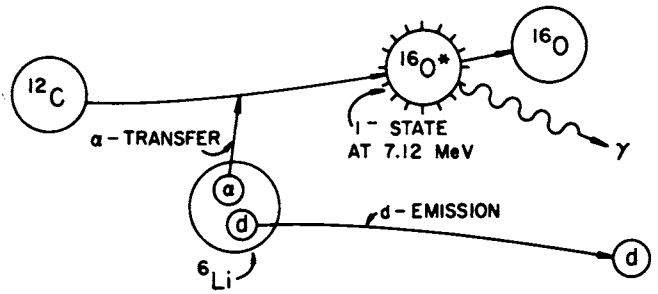

FIGURE 10. Alpha-particle transfer from ^{6}Li to ^{12}C in the reaction ^{6}Li(^{12}C,d)^{16}O*. Direct transfer is a measure of the alpha-particle width[35] of the 7.115-MeV state of ^{16}O shown in Figure 9.

the yield of the deuteron group corresponding to 7.115-MeV residual excitation of ^{12}C is, to the extent that the reaction is direct, proportional to the product of the alpha-particle widths of ^{16}O (7.115 MeV) and of ^{6}Li. The interpretation of this experiment is not unambiguous, but the experiment itself embodies the essence of nuclear astrophysics—a pains-

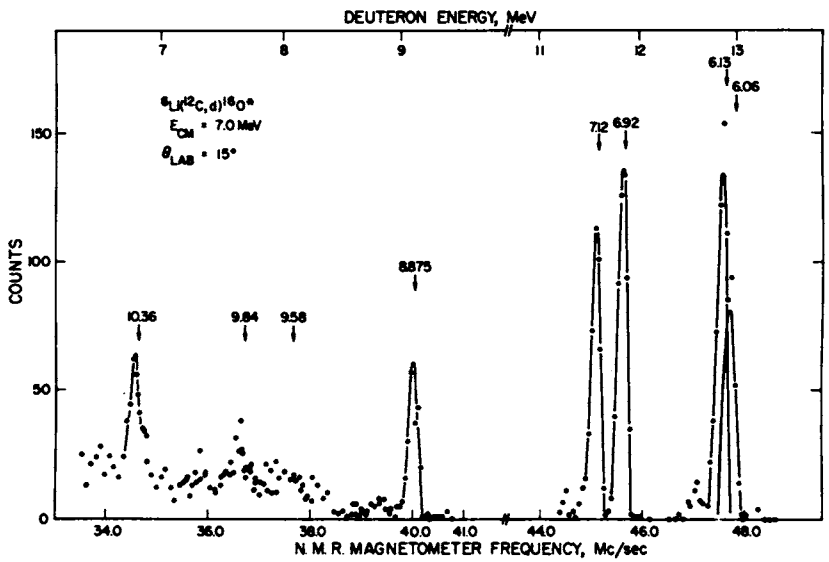

FIGURE 11. Energy spectrum of the deuterons from ^{6}Li(^{12}C,d)^{16}O* at 7.0-MeV center-of-mass bombarding energy and 15° laboratory angle with the incident beam. The relative yields to the 7.12-MeV and 9.84-MeV states of ^{16}O were taken to be measures of their alpha-particle widths. Γ_γ (9.84) has been measured directly by ^{12}C(α,γ)^{16}O, so Γ_γ(7.12) can be obtained from the ratio.[35]

taking nuclear experiment performed to obtain a single number important to the evolution of the universe. With the result inferred from this experiment,[35] $\theta_\alpha^2(7.12) = 0.10 \pm 0.04$, it is found [36] that helium burning in stars produces comparable amounts of ^{16}O and ^{12}C, similar to the ratios found naturally. If, however, the rate of $^{12}C(\alpha,\gamma)^{16}O$ were considerably faster or slower compared to the 3α rate, the relative production $^{16}O/^{12}C$ would be, respectively, too large or too small to fit known abundances.

After the exhaustion of helium, a star contracts until the temperature reaches a sufficient value for ^{12}C to interact with itself. The experimental study of the resulting reactions is quite complicated because of the large number of final states, as shown in the energy level diagram of Figure 12. Possible end products are $^{23}Na+p$, $^{23}Mg+n$, $^{20}Ne+^4He$, $^{16}O+2^4He$, and $^{24}Mg+\gamma$. Available low-lying states of the final nuclei are also shown. The Coulomb barrier for $^{12}C+^{12}C$ is about 7 MeV, whereas the most effective stellar energy is $E_0 = 2.41 T_9^{\frac{2}{3}}$ MeV. Because it has been found that carbon will burn near $T_9 = 1$ in stars, the reaction occurs over a spread of energies from about 1 MeV to almost 4 MeV, whereas laboratory studies have been pushed down only to 3.23 MeV. Because protons,

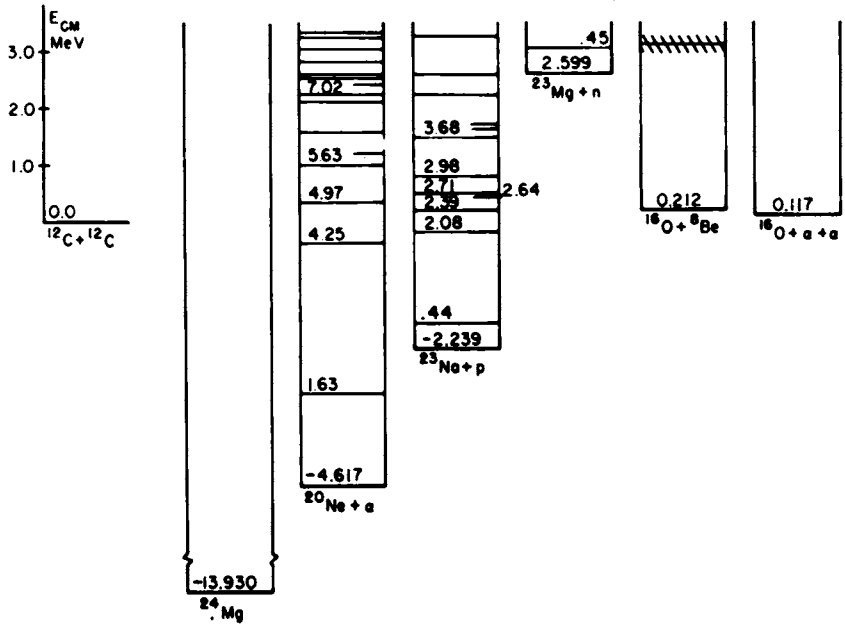

FIGURE 12. The decay modes of the system $^{12}C + ^{12}C$. The masses of the ground states are relative to $^{12}C + ^{12}C$, whereas the excitation energy of the final nucleus is relative to the ground state of that nucleus.

neutrons, and alpha particles are all liberated by carbon reactions, it is also necessary to study the reactions of p, n, and α with all nuclei that are present at temperatures near 10^9 K. Thus, for example, the $^{12}C(p,\gamma)^{13}N$ reaction, which was shown in Table 1 to be important near $E=34\pm20$ keV in the carbon–nitrogen cycle of hydrogen burning, is also found to be of interest during carbon burning up to almost 1 MeV for nonresonant interactions. Because of the large number of possible secondary reactions, it is found that during carbon burning and later thermonuclear epochs a reaction network must be solved to understand the thermonuclear products.[37]

Of prime importance, however, is the experimental study of the $^{12}C+^{12}C$ reaction itself. Low-energy accelerators are quite useful for such studies provided compact ion sources capable of producing doubly and triply ionized ^{12}C ions can be developed. In addition, one requires a scattering chamber and particle detectors capable of unraveling the multifaceted spectrum. The total reaction cross section measured by one such study[38] is shown in Figure 13. It can be seen that $S(E)$ is by no means constant, but is a rapidly varying function of energy showing considerable detail. The resonance-like peaks, whose actual nature is not clearly understood, are associated with a simultaneous rise in each of the

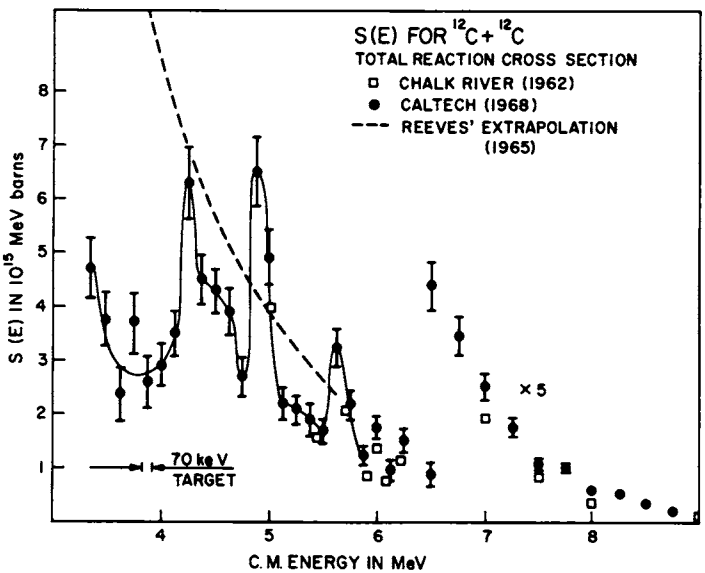

FIGURE 13. Cross-section factor $S(E)$ for reactions between $^{12}C+^{12}C$.[38] The values at the lowest energies are far below Reeves' extrapolation with the aid of optical-model transmission functions of data obtained at Chalk River near 6 MeV.

proton, neutron, and alpha-particle channels. Although the exact structure of $S(E)$ near E_0 remains unknown, studies like this one may well show how $S(E)$ should be averaged in the measured region to obtain a realistic estimate of $S(E)$ at lower energy. It is also clear that $S(E)$ is generally smaller than the value obtained by extrapolating measurements made between 5 and 10 MeV downward to 3 MeV with the aid of optical model transmission functions. There can be no doubt that observations on this reaction should be made below $E_{CM}=3$ MeV or $E_{lab}=6$ MeV. A strong source of triply ionized ^{12}C atoms in a 2-MV accelerator would do the trick.

Many of the features of the experimental study of carbon burning find analogs in the study of oxygen burning. At the time of writing of this report, experimental studies of $^{16}O+^{16}O$ are badly needed, but at least one such experiment is already under way.

During the thermonuclear burning of ^{28}Si, which is actually a complicated rearrangement process[39,40] following photodisintegration, a host of reactions of protons, neutrons, and alpha particles with intermediate mass nuclei become important. Ideally one would like individual measurements of the cross sections for all the various alpha-particle, nucleon, and gamma-ray induced reactions. These reactions find many compound nuclear resonances within the energy range $E_0 \pm \Delta$, and the properties of these resonances are almost entirely unknown. However, it by no means follows that direct study of them is a feasible approach. The example $^{44}Ti(\alpha,p)^{47}V$ listed in Table 1 is typical of this class of reaction. Its rate is important and would be measurable near E_0 *provided* all proton groups could be counted and *provided* targets of radioactive ^{44}Ti ($\tau_{\frac{1}{2}}=47$ yr) existed in sufficient abundance. However, even for stable targets there are problems, because if the reaction does not lend itself to a radiochemical determination of cross section, then one may encounter experimental difficulties in attempting to count the contributions of outgoing particles to all levels of the residual nucleus. Much more troublesome, however, is the fact that the most abundant nuclei in silicon burning tend to lie on the proton-rich side of the stable valley. Thus, many of the most relevant target nuclei are unstable, and the interesting reactions are difficult to study in accelerator experiments. More specifically, for a typical silicon burning process,[39] the most abundant product at each A (for $28 \leq A \leq 60$) is unstable except for ^{28}Si, ^{32}S, ^{36}Ar, ^{39}K, ^{40}Ca, ^{46}Ti, ^{50}Cr, ^{54}Fe, and ^{58}Ni. For these reasons, one goal of an experimental program would be to develop a quantitative understanding of the systematics of the cross sections. Some reactions, on the other hand, such as $^{32}S(p,\gamma)^{33}Cl$, may be directly "studyable" by conventional techniques.

The systematic behavior of average cross sections (averaged to avoid

possible confusion from Ericson fluctuations[41]) can be surveyed by considering the following questions:

(a) To what extent do the reactions proceed via compound nucleus formation? At low energies the compound nuclear mechanism is usually thought to be dominant. However, there is little information concerning subbarrier reaction mechanisms and further experimental and theoretical work (such as the measurement and analysis of angular distributions) appears desirable before one can be confident about assuming predominantly compound nuclear reactions. Should direct reactions play a nontrivial role, then the goal of establishing the systematics of the reaction cross sections will be harder, because detailed properties of individual nuclei will become important.

(b) Tentatively assuming that the reaction is mostly compound, what is the cross section for compound nucleus formation? This essentially involves determining the barrier penetration. The best calculations of barrier penetration use the optical model, with parameters determined from experiments carried out at higher energies than considered here. Comprehensive tests of the validity of the extrapolation have not been made, but there is evidence, at least for alpha particles, that it is not yet possible to calculate low-energy reaction cross sections reliably. In particular, experimental total reaction cross sections for 5- to 6-MeV alpha particles in ^{58}Ni have been reported to lie a factor of 5 to 10 below reasonable optical model predictions.[42] The choice of particular individual reactions for the necessary further study depends, in the first instance, primarily on experimental convenience. Eventually, of course, a broad sampling of nuclei should be covered.

(c) What are the branching ratios for the competing decay modes of the compound nucleus, including gamma decay? Here barrier penetration (for the specific spin distribution of the compound nuclear states) and the level structure of the residual nucleus both enter. The level structure may be treated either by using a statistical prescription for level densities[43] or by explicit knowledge of the individual levels. Where practical, the latter course is to be preferred, especially since many of the reactions are endoergic, and thus only a few levels can be reached in the residual nucleus. When one believes that one can calculate branching ratios with reasonable accuracy, this belief should be tested by selected measurements involving competing proton, neutron, alpha-particle, and gamma-ray yields.

In implementing the procedure described above, for the calculation of reactions in cases of astrophysical interest, one will encounter considerable gaps in the existing knowledge of the level structure of many of the nuclei on the proton-rich side of the stable valley. Some of these levels

are accessible via (τ,n) reactions. An associated benefit of determining the level structure (at least for the very low-lying levels) accrues even to the equilibrium model of silicon burning,[39] because the equilibrium abundances depend upon the nuclear partition functions.

Reciprocity in Thermonuclear Reaction Rates; Photonuclear Rates

The quantum principles of reciprocity relate the cross section for ①+②→③+④+$Q_{12,34}$ to the cross section for ③+④→①+②−$Q_{12,34}$ by

$$(2J_1+1)(2J_2+1)\frac{\sigma(12,34)}{\lambda\!\!\!^{-2}_{12}}=(2J_3+1)(2J_4+1)\frac{\sigma(34,12)}{\lambda\!\!\!^{-2}_{34}}. \quad (12)$$

For the specific reaction involving only the ground states of all particles, it can rather easily be shown that because of this reciprocity principle the thermal average $\langle\sigma v\rangle_{12,34}$ for a reaction is proportional to the thermal average $\langle\sigma v\rangle_{34,12}$ for the inverse reaction:

$$\langle\sigma v\rangle_{34,12}^{\text{ground states}}=\langle\sigma v\rangle_{12,34}^{\text{ground states}}\left(\frac{M_{12}}{M_{34}}\right)^{\frac{3}{2}}\frac{(2J_1+1)(2J_2+1)}{(2J_3+1)(2J_4+1)}\times\exp\left(-\frac{Q_{12,34}}{kT}\right), \quad (13)$$

where $M_{12}=M_1M_2/(M_1+M_2)$ and $M_{34}=M_3M_4/(M_3+M_4)$.

The total reaction rate appropriate to the thermal environment of the stellar interior requires an average over the thermal distribution of excited states of the initial nuclei and a sum of the cross sections over all energetically open channels for the residual nuclei. For the projectile nuclei, the average thermal population in excited states is given by the Boltzmann distribution:

$$\frac{n(E_i,J_i)}{n(\text{all states})}=\frac{(2J_i+1)e^{-E_i/kT}}{G}, \quad (14)$$

where G is the nuclear partition function

$$G=\sum_i(2J_i+1)\exp(-E_i/kT). \quad (15)$$

With the use of these quantities and the application of Eq. (12) to each pair of distinct initial and final states it turns out simply that[22]

$$\langle\sigma v\rangle_{34,12}^{\text{all states}}=\langle\sigma v\rangle_{12,34}^{\text{all states}}\left(\frac{M_{12}}{M_{34}}\right)^{\frac{3}{2}}\frac{G_1G_2}{G_3G_4}\exp\left(-\frac{Q_{12,34}}{kT}\right), \quad (16)$$

where the reaction rate on the left is for particles ③ and ④ thermally distributed among their excited states going to all energetically allowable

final states of ① and ②, and the cross section on the right is for particles ① and ② thermally distributed among their excited states going to all energetically allowable final states of ③ and ④. This result has the happy feature of allowing some thermonuclear reaction rates to be measured by study of the inverse reaction. By far the most important case is the thermal average of photonuclear cross sections, because they are generally more difficult to measure than are the inverse radiative capture reactions. For this case the average $\lambda_\gamma(3)$ over the Planck spectrum of the photonuclear rate for the reaction $\gamma+3\rightarrow 1+2$ becomes

$$\lambda_\gamma(3)=\left(\frac{M_{12}kT}{2\pi\hbar^2}\right)^{\frac{3}{2}}\frac{G_1G_2}{G_3}\exp\left(-\frac{Q_{12,3\gamma}}{kT}\right)\langle\sigma v\rangle_{12,3\gamma}, \qquad (17)$$

where the thermal average $\langle\sigma v\rangle$ is evaluated at the same temperature for which $\lambda_\gamma(3)$ is desired. Photonuclear rates are very important in nuclear astrophysics, so it is fortunate that they are usually obtainable from $\langle\sigma v\rangle$.

One must not lose sight of the fact that Eq. (17), like Eq. (16), automatically sums the photodisintegration rates from all excited states of ③ provided that $\langle\sigma v\rangle_{12,3\gamma}$ includes reactions from the ground state and *all* the thermally excited states of ① and ② which leave nucleus ③ in *all* of its energetically allowed excited states. The latter requirement for studies involving the ground states at ① and ② is easy, because laboratory measurements lead, when properly designed, to the measurement of the cross section to all excited states of the residual nucleus, ③. The former requirement involving all states of ① and ② deserves special consideration. Laboratory targets lie exclusively in their ground states, so if the inverse reaction involves an excited state of that target it cannot be studied directly. As a concrete example to illuminate this point, the photonuclear reaction ^{24}Mg(γ,p)^{23}Na* to an excited state of ^{23}Na cannot be studied by the reaction ^{23}Na(p,γ)^{24}Mg. Fortunately, this complication is seldom of practical importance in light nuclei because of the large energy required to leave photodisintegration products in excited states. In medium and heavy nuclei, however, where the energies of excited states may not be large compared to kT, this complication must not be overlooked. The contribution of the excited states to $\langle\sigma v\rangle$ must be calculated, but laboratory measurements can sometimes guide the calculation. Certainly J^π for the excited target state can be measured, so the partial waves contributing to specific compound nuclear resonances can be ascertained. In the case ^{23}Na*(p,γ)^{24}Mg, the proton width Γ_p' can be obtained by measuring resonant inelastic scattering ^{23}Na(p,p′)^{23}Na* and comparing it with resonant elastic scattering ^{23}Na(p,p)^{23}Na.

Two typical examples of prominence during silicon burning were listed in Table 1. The reaction ^{16}O(γ,α)^{12}C participates in the chain of alpha-

particle photoejections which moderate the destruction of ^{28}Si. The most effective photons within the Planck distribution are those which eject the alpha particle with that same energy E_0 that is most effective for the inverse radiative capture at the same temperature. Thus this photodisintegration rate is studied by the same $^{12}C(\alpha,\gamma)^{16}O$ reaction that was important during helium burning and carbon burning. For photodisintegration near $T_9=4$, moreover, the reaction is easy to study because it proceeds through resonances a few MeV up in the $^{12}C+\alpha$ system—resonances that have been amenable to careful study.[44]

A more complicated case is the reaction $^{28}Si(\gamma,p)^{27}Al$, which is the first reaction to occur whenever ^{28}Si is heated. The study of the inverse reaction $^{27}Al(p,\gamma)^{28}Si$ at energies near $E_0=1680$ keV and above is possible in the laboratory. The corresponding cross section has a great deal of resonant structure, as shown by thin target yield curves[45] in Figure 14. Such yields raise an interesting experimental point for radiative capture reactions in nuclear astrophysics. What is required is the sum of radiative capture to all levels of the final nucleus, so it is not sufficient to

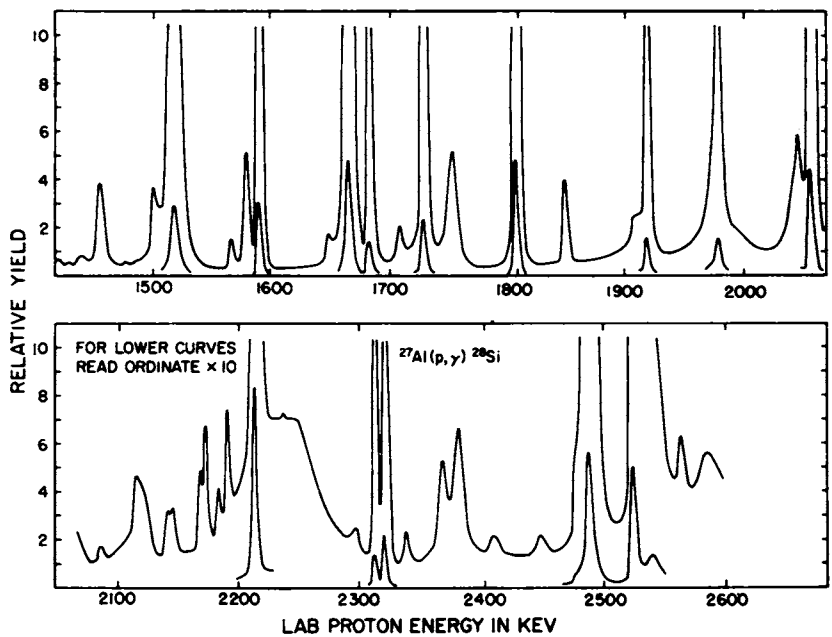

FIGURE 14. Relative yield of resonances observed[45] in the $^{27}Al(p,\gamma)^{28}Si$ reaction. The contribution of each resonance to $\langle\sigma v\rangle$ is proportional to the contribution of that state to the rate of photodisintegration of ^{28}Si at the same temperature.

measure the yield by the intensity of gamma radiation to a selected level. It is not necessary, in cases like this one, to extract the gamma-ray cascade scheme at each bombarding energy. The relevant yield is that measured by a gamma-ray spectrometer which sums the gamma energies in the cascade—a total-energy spectrometer. Such spectrometers have, for example, been used at Oak Ridge National Laboratory in their studies of radiative neutron capture.[46] The combined effect of the resonances like those in Figure 14 is obtained by the sum, weighted by the Maxwellian distribution, of the area beneath the capture yield curve. Careful attention to target thickness allows the summation to be made automatically over a selected energy region. The continuous nonresonant capture must be considered as well, because it may have greater area than the resonances. Figure 15 shows the nonresonant capture cross section extracted from the total yield measurements of Figure 14. This contribution too must be numerically integrated to determine its contribution to $\langle \sigma v \rangle$.

The highest thermonuclear temperatures of interest occur when matter at such high temperature and density that all nuclei have been broken down into nucleons is quickly expanded and cooled. A highly varied reaction chain occurs at temperatures $1 < T_9 < 10$ by which nucleons are reassembled into nuclei. The so-called "explosive nucleosynthesis" in

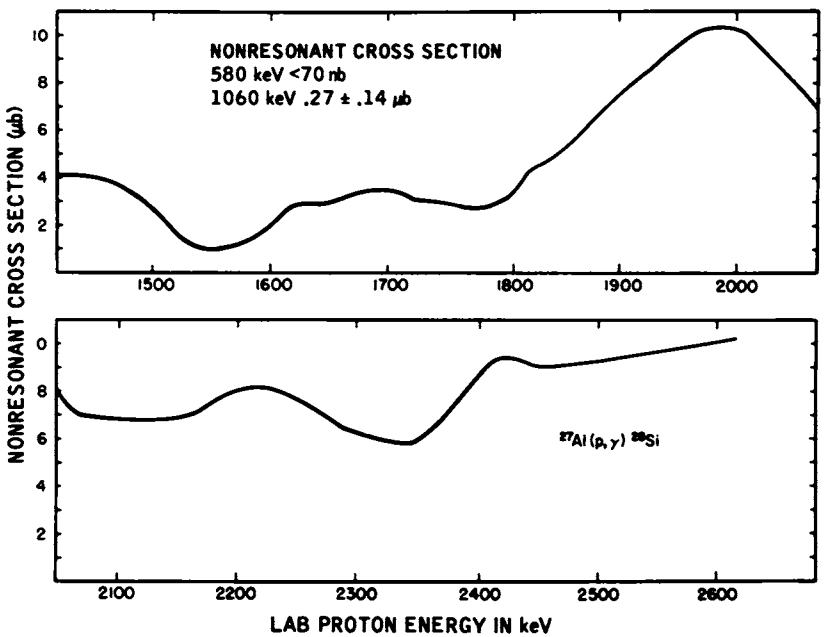

FIGURE 15. The nonresonant cross section[45] for the $^{27}Al(p,\gamma)^{28}Si$ reaction.

"big and little bangs" involves almost all reactions between the light nuclei and protons, neutrons, alpha particles, and gamma rays.[47] Two examples were listed in Table 1.

Neutron Reactions

The primary distinguishing feature of neutron-induced thermonuclear reactions is the absence of a Coulomb barrier in the entrance channel. Neutron cross sections are accordingly most important near the peak of the thermal distribution; $E_n \approx kT = 86T_9$ keV. In stars, the temperatures for which detailed knowledge of the neutron cross sections is important are roughly $0.2 < T_9 < 4$, and in explosions from very high temperature (big and little bangs) up to $T_9 = 10$.

The most extensive applications made so far have been to the theory of the nucleosynthesis of heavy elements by chains of radiative neutron captures. Thermonuclear fusion of charged particles synthesizes nuclei only up to the abundance peak near $A = 56$, whereas a sequence of (n,γ) reactions can build the heaviest known elements provided that an adequate thermonuclear neutron source exists. Accurate values of thermally averaged (n,γ) cross sections are important tests of our understanding of these processes.[48]

In dealing with thermally averaged neutron-capture cross sections it has become conventional to define an average cross section $\langle\sigma(kT)\rangle$, which has the property that its product with the most probable thermal velocity $v_T = (2kT/M)^{\frac{1}{2}}$ equals $\langle\sigma v\rangle$:

$$\langle\sigma(kT)\rangle \equiv \frac{\langle\sigma v\rangle_T}{v_T} = \frac{1}{v_T}\int_0^\infty \sigma(v) v \varphi(v,T)\, dv. \qquad (18)$$

This effective neutron cross section depends upon the temperature, and it is the laboratory task to obtain sufficient data to calculate $\langle\sigma\rangle$ for each temperature. For most heavy nuclei of interest, one requires knowledge of the cross section from zero energy up to several hundred keV, with the range $1 < E_n$ (keV) < 100 of greatest interest, whereas for light-element neutron reactions in explosive nucleosynthesis, the cross section is of interest up to about 3 MeV of neutron energy. Note that to determine $\langle\sigma\rangle$ it is not necessary to have particularly high-energy resolution in the measurement of σ.

The neutron cross sections may involve either resonances or a nonresonant continuum, depending upon the nucleus involved. The cross sections for the light elements participating in high-temperature explosive nucleosynthesis require study of individual resonances in the hundreds

TABLE 2 Light-Element Neutron Resonances of Importance to Explosive Nucleosynthesis

REACTION	Q (MeV)	RESONANCES E_r(cm,keV),J^π	REACTION	Q (MeV)	RESONANCES E_r(cm,keV),J^π
^{6}Li(n,γ)^{7}Li	7.253	222, $\frac{5}{2}^-$	^{13}C(n,γ)^{14}C	8.176	147, 1^+ or 2^+
^{9}Be(n,γ)^{10}Be	6.815	562, 3^- 733, 2^+	^{14}N(n,γ)^{15}N	10.835	470, 600,
^{10}B(n,γ)^{11}B	11.456	220, $\frac{5}{2}^+$ or $\frac{7}{2}^+$ 490, $\frac{3}{2}^-$ or $\frac{5}{2}^+$	^{16}O(n,γ)^{17}O	4.143	409, $\frac{3}{2}^-$
^{11}B(n,γ)^{12}B	3.369	18, $\leq 3^+$ 390, 2^+	^{17}O(n,γ)^{18}O	8.046	160, 2^+ 233, 3^-
^{12}C(n,γ)^{13}C	4.947	560 ?	^{18}O(n,γ)^{19}O	3.956	150,
^{7}Be(n,α)^{4}He	18.991	~ 0, 2^- 150, 3? 320, 3^+	^{20}Ne(n,γ)^{21}Ne	6.760	540,
			^{17}O(n,α)^{14}C	1.819	160, 2^+ 233, 3^-

of keV region. In Table 2 we have listed several of the more important of these, although we do not wish to imply that interest is limited to only the resonances shown there. The possibility of nucleosynthesis in supermassive stars in the early life of the Galaxy depends in part on the measurement of such resonant cross sections. For atomic weights $A>20$, many resonances become important, and their identification and study is a formidable long-range task for neutron physicists. Near the closed neutron shells, moreover, the study of individual resonances is required even in heavier nuclei. The measurements for one such example, ^{51}V with $N=28$, are shown in Figure 16, where the points are cross-section measurements and the arrows across the top locate the energies of known resonances (from total cross-section measurements). Very-low-energy resonances must be detected, because the contribution of a single narrow resonance to the thermal average

$$\langle\sigma\rangle_{\text{res}} = \frac{2\pi^{\frac{3}{2}}\hbar^2}{(kT)^2M}\frac{\omega\Gamma_\gamma\Gamma_n}{\Gamma}\exp\left(-\frac{E_r}{kT}\right) \qquad (19)$$

is greatest for $E_r<kT$. Since usually $\Gamma\approx\Gamma_n$ one needs both E_r and $\omega\Gamma_\gamma$ to evaluate the contribution of the resonance. Shown as a solid curve in Figure 16 is the thermal average $\langle\sigma\rangle$, for ^{51}V(n,γ) as calculated from the measured cross section and the known resonances. For a nucleus of this type, $\langle\sigma(kT)\rangle$ is not well estimated by the measurement of the cross sec-

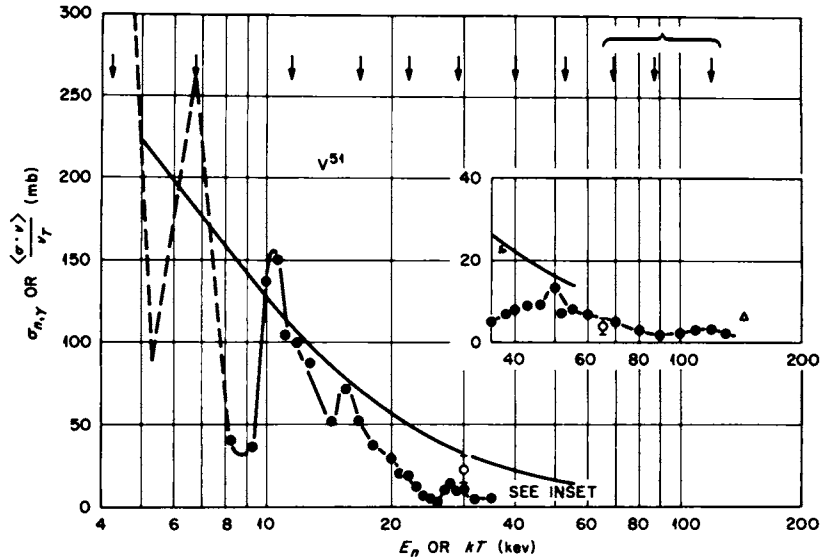

FIGURE 16. Neutron-capture cross section of the neutron-magic nucleus ^{51}V. The connected points represent measured values $\sigma(E_n)$ and the arrows across the top show the positions of neutron resonances known from total cross section.[48] The smoothly falling solid curve represents the value of $\langle\sigma(kT)\rangle$ as a function of kT. For nuclei such as this one individual resonances dominate the cross section and one finds that $\langle\sigma(kT)\rangle$ is not well estimated by a measurement near $E_n = kT$.

tion at a single energy near $E_n = kT$, and the associated problems are the hardest of those in neutron astrophysics. Judicious use must be made of the fact that the energy spread in the neutron beam with which the measurements are being made already averages the cross section over a limited energy region. A total-energy gamma-ray spectrometer is almost a necessity to avoid the tedious unraveling of cascade schemes.

Most of the nonmagic heavy nuclei have neutron resonance spacings less than a few keV. Data are now available for most heavy *elements,* but isotope cross sections still require extensive studies. The characterization of the (n,γ) cross section of heavy nonmagic nuclei is most conveniently made in terms of the average behavior of resonances—*s*-wave and *p*-wave strength functions, Porter-Thomas distributions, and the ratio of radiative width to level spacing. When measured capture cross sections have been fitted with four main parameters (Γ_γ, D, S^0, S^1) the thermal average $\langle\sigma\rangle$ can be calculated in terms of those same parameters. For example the excitation curve for ^{181}Ta(n,γ) is shown in Figure 17. Because the cross section is smoothly decreasing between 1 keV and 100 keV, it happens that $\langle\sigma(kT)\rangle \simeq \sigma(E_n = kT)$. Thus for nuclei of this

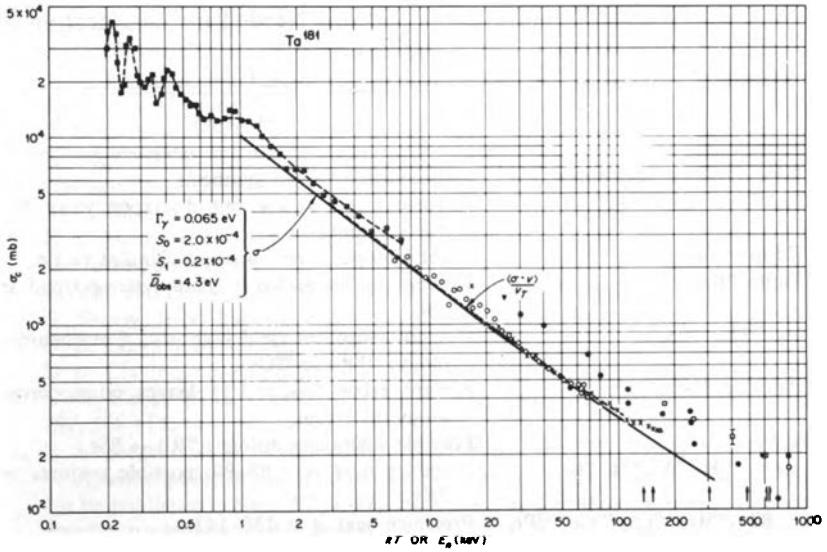

FIGURE 17. The neutron-capture cross section of ^{181}Ta. The points are measurements[48] of $\sigma(E_n)$, whereas the solid curve is a fit of $\sigma(E_n)$ made with the average resonance parameters and strength functions shown on the figure. The dashed curve overlying the solid one shows the value of $\langle\sigma(kT)\rangle$ as a function of kT. For nuclei like this one, many broad overlapping resonances dominate the cross section and one finds that $\langle\sigma(kT)\rangle$ is well estimated by a measurement near $E_n = kT$.

type the value of $\langle\sigma\rangle$ is well estimated by a measurement of the cross section at $E_n = kT$. Further experimental and theoretical studies of the best techniques for determining $\langle\sigma\rangle$ for heavy nuclei are needed. In some cases accuracy of a few percent in $\langle\sigma\rangle$, or more properly in ratios of two $\langle\sigma\rangle$'s, is needed to test the accuracy of the astrophysical theory to its limit. Macklin and Gibbons[49] have summarized nicely the experimental status of the theory. The questions here are of extraordinary importance, because if the theory is correct it can be used to measure the time of the origin of the elements,[50] a cosmological datum of the first rank.

The experimental problems are probably somewhat more demanding than those of charged-particle nuclear astrophysics. The challenge is to develop a collimated neutron beam capable of fair energy resolution between 1 keV and 100 keV for heavy-nucleus radiative capture and to develop precise counting techniques for the smallest possible samples. Such a program is, moreover, in direct competition with the functioning program at Oak Ridge National Laboratory (ORNL). Competition is undeniably healthy, but the individual researcher must estimate his

TABLE 3 Neutron Capture Cross Sections Needed for Clarification of *s*-Process

NUCLEI	REMARKS
All Fe, Co, Ni, Cu isotopes	Required for Cu–Ni synthesis.
^{70}Ge, ^{72}Ge, ^{73}Ge, ^{74}Ge	Reverse trend in σN but discrepancy in ^{74}Ge measurements.
^{106}Cd to ^{116}Cd	Eight isotopes, five *s*-process. Similar to tin.
^{130}Ba to ^{138}Ba	Current *estimates* for σ yield reverse trend in σN.
^{186}Os, ^{187}Os, ^{188}Os	Current estimates yield high σN. Cosmochronology: $^{187}\text{Re} \rightarrow {}^{187}\text{Os}$.
^{208}Pb, ^{207}Pb, ^{206}Pb, ^{204}Pb	Present error ($\sigma_{208} = 3^{+1}_{-2}$) leaves cosmochronology uncertain.
^{86}Sr, ^{87}Sr	Possible cosmochronology: $^{87}\text{Rb} \rightarrow {}^{87}\text{Sr}$.
$N = 50$: ^{88}Sr, ^{89}Y, ^{90}Zr, ^{86}Kr	Precipice near $A = 88$–90; possible *s*-source of ^{86}Kr.
$N = 82$: ^{138}Ba, ^{139}La, ^{140}Ce, ^{141}Pr, ^{142}Nd	Precipice near $A = 138$–142.
All shielded *s* nuclei	σN, curve, element abundances.

laboratory resources carefully to ascertain whether he can compete effectively. The ORNL uses a 3-MV pulsed proton beam on a ^{7}Li target as a neutron source, time-of-flight counting techniques to select the neutron energy whose capture is observed, and a variety of total-energy gamma-ray spectrometers to separate the desired counts from the background.[51]

We do not list here the many neutron-capture reactions needed in the 1–100 keV region, for the list is too long. Quantitatively the most significant applications are to nucleosynthesis by chains of slow neutron captures—the so-called "*s*-process." The papers[52] on this process delineate the capture chain of interest for $A > 56$ and cite several (n,γ) cross sections as being of special interest, some of which are listed in Table 3. Every nucleus on the *s*-process chain can usefully be measured, but the most important measurements are those of neutron-magic nuclei and nuclei shielded from *r*-process production. Below $A = 56$, measurements of the (n,γ) cross sections of the isotopes of Si, S, Ar, Ca, Ti, and Cr are needed to ascertain the extent to which their neutron-rich isotopes have resulted from a *s*-process on the $A = 4n$ seed.[39]

REFERENCES

1. D. D. Clayton, *Principles of Stellar Evolution and Nucleosynthesis* (McGraw-Hill Book Co., Inc., New York, 1968).

2. B. S. P. Shen, ed., *High Energy Nuclear Reactions in Astrophysics* (W. A. Benjamin, Inc., New York, 1967).
3. D. D. Clayton, *op. cit.*, p. 303.
4. D. F. Hebbard and J. L. Vogl, Nucl. Phys. *21*, 652 (1960). For additional details see reference 22.
5. D. D. Clayton, Phys. Rev. *128*, 2254 (1962).
6. A. McKellar in *Stellar Atmospheres*, J. L. Greenstein, ed., (University of Chicago Press, Chicago, 1960), pp. 569–584.
7. A. D. Bacher and T. A. Tombrello, *Phys. Rev.* (to be published).
8. H. C. Winkler and M. R. Dwarakanath, Bull. Amer. Phys. Soc. *12*, 16 (1967) and to be published.
9. R. May and D. D. Clayton, Astrophys. J. *153*, 855 (1968).
10. G. Shaviv, J. N. Bahcall, and W. A. Fowler, Astrophys. J. *150*, 725 (1967).
11. D. D. Clayton, *op. cit.*, Chapters 5 and 7.
12. D. D. Clayton, *op. cit.*, p. 352.
13. C. W. Cook, W. A. Fowler, C. C. Lauritsen, and T. L. Lauritsen, Phys. Rev. *107*, 508 (1957).
14. P. A. Seeger and R. W. Kavanagh, Nucl. Phys. *46*, 577 (1963).
15. F. Ajzenberg-Selove and T. Lauritsen, "Energy-Levels of Light Nuclei VII" (to be published); Nucl. Phys. *11*, 1 (1959), *78*, 1 (1966). For data on more massive nuclei the reader should consult P. M. Endt and C. Van der Leun, Nucl. Phys. *34*, 1 (1962), *A105*, 1 (1967); C. M. Lederer, J. M. Hollander, and I. Perlman, *Table of Isotopes*, 6th ed. (John Wiley & Sons, Inc., New York, 1967); *Nuclear Data Sheets 1959–1965* (Academic Press, New York, 1966); *Landolt-Börnstein Energy Levels of Nuclei: $A = 5$ to $A = 257$*, K. Hellwege, ed. (Springer-Verlag, Berlin, 1961).
16. R. F. Christy and I. Duck, Nucl. Phys. *24*, 89 (1961).
17. D. C. Hensley, Astrophys. J. *147*, 818 (1967).
18. D. E. Alburger and E. K. Warburton, Phys. Rev. *152*, 914 (1966).
19. W. P. Bidelman, Astrophys. J. *117*, 25 (1953); G. Wallerstein, T. F. Greene, and L. J. Tomley, Astrophys. J. *150*, 245 (1967).
20. R. Davis, Jr., D. S. Harmer, and K. C. Hoffman, Phys. Rev. Lett. *20*, 1205 (1968).
21. T. A. Tombrello, "Astrophysical Problems," in *Nuclear Research with Low-Energy Accelerators*, J. B. Marion and D. M. VanPatter, eds. (Academic Press Inc., New York, 1967).
22. W. A. Fowler, G. R. Caughlan, and B. A. Zimmerman, Ann. Rev. Astron. Astrophys. *5*, 525 (1967) is the latest summary of thermonuclear reaction rates involving charged particles.
23. J. N. Bahcall, N. A. Bahcall, and G. Shaviv, Phys. Rev. Lett. *20*, 1209 (1968).
24. P. D. Parker and R. W. Kavanagh, Phys Rev. *131*, 2578 (1963).
25. K. Nagatani, D. Ashery, and M. R. Dwarakanath (to be published).
26. P. D. Parker, Phys. Rev. *150*, 851 (1966).
27. F. J. Vaughn, R. A. Chalmers, D. A. Kohler, and L. F. Chase, Jr., Bull. Amer. Phys. Soc. *12*, 1177 (1967) and private communication.
28. R. W. Kavanagh, Nucl. Phys. *15*, 411 (1960).
29. W. L. Imhof, R. G. Johnson, F. J. Vaughn, and M. Walt, Phys. Rev. *114*, 1037 (1959).
30. T. A. Tombrello, Nucl. Phys. *71*, 459 (1965).
31. R. E. Brown, Phys. Rev. *125*, 347 (1962).
32. J. B. Marion and W. A. Fowler, Astrophys. J. *125*, 221 (1957).

33. S. Hinds, H. Marchant, and R. Middleton, Nucl. Phys. *51*, 427 (1964).
34. P. M. Endt and C. Van der Leun, Nucl. Phys. *A105*, 1 (1967).
35. H. M. Loebenstein, D. W. Mingay, H. Winkler, and C. S. Zaidins, Nucl. Phys. *A91*, 481 (1967).
36. W. Deinzer and E. E. Salpeter, Astrophys. J. *140*, 499 (1964).
37. W. D. Arnett and J. W. Truran, Astrophys. J. (to be published).
38. J. R. Patterson, H. C. Winkler, and C. S. Zaidins, Astrophys. J. (to be published).
39. D. Bodansky, D. D. Clayton, and W. A. Fowler, Astrophys. J. Suppl. No. 148 (1968).
40. J. W. Truran, A. G. W. Cameron, and A. Gilbert, Can. J. Phys. *44*, 563 (1966).
41. T. Ericson and T. Mayer-Kuckuk, Ann. Rev. Nucl. Sci. *16*, 183 (1966).
42. F. K. McGowan, P. H. Stelson, and W. G. Smith, Phys. Rev. *133*, B907 (1964).
43. J. W. Truran, C. J. Hansen, A. G. W. Cameron, and A. Gilbert, Can. J. Phys. *44*, 151 (1966) discusses the statistical approach to thermonuclear reactions and has a good bibliography to source papers.
44. J. D. Larsen and R. H. Spear, Nucl. Phys. *56*, 497 (1964).
45. P. Lyons, J. Toevs, and D. G. Sargood (to be published).
46. R. L. Macklin, J. H. Gibbons, and T. Inada, Nucl. Phys. *43*, 353 (1963).
47. R. V. Wagoner, W. A. Fowler, and F. Hoyle, Astrophys. J. *148*, 3 (1967); R. V. Wagoner, "Synthesis of Elements Within Exploding Objects," Astrophys. J. (to be published).
48. The reader is referred to these papers and references therein: R. L. Macklin and J. H. Gibbons, "Neutron Capture Data at Stellar Temperatures," Rev. Mod. Phys. *37*, 166 (1965); G. I. Bell, "Cross Sections for Nucleosynthesis in Bombs and Stars," Rev. Mod. Phys, *39*, 59 (1967); W. A. Fowler, "The Role of Neutrons in Astrophysical Phenomena," in Proceedings of Conference on Neutron Cross Sections and Technology, Washington, D.C., 1968.
49. R. L. Macklin and J. H. Gibbons, Astrophys. J. *149*, 577 (1967).
50. D. D. Clayton, Astrophys. J. *139*, 637 (1964).
51. See R. L. Macklin and J. H. Gibbons, Phys. Rev. *159*, 1007 (1967) and references therein for their laboratory setup.
52. E. M. Burbidge, G. R. Burbidge, W. A. Fowler, and F. Hoyle, Rev. Mod. Phys. *29*, 547 (1957); D. D. Clayton, W. A. Fowler, T. E. Hull, and B. A. Zimmerman, Ann. Phys. *12*, 133 (1961); P. A. Seeger, W. A. Fowler, and D. D. Clayton, Astrophys. J. Suppl. No. 97, *11*, 121 (1965).

CHAPTER 2

Practical Considerations in Experimental Nuclear Astrophysics

This chapter is intended as an introduction for someone entering the field of experimental nuclear astrophysics for the first time and attempts to point out the important experimental problems and practical considerations. It is not intended to be a complete or definitive encyclopedia on the hardware and instrumentation related to nuclear astrophysics. This chapter contains much information which is relevant to general nuclear physics because nuclear astrophysics is to a large extent just nuclear physics applied to the interesting problems of astrophysics. However, because of the nature of these astrophysical problems there are many special requirements and considerations in experimental nuclear astrophysics (such as the need for total, absolute cross-section measurements at energies far below the Coulomb barrier) which are not encountered in ordinary nuclear physics. Throughout the following discussion (beginning with the accelerator ion source and continuing through the beam-analysis system, targets, detectors, and the like), we have tried to emphasize the sources and solutions for those problems and considerations that are peculiar to this field. (If it seems that we have devoted an inordinate amount of space to the problems of gamma-ray detectors, this is because of the importance of both resonant and nonresonant capture reactions in nuclear astrophysics and because of the inherent difficulties in determining quantitatively the spectrum of these capture gamma rays from the complicated response characteristics of gamma-ray detectors.)

Ion Sources

In addition to the traditional radio-frequency (rf) and duoplasmatron ion sources that have been faithfully producing beams of protons, deuterons,

^{3}He, and ^{4}He for several decades, several new sources are now available which make it possible to generate beams of almost every ion. It is true that proton and alpha-particle beams are of the greatest direct importance in experimental nuclear astrophysics, yet many relevant studies can be made with deuteron, triton, ^{3}He, and heavy-ion beams.

The traditional ion sources are already capable of producing triton beams, but the use of tritium gas requires that many added precautions be taken to prevent unnecessary exposure of personnel and contamination of the laboratory. A few laboratories (e.g., Brookhaven, Lockheed Palo Alto, Los Alamos, and Chalk River in Canada) are now operating low-energy accelerators with triton beams, and a good description of the instrumentation necessitated by this use of tritium gas in an ion source is given by Chase.[1]

Moving up the periodic table, lithium beams would be very useful for the study of alpha-transfer reactions via (^{6}Li,d) and (^{7}Li,t) reactions,[2] and the techniques for producing these beams have already been developed by Allison and Kamegai[3] and by Carlson.[4] Carlson notes that he has been able to obtain Li^{3+} beams at energies of up to 14.5 MeV from a CN Van de Graaff accelerator by using a stripper foil part way down the accelerator tube. The astrophysically interesting beams of carbon, nitrogen, and oxygen can be extracted from standard duoplasmatron and rf ion sources by using gases such as CO_2 and N_2O.

With the development of compact heavy-ion sources,[5] which include sublimation furnaces capable of temperatures in excess of 1100°C for handling solid materials, it is now apparently possible to produce beams of virtually any element with intensities of several microamperes. Originally designed for use with isotope separators, these heavy-ion sources are now also being marketed commercially for use as ion sources for particle accelerators. (Danfysik Model 910 marketed in the U.S.A. by Physicon, Boston, Massachusetts, for example.) However, the power requirements for the present design (1200 to 2400 W) are too large to make these sources feasible for installation in the terminals of standard Van de Graaff accelerators.

Beam-Energy Analysis

In almost all nuclear astrophysics experiments, once a beam of the appropriate ions has been extracted from the accelerator, it is very important to determine accurately both the centroid and the width of the energy distribution of these ions. Accurate measurements of these quantities are necessary because of the importance of locating and measuring the posi-

tions and properties of narrow resonances and because of the effects of the Coulomb barrier on the cross sections for charged-particle reactions. For example, in studying the reaction $^{14}N(a,\gamma)^{18}F$ a change in the bombarding energy of 1 percent, from 1000 keV to 990 keV, would cause a 15 percent reduction in the nonresonant direct-capture cross section. Although time-of-flight techniques have been used, the most usual ways for accomplishing this energy or momentum analysis of the accelerated beam are by means of magnetic or electrostatic deflection.

In a magnetic analyzer, the beam travels along a circular orbit whose radius of curvature is determined by the energy, charge, and mass of the particles and the strength of the magnetic field. The strength of the magnetic field can be measured by instruments such as rotating-coil or torque-balance fluxmeters and nuclear-magnetic-resonance probes. In the latter case, the energy of the particles deflected along a particular orbit is given by

$$E=kf^2\left(\frac{Q^2}{m}\right)\left(1+\frac{E}{2mc^2}\right)^{-1}, \tag{1}$$

where k is a "constant," characteristic of the particular magnet, and includes all the geometrical factors concerned with the particular orbit in question, including any field nonuniformities along that orbit; f is the NMR frequency; Q is the charge of the ion; m is the rest mass of the ion; and E is its relativistic kinetic energy. In many cases the nonrelativistic expression, $E\approx kf^2Q^2/m$, can be substituted into the relativistic correction term, $(1+E/2mc^2)^{-1}$.

In an electrostatic analyzer,[6,7] the beam is passed between two "parallel" electrodes, each of which has a radius of curvature (r_1 and r_2) such that they have a constant separation, d,

$$r_2=r_1+d. \tag{2}$$

An ion which passes through the center of such an electrode system, as defined by entrance and exit slits, has an energy given by

$$E=Q\frac{Vr}{2d}\left(1+\frac{d^2}{24r^2}\right)^{-1}\left(1+\frac{E}{mc^2}\right)\left(1+\frac{E}{2mc^2}\right)^{-1}, \tag{3}$$

where Q is the charge of the ion; V is the potential difference between the two electrodes; d is the separation between the two electrodes; r is the mean radius of curvature of the electrodes, $(r_1r_2)^{\frac{1}{2}}$; m is the rest mass of the ion; and E is its relativistic kinetic energy. In many cases the nonrelativistic expression, $E\approx QVr/2d$, can be substituted into the two relativistic correction terms. Since the deflection of an electrostatic analyzer is to first order independent of the mass of the particles in the beam, it is necessary to supplement its operation with some sort of mag-

netic deflection in order to separate out the various mass components in the beam with the same energy, e.g., H^+, H_2^+, and possible heavy contaminants such as N_2^+.

Each of these instruments has its own advantages and disadvantages. For example, while it is much easier to make absolute energy measurements using a carefully constructed electrostatic analyzer, the problems of voltage conditioning of the plates and secondary emission caused by particles striking the plates make the electrostatic analyzer (compared with the magnetic analyzer) slightly less convenient for general use and considerably less desirable for handling the large beam currents which are often necessary for nuclear astrophysics experiments because of the small cross sections being measured. The calibration of these analyzers need not be carried out in an absolute manner but can be accomplished by using field or voltage measurements relative to a set of independently determined referenced energies such as narrow resonances or neutron thresholds.[8]

Vacuum Requirements

In addition to the normal vacuum requirements for accelerator operation, many experiments in nuclear astrophysics require special precautions to prevent the deposition of any carbon onto the target surface from organic compounds in the vacuum system, e.g., pump oil, O-rings, and vacuum grease. Such a buildup not only degrades the energy of the incident beam before it can strike the "true" target surface but also introduces an additional spread in the beam energy due to straggling. Both of these effects are important in view of the requirements noted above for an accurate determination of the energy distribution of the beam, and corrections for these effects must be made in analyzing the data.

The prevention of the buildup of carbon on the target is particularly important for studies involving (α,γ) reactions since the ^{13}C component in natural carbon will give rise to very serious background contributions via the neutrons resulting from the $^{13}C(\alpha,n)^{16}O$ reaction. How serious a problem the $^{13}C(\alpha,n)^{16}O$ reaction represents clearly depends on the particular reaction being studied, but a rough estimate of its effects can be obtained from a comparison of the cross sections involved. Whereas (α,γ) reactions may typically have total cross sections ranging from 0.1 to 5.0 μb at alpha-particle energies from 0.5 to a few MeV, the total cross section for the $^{13}C(\alpha,n)^{16}O$ reaction rises from $\sim$1 mb at 1 MeV to typically 50 mb for alpha-particle energies above 1.8 MeV.[9] This is

$\sim 10^4$ times greater than the (α,γ) cross sections one is trying to measure so that (even though ^{13}C has only a 1.1 percent abundance in natural carbon) atom for atom any "natural" carbon contamination will produce ~ 100 times more neutrons than the target material will produce gamma rays. [For additional information on the $^{13}C(\alpha,n)^{16}O$ reaction at energies below 1 MeV see Davids,[10] and for information at alpha-particle energies above 5 to 6 MeV, where the various $^{13}C(\alpha,n\gamma)^{16}O$ reactions become possible, see Spear *et al.*[11]]

Some of the precautions that can be taken to minimize carbon buildup include (a) liquid nitrogen trapping of all oil diffusion pumps or the use of ion pumps, (b) the use of molecular-sieve traps on roughing lines to prevent the backstreaming of oil from roughing pumps, (c) the use of an all metal and glass system with metal gaskets, low-vapor-pressure epoxies (e.g., "Torr Seal," Varian Associates, Palo Alto, California) or at least viton O-rings so that the entire system can be baked out, (d) the use of liquid nitrogen trapping in the beam line immediately in front of the target and in the region surrounding the target, (e) heating the target relative to its surroundings, (f) *no* vacuum grease, etc. For an example of a system employing many of these precautions see Spear *et al.*[11]

One way to bypass the problem of the neutron backgrounds from reactions such as $^{13}C(\alpha,n)^{16}O$ involves the use of a pulsed beam and time-of-flight techniques to discriminate between the prompt gamma rays from the target and the neutron induced background.[12]

TARGETS

Today, a very wide variety of target nuclei are available to the experimental nuclear physicist in isotopically enriched forms. Many of the more common isotopes, such as the carbon, nitrogen, and oxygen isotopes, are available in enriched forms from various commercial establishments. Of the remaining isotopes, which are not available commercially, virtually *all* of the stable, nongaseous isotopes are now available in an enriched form from Oak Ridge National Laboratory. There are only a few exceptions to this, such as ^{181}Ta, where the natural abundance is already 99.9877%. (^{180}Ta, the other stable tantalum isotope, is available in enrichments of up to 5.1%.) All the noncommercial, stable, gaseous isotopes (except some of the rarer xenon and krypton isotopes) are available in enriched forms from Mound Laboratory, operated for the AEC by Monsanto in Miamisburg, Ohio. Listings of the available isotopes, together with their enrichments, chemical forms, and prices, can

be obtained from Isotopes Sales, ORNL, Oak Ridge, Tennessee, and Isotopes Sales, Monsanto Research Corporation, Mound Laboratory, Miamisburg, Ohio.

[Concerning this essentially complete availability of enriched isotopes, it should also be noted that these materials do come with price tags. While these prices may be as low as a few dollars per gram for some of the more common isotopes (e.g., ^{7}Li enriched from 92.5% to 99.99% is only \$1/g, and ^{10}B enriched from 19.6% to 92% is only \$7/g), these figures can also become "astronomical" as in the case of ^{180}Ta enriched from 0.0123% to 5.1% at \$1175/mg. Most of the isotopes, of course, lie in the middle ground and generally are available at prices of approximately a few dollars per milligram for enrichments in the range of 90 to 99%. It should also be noted that some of the very high-priced isotopes are available through Isotopes Sales, ORNL, on a rental basis.]

The conversion of the target material into usable targets is accomplished by a variety of chemical techniques. This is not the place to even attempt to compile a list of these procedures; we will note below only some of the alternatives available. Many elements can be made into self-supporting targets by evaporating the material onto a substrate such as NaCl or Teepol and subsequently floating off and mounting the target by dissolving the substrate in water. For targets where this is not feasible, it is often possible to evaporate the material directly onto a very thin, previously mounted carbon foil (available in thicknesses down to 10 μg/cm^2 from Yissum Research Development Company, Hebrew University, Jerusalem, Israel). Also, the possibility of using thick targets or targets on heavy backings should not be ignored, especially at low energies where the Coulomb barrier will inhibit any competing reactions in the backing. Some general surveys of target making techniques are presented elsewhere.[13–18]

In addition to solid targets, as discussed above, it is also often possible to use gas targets. Compared to solid targets, gas targets have many advantages, such as chemical purity, which often make them desirable not only for noble gases but also for other gaseous elements and compounds. (It should also be noted that one can make "solid" noble-gas targets by ion implantation into a metallic backing. These targets may be quite satisfactory for some applications, but they generally tend to be nonuniform and very susceptible to gas loss due to beam-induced heating of the metallic backing.) With regard to gas targets, two major options are available: differential-pumping techniques or containing the gas within a cell with ultrathin foil windows.

In the case of differentially pumped gas targets, a number of descriptions have been published in the literature, e.g., Silverstein *et al.*[19] and

Winkler and Dwarakanath.[20] In the latter case, by using the first pumping stage as the backing pump for the diffusion pump in the second stage and then recirculating the output of the first stage through a repurifier back to the gas target, it was possible to keep gas losses down to less than 1 percent per 24 h. This has obvious application to the use of rare or expensive gases (such as the ^{3}He used in this case) in differentially pumped systems. Winkler[21] has also shown that it is possible to increase by 30 to 50 percent the maximum attainable gas-target pressure in a differentially pumped chamber by using a gas inlet in the form of a 45° cone-shaped opening located at the high-pressure end of the beam entrance canal and directed toward the gas target.

Whereas in the case of differentially pumped gas targets the maximum attainable pressures are typically in the range from 15 to 25 mm Hg, pressures as high as several atmospheres can be achieved for targets where the gas is contained by an entrance foil through which the incident beam must pass. As might be expected, the most critical part of such a target is the entrance foil. At low energies the most commonly used material for these foils is nickel; nickel foils with thicknesses as small as 2×10^{-6} in. (45 μg/cm^2) are available from Chromium Corporation of America, Waterbury, Connecticut. Of course, such a thin foil will not withstand a 1-atm pressure differential across even a $\frac{1}{8}$-in.-diameter aperture, but for thicknesses $\gtrsim 20\times10^{-6}$ in., a 1-atm pressure differential is easily supported across a $\frac{1}{8}$-in.-diameter aperture. A 20×10^{-6} in. foil (450 μg/cm^2) represents an energy loss of only 54 keV for a 1-MeV proton; however, for heavier projectiles this energy loss increases, and for 1 MeV ^{4}He's the energy loss is up to 380 keV. Discussions of the energy losses by charged particles are relevant not only to gas-target entrance foils but also to solid targets and even to the design and choice of detector specifications. Several useful tables and graphs of dE/dx, stopping cross sections, and particle ranges have been compiled for p, d, t, ^{3}He, and ^{4}He by Whaling and Demirlioglu[22] and Williamson *et al.*[23] An extension of this work to heavy ions has been presented by Northcliffe.[24]

In obtaining higher-pressure gas targets by the use of an entrance foil, a price is paid not only in the form of beam-energy degradation, but also in the form of (a) a deterioration in the beam-energy resolution due to straggling, (b) possible background effects due to reactions taking place in the foil, and (c) a limitation on the usable beam intensities. This latter limitation arises because the heating of the foil, due to the energy lost by the incident beam, weakens the foil and can cause it to rupture. Typically this limitation is $\sim$1.2 μA for 1-MeV protons and $\sim$0.2 μA for 1-MeV alpha particles, and for other particles and energies this

limit scales roughly as the inverse of the stopping cross section involved. One technique that can be used to alleviate this problem is the evaporation of a very thin layer of copper onto the nickel foil in order to increase its thermal conductivity. (For example, the addition of 70 $\mu g/cm^2$ of copper to a 450 $\mu g/cm^2$ nickel foil adds little in the way of energy loss but will double the thermal conductivity of the foil.)

Some of the other materials which are commonly used for entrance windows to gas targets include organic compounds, such as formvar and havar (a cobalt-base steel alloy manufactured by Hamilton Watch Company, Lancaster, Pennsylvania). Formvar-type foils are useful where a very small energy loss or straggle by the incident beam is particularly important, but because of their very poor thermal conductivity they are only practical for experiments involving very low beam intensities. Havar, because of its convenience, has found wide application in "high"-energy work, but for low-energy experiments (below 3 MeV) it is not nearly so suitable as nickel since its minimum available thickness, 90×10^{-6} in., represents a 225-keV energy loss for 1-MeV protons and stops alpha particles at energies $\lesssim$1.3 MeV.

Since it is important to know the energy of the beam *in* the gas cell, it is necessary to obtain an accurate measurement of the foil thickness and the energy lost in the foil by the incident projectile. The simplest and most direct way to accomplish this is to measure the position of a well-known resonance with and without the foil inserted in front of the target. This measures the energy loss in the foil directly, and by using Whaling's stopping cross sections[22] this loss can be scaled to any other incident energy for this same foil. Furthermore, if the calibration resonance is narrow, this measurement can also provide information regarding the straggling of the beam in the foil.

One of the desirable features of a gas target is the ease with which one can obtain the target thickness directly from a measurement of the gas temperature and gas pressure. Robertson *et al.*[25] have pointed out, however, that care should be taken in determining the gas temperature to take into account beam-heating effects in the gas which may raise the temperature along the beam path by as much as 50°C or more. While on the topic of target thickness determinations, some mention should also be made about ways for measuring thicknesses for solid targets. Some of the standard techniques for this include (a) (for targets mounted on thick, heavy backings) the use of a magnetic spectrometer at a back angle to measure the target profile,[26] (b) (for thin targets) the use of an "alpha gauge" to measure the energy loss of transmitted alpha particles,[27,28] (c) excitation function measurements across a narrow resonance (narrower than the target thickness), (d) a comparison with

a *reliable,* previously measured cross section, and (e) the comparison of a particular reaction yield in the uncalibrated target with the yield from that same reaction in a target whose thickness is known.

Finally, it should be added that all these endeavors need not be restricted to stable isotopes. There are many interesting and important measurements to be made with radioactive targets such as ^{7}Be, ^{10}Be, ^{14}C, ^{37}Ar, and ^{44}Ti, and a small laboratory with a strong radiochemistry background might well consider that the development of such a target could be as important a stimulus for the creation of an active research program as the acquisition of a lot of complicated and expensive hardware for use in studying more mundane nuclei.

Beam Integration

Since many of the problems in nuclear astrophysics require information in the form of absolute cross sections, it is necessary to have an accurate, *absolute* measurement of the number of incident particles corresponding to a given "run." This is normally obtained by simply integrating the incident beam current to obtain a measurement of the total charge accumulation. As in all nuclear physics experiments, in order that the measured beam current be accurate, precautions must be taken in the design of a properly shielded Faraday cage and in the use of magnets and electrostatic guard rings to ensure (a) that secondary electrons produced in the collimating slits and in the target do not enter the Faraday cup and (b) that secondary electrons produced in the Faraday cup do not escape. One way of checking on the effectiveness of secondary electron suppression is to compare the forward-angle elastic scattering from a heavy target nucleus at low energies with the calculated Rutherford cross section. This technique, of course, requires that the absolute target thickness already be known from an independent measurement, as described earlier. Once the accuracy of the charge collection has been established, however, this technique can then be turned around and used as an additional method for determining target thicknesses. A quantitative assessment of the ways in which the effects of secondary electrons can be exaggerated when using heavy-ion beams is presented by Loebenstein *et al.*[29] together with one way in which these problems can be handled successfully.

An additional problem, which arises especially at low energies, involves the question of the ionization state of the incident ion. The ionization state is initially well defined by the magnetic or electrostatic energy analysis, but after leaving the analyzer this charge state can change

during any collision in the target or during any collisions with residual gas molecules in the vacuum system—another good reason to work for as good a vacuum as possible. For example, for 4.0-MeV ^{16}O ions the equilibrium charge distribution is 3+ (11%), 4+ (40%), 5+ (40%), and 6+ (9%), while for 400-keV ^{4}He ions it is neutral (15%), 1+ (65%), and 2+ (20%). This problem can be important even for protons for which the equilibrium charge distribution does not get to 1+ (>99%) until proton energies are above 350 keV. For alpha particles one has to get over 2.5 MeV before the equilibrium charge distribution becomes 2+ (>99%). A compilation of equilibrium charge-state distributions as a function of energy has been prepared by Zaidins.[30] For cases where the charge changes occur in the target (target-in versus target-out changes in the apparent beam intensity) the most direct solution is simply to include the target as part of the Faraday cup system, though this will almost certainly require some additional shielding and secondary electron suppression. For cases where it is not possible to make an accurate or meaningful charge integration because of charge changing collisions before the beam enters the Faraday cup, Winkler and Dwarakanath[20] have devised a method for ignoring the charge of the incident beam and instead simply measuring the beam power using a balanced calorimeter. This method treats particles of all charge states equally, and when combined with an accurate energy determination it gives an accurate determination of the number of incident particles corresponding to a given "run."

Charged-Particle Detectors

During the past 10 years enormous advances have been made in the techniques and devices available for detecting and measuring the radiations produced in nuclear reactions. For charged particles,[31] silicon surface-barrier devices, Si(SB), are now available commercially in thicknesses from 6 μ (uniform to ± 0.5 μ) to 2000 μ, and lithium-drifted silicon devices, Si(Li), now extend this range from 2 mm to as much as 5 mm. The active surface areas for all but the thinnest of these detectors span the range from 25 mm^2 to several hundred mm^2 and even to 1000 mm^2 in some cases. As far as resolution is concerned, based on the 5.47-MeV alpha particles from ^{241}Am, Si(SB) detectors of all thicknesses are now available with dead layers (gold or aluminum surface contacts) of 30 to 40 $\mu g/cm^2$ (≈ 1 keV for 5-MeV protons and ≈ 7 keV for 5-MeV alpha particles) and with guaranteed resolutions (when used with suitable preamplifiers and amplifiers) in the range from 15 to

30 keV for active areas up to 150 mm². For larger areas, the increase in capacitance causes a deterioration in resolution to figures approaching 40 to 50 keV. For Si(Li) detectors the resolution figures begin at 35 to 50 keV for 2-mm devices with active areas of 50 to 100 mm² and go to 100 keV for 5-mm devices in this area range and even higher for larger areas. Dead-layer specifications for Si(Li) detectors are also somewhat higher, $\lesssim 1$ mg/cm², but this need not be too important since these devices are primarily intended for the very energetic particles that cannot be stopped in the thinner surface-barrier detectors. A discussion of the straggling effects of these dead layers on energy resolution is given by Fabri *et al.*[32]

The specifications for detector performance given above refer to the operation of the detectors at room temperature. Considerable improvements in the resolution can normally be obtained by cooling the detectors to temperatures between 0°C and −80°C using, for example, CO_2 expansion refrigerators, Freon coolant systems, or thermoelectric coolers. Operating under actual experimental conditions, one such system has achieved resolutions of 11.2-keV FWHM for 12-MeV protons using a 50-mm², 1500-μ-thick Si(SB) detector.[33] This reference is particularly useful as it also points out and examines a number of other precautions (such as magnetic suppression of secondary electrons from the target) which are essential in obtaining this high resolution.

It should be noted that in general Si(SB) and Si(Li) detectors do not compete but rather complement one another; i.e., the Si(Li) detectors, which give poorer resolution, offer a much larger depth for stopping high-energy particles with a single detector. Si(SB) detectors can also be used for measuring high-energy particles by stacking several transmission mounted detectors in tandem, but this results in a considerable increase in cost—~$700 for one 3-mm-deep, 80-mm² Si(Li) detector versus ~$2100 for an equivalent stack (two 1500-μ or 1000-μ plus 2000-μ) of 50-mm² Si(SB) detectors. [In spite of the contributions to peak width from each of the members of such an array, a 5-mm stack of Si(SB) detectors would still have better resolution ($\approx$50 keV uncooled) than the one Si(Li) detector. Thus for a case where resolution, not cost, is of ultimate importance this stacking technique might still be preferable.]

Prices for each of these detectors, Si(SB) and Si(Li), will run in the neighborhood of $1200 to $1600 for the very thin, very thick, or very large area models, dropping to $300 to $400 for the less demanding sizes. Regarding these high costs, in view of the present tight budget limitations, it is interesting to note that at least one detector manufacturer is talking about "detector rental plans."

Finally, it should be cautioned that these detectors do not last indefinitely but are subject to radiation damage resulting in an appreciable degradation in pulse shape and resolution presumably caused by carrier-trapping centers generated at actual damage sites in the crystal lattice. Generally, Si(Li) detectors are much more sensitive to this type of damage than are Si(SB) detectors. For example, for Si(Li) detectors significant deterioration appears to occur after exposures of $\approx 10^{10}$ fast neutrons/cm^2, whereas for Si(SB) detectors this figure is at least 100 times higher. There is still much black magic involved in the handling of this problem, but in general the application of increased bias levels to the detector (i.e., higher field strengths in the crystal) seems to restore its performance at least temporarily.

Neutron Detectors

For neutron detectors, the standard "Long Counter"[34] still provides a very important method for detecting fast neutrons of varying energies because of its more or less constant efficiency as a function of neutron energy. Because of this "constant" efficiency, when coupled to a pulsed-beam, time-of-flight system the Long Counter can provide detailed information about the energy spectrum in the neutron flux. Organic scintillators, e.g., Pilot-B, with their fast rise times are also well suited for accurate time-of-flight work. Slow or thermal neutrons can be detected selectively by taking advantage of the relatively large thermal cross sections and large positive Q-values for the ^{6}Li(n,α)^{3}H and ^{10}B(n,α)^{7}Li reactions by utilizing charged-particle sensitive scintillators doped with these isotopes, e.g., NE-401.

The development of semiconductor devices has also had its impact on neutron detectors. By sandwiching a thin ^{6}Li or ^{10}B layer between two Si(SB) detectors one can obtain neutron energy spectra by taking advantage of (a) the ^{6}Li(n,α)^{3}H and ^{10}B(n,α)^{7}Li reactions, (b) the energy response of the Si(SB) detectors to charged particles, and (c) the nearly 4π total collection efficiency of the sandwich geometry.[35] Because of the large positive Q-values for these reactions, this technique is not troubled by low-energy background events from photons and charged particles interacting with the detectors. Individual detector backgrounds can also be further reduced by utilizing coincidence requirements between the two Si(SB) sandwiching detectors.

A completely different fast neutron spectrometer is provided by making use of the (n,p) and (n,α) reactions in the silicon of the detector itself.[36,37] [Because of the importance of their larger volumes toward

increasing the efficiency of such a detector, Si(Li) devices are normally used for this work, but this has nothing to do with the nuclear properties of the lithium.] The Q-values for all of these Si + n reactions are negative, the most important being the $^{28}Si(n,\alpha_0)^{25}Mg$ reaction with a Q of -2.65 MeV. Miller and Kavanagh[37] have applied this technique successfully to neutrons with energies from 6 to 17 MeV. Using liquid nitrogen-cooled detectors they have been able to achieve neutron energy resolutions as good as 125 keV and have been able to determine the energies of various "unknown" neutron groups with a precision of 5 to 15 keV by comparisons with the detector's response to other neutron groups of "known" energy.

Gamma-Ray Detectors

In the field of gamma-ray spectroscopy, the work load is now shared between NaI(Tl) and Ge(Li) detectors. In spite of their poorer resolution, NaI(Tl) detectors still have an important advantage over the Ge(Li) detectors in terms of bulk size for applications where high efficiency is important or where high-energy gamma rays are involved.

NaI(Tl) crystals are now available commercially in diameters up to 15 in. with lengths of 12 in. and longer for prices of $30,000 and more. Typical intermediate-size detectors such as 3 in. × 3 in. (with better than 7 percent resolution for 662-keV gamma rays) or 5 in. × 5 in. ($\lesssim 7\frac{1}{2}$ percent resolution at 662 keV) come with price tags (including photomultiplier tube) of about $1000 and $2400 each. For Ge(Li) detectors, active volumes in the range 20 to 40 cc with resolutions better than 3 keV at 662 keV have prices in the neighborhood of $5000 to $7500, while the smaller detectors (4 to 8 cc) fall in the range from $2000 to $4000.

Having noted the quality and sizes that are presently avaliable for those two types of detectors, in order to make a more meaningful comparison of their performances it is necessary to first discuss their responses to monoenergetic photons. Gamma rays incident on either of these detectors will normally interact via photoelectric absorption, Compton scattering, or (for energies above 1022 keV) pair production. The relative probabilities of these interactions depend on the energy of the gamma ray. In the case of photoelectric absorption, the entire energy of the gamma ray is transferred to the photoejected electron, and if that electron stops in the crystal the resulting pulse will correspond to the full energy of the gamma ray. For a Compton scattering event, a full-energy pulse will result only if the Compton-scattered electron stops in

the crystal *and* the scattered gamma ray also deposits the rest of its energy in the crystal through a series of subsequent Compton scatterings and/or a photoelectric absorption. If the energy of the gamma ray is above the pair-production threshold ($2m_0c^2 = 1022$ keV), then it can also interact in the crystal to create an electron–positron pair. If the size of the crystal is sufficient, both members of the pair will stop in the crystal, and the positron will annihilate with an atomic electron to form two 511-keV gamma rays. A full-energy pulse will result from such an event only if both members of the pair are stopped in the crystal *and* if *both* of the subsequent annihilation quanta also interact via Compton scattering or photoelectric events to deposit all of their energy in the crystal. Because of the quantized energy of the 511-keV annihilation radiation, if one or both of these quanta escape from the crystal, the detector output pulse will correspond to the gamma-ray energy minus 511 keV or 1022 keV, respectively.

The response functions of NaI(Tl) and Ge(Li) detectors to a monochromatic gamma ray will include contributions from all these interactions, with peaks corresponding to the full photon energy and (for $E_\gamma > 1022$ keV) to the escape of one or two of the annihilation quanta, plus a broad continuum corresponding to interactions where the electrons do not stop in the crystal and to Compton events in which the scattered photon escapes. With such a complex spectrum, the advantages of good energy resolution are obvious, especially when the spectrum contains contributions from several gamma rays of differing energies. At the present state of technology, good NaI(Tl) crystals are available with resolutions at 662 keV of $\lesssim 7$ percent (46 keV), whereas good Ge(Li) detectors can be purchased commercially with resolutions of $\lesssim 3$ keV at 662 keV. As the gamma-ray energy increases, the NaI(Tl) resolution goes to ≈ 4 percent at 3 MeV (120 keV), while the Ge(Li) resolution has only deteriorated to 6–8 keV at 3 MeV.

For gamma rays with energies above the pair-production threshold, a considerable simplification of the complex NaI(Tl) spectrum can be achieved by using a three-crystal pair spectrometer consisting of one main NaI(Tl) crystal with two additional NaI(Tl) crystals 180° apart (or a split annulus) on either side of the main crystal. Events from the main crystal are then stored only when there is a coincidence between two 511-keV gamma rays in the peripheral crystals. All full-energy, single-escape, and Compton contributions are eliminated, and one is left with *only* the double-escape peaks in the main spectrum. Three-crystal pair spectrometers are now also being built with a central Ge(Li) detector and a surrounding split annulus of NaI(Tl).[38,39]

Because of their magnificent resolution, precision gamma-ray energy measurements with Ge(Li) detectors now often provide the most accurate method for determining the excitation energy of gamma-emitting nuclear levels. A convenient set of calibration lines with energies covering the range from 2.3 to 7.1 MeV have been measured by Chasman *et al.*[40] In such precision measurements, in converting the measured gamma-ray energy to the nuclear-level energy, proper consideration must be given to Doppler shift effects as well as corrections for the recoil energy of the emitting nucleus,

$$E_{\text{recoil}} = \frac{E_\gamma^2 \text{ (MeV)}}{A \text{ (n.m.u.)}} \times 0.536781 \text{ keV}. \qquad (4)$$

An example of the application of this technique to the precise location of levels of astrophysical importance is given by Alburger and Warburton in a study of the 7276-keV state in ^{15}O, which is relevant to the $^{14}N(p,\gamma)^{15}O$ reaction rate in the CNO cycle.[41] (Also see D. C. Hensley.[42,43])

Another interesting technique that has been suggested to take advantage of the high resolution of the Ge(Li) detectors is the measurement of radiative-capture excitation functions using a thick target and one fixed bombarding energy. "The measured thick target gamma-ray spectrum, after correction for energy variations in target stopping power and detector efficiency becomes a plot of the capture cross section vs. energy. The effective bombarding-energy resolution is determined by the resolution of the detector, and is independent of accelerator stability and energy spread and of target thickness uniformity."[44] This method should be useful in many cases where the capture gamma-ray cascade is simple, as in the case of the $^{12}C(p,\gamma)^{13}N$ reaction at low energies.

Resolution, however, is not the only important consideration in choosing gamma-ray detectors; the detector must also have an efficiency high enough to make accurate measurements for reactions whose cross sections may be as low as 10^{-11} b. In considering the determination of *absolute* cross sections from a gamma-ray spectrum, one of the problems that must be recognized is that gamma rays which were originally outside the solid angle subtended by the detector can be subsequently scattered into the detector by the material in the target chamber and the shielding material near the detector, for example, adding extra counts to the spectrum. Because these gamma rays must lose energy in the scattering process, they cannot possibly contribute counts to the full-energy peak in the spectrum. In fact, this is the only region in the spectrum where such scattered gamma rays cannot contribute, and for this reason, quantitative gamma-ray experiments are normally carried out using

measurements of the full-energy peaks. Therefore, the efficiencies which we will discuss below will always refer to the efficiency of the full-energy peak, unless specifically noted otherwise.

Because of their homogeneity and well-defined dimensions, very standard techniques can be used to calculate the "total" efficiency for gamma-ray detection by NaI(Tl) crystals, including all the interactions noted above. In general,

$$\eta_0 = \frac{1}{4\pi} \int_{\text{crystal}} \int W(\alpha,\beta)\,(1-e^{-\sigma\rho l(\theta,\phi)}) \sin\theta\, d\theta\, d\phi, \tag{5}$$

where $W(\alpha,\beta)$ is the normalized angular distribution of the gamma radiation which can be re-expressed in terms of the coordinates of the crystal using the method of Rose[45]; σ is the total interaction cross section as tabulated by Grodstein[46]; ρ is the density of NaI, 3.667 g/cm^3; and l is the path length in the crystal. For the usual case of a cylindrical crystal with a source of isotropic radiation located on the crystal axis, this reduces to

$$\eta_0 = \tfrac{1}{2} \int_{\text{crystal}} (1-e^{-\sigma\rho l(\theta)}) \sin\theta\, d\theta. \tag{6}$$

Many compilations of these "total" efficiencies already exist for isotropic radiation for a variety of cylindrical crystal sizes and source-to-detector distances.[47]

By combining such a calculation with a measurement of the ratio of the area of the full-energy peak to the area of the total spectrum, one determines the full-energy-peak efficiency of the crystal. Attempts have been made using Monte Carlo techniques to calculate this peak-to-total ratio but without quantitative success, so that the only way to really determine this ratio is by experimental measurement. In making such measurements, care must be taken to eliminate any nearby objects which could cause secondary scattering into the crystal which (since it cannot contribute to the full-energy peak) would decrease the peak-to-total ratio. An analytical solution to the problem of how to extrapolate the low-energy Compton tail, through regions where other backgrounds invariably contribute, to zero energy has been presented by Zerby and Moran.[48] A number of measurements have already been made of the peak-to-total ratios for such standard crystals as 3 in. $\times$ 3 in. and 5 in. $\times$ 5 in. Because of the reasonably good uniformity which exists in the manufacture of these detectors, these measurements should be generally applicable and are therefore presented in Figure 18. Although very good agreement exists between these measurements for energies above $\approx$ 1.0 MeV, it is

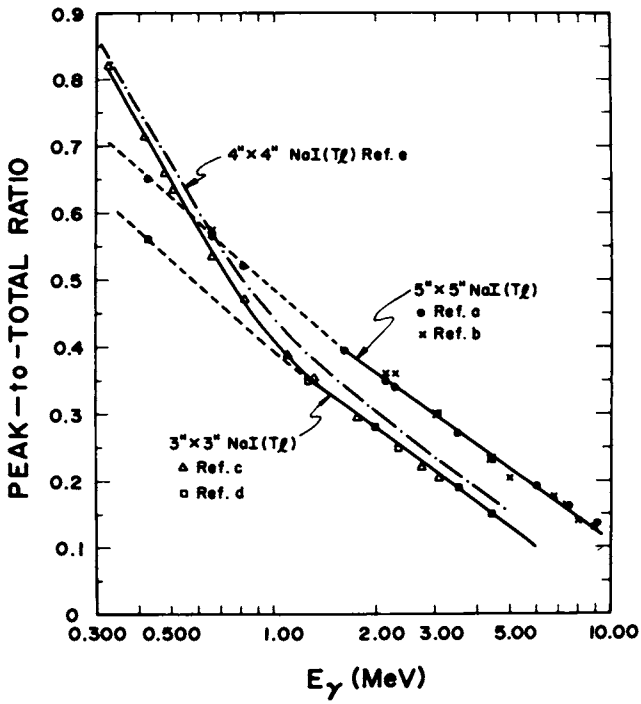

FIGURE 18. Peak-to-total ratio for NaI(Tl) detectors as a function of gamma-ray energy. Reference a, Young *et al.*[49]; reference b, BNL Van de Graaff Group[50]; reference c, Heath[47]; reference d, Parker[51]; reference e, Christaller.[52]

clear that there is a very serious disagreement between the results of references c and e and the results of references a, b, and d concerning the low-energy behavior of this ratio. This discrepancy is not presently understood and should be resolved.

There is a small dependence of this ratio on the distance of the source from the detector, with the ratio getting larger at larger distances, but this effect is not very pronounced. Heath[47] finds at most a 2 percent increase for a change in the source-to-detector distance from 3 cm to 10 cm. The effect is unobservable in Christaller's data[52] for a distance change by a factor of 6, from 7.5 cm to 45 cm.

Once these peak-to-total ratios have been measured and combined with calculations of the total efficiency to yield the "peak" efficiency, a good check can be obtained by making measurements on a calibrated source; just be sure that the source was *accurately* calibrated. In principle, such sources could be used for the complete calibration of the crystal without

peak-to-total measurements or total efficiency calculations. However, such sources are not readily available for energies above 2.6 MeV, and even if they were available, their use for such efficiency calibrations would require measurements with *each* source at a number of different source-to-crystal distances in order to determine the dependence of the efficiency of the crystal on both energy and distance.

Techniques such as Compton suppression (using an anticoincidence shield around the detector) or simply the collimation of the crystal (allowing gamma rays to enter the crystal only near its axis) can be used to improve the peak-to-total ratio in the spectrum, increasing the "quality" of the spectrum. However, these techniques can only make a complex spectrum easier to interpret while making the absolute efficiency smaller and more difficult to determine. These techniques can never increase the full-energy-peak efficiency of the detector.

In general, all this discussion can be applied equally as well to Ge(Li) detectors. In practice, however, because of their frequently irregular or poorly defined shapes (as in the case of ingot-shaped devices or coaxially drifted devices where the drifting depth is not accurately defined) a direct calculation of the "total" efficiency is not usually satisfactory. At least until somewhat better uniformity exists in their manufacture, efficiency measurements must be made directly for each Ge(Li) detector using sources in the empirical technique described earlier. Such measurements are almost always made only in terms of the full-energy peak, since it is so well separated from the rest of the spectrum. A few series of measurements of this sort are available for absolute efficiencies[53,54] and for relative efficiencies[55–57] and should be worthwhile for comparison.

In general, these measurements indicate that, *relative* to a 3 in. $\times$ 3 in. NaI(Tl) detector located at the same distance, for 1-MeV gamma rays the efficiency of a 1-cc Ge(Li) detector is only 1×10^{-3} (1000 times smaller), for an 8-cc Ge(Li) it is 1×10^{-2}, and for a 35-cc Ge(Li) it is 3×10^{-2}; for 3-MeV gammas these figures have all decreased by roughly a factor of 2. In a comparison of this sort, however, consideration must also be given to the difference in resolution between these types of detectors, since fewer counts are necessary for the higher-resolution instrument to show a peak above the background continuum. This effect is essentially proportional to the ratio of the resolutions of the detectors, and this ratio is typically of the order of 15 to 20 in favor of the Ge(Li) detector. Therefore, it may be more reasonable to compare "effective" efficiencies (including the resolution factor) in which case at 1 MeV one obtains for 1-cc Ge(Li) $\rightarrow 2 \times 10^{-2}$, for 8-cc Ge(Li) $\rightarrow 0.2$, and for 35-cc Ge(Li) $\rightarrow 0.5$ relative to a 3 in. $\times$ 3 in. NaI(Tl). For larger NaI(Tl)

crystals this ratio gets considerably smaller, e.g., 35-cc Ge(Li)/5 in.×5 in. NaI(Tl)→0.2, etc.

When either of these types of detectors is used in a real experimental situation, corrections must be made to the ideal efficiencies in order to take into account the absorption by any material which is between the source and the detector. This absorption can be calculated as $e^{-\sigma\rho l}$, where σ is the absorption cross section for the material (cm^2/g) as tabulated by Grodstein[46] and by Plechaty and Terrall[58]; ρ is the density of the material; and l is the path length in the material. Strictly speaking, the angular dependence of this factor should be taken into account by rewriting it as (for composite absorbers) $e^{-\sum_i \sigma_i \rho_i l_i(\theta,\phi)}$ and including it in the efficiency integral. However, in many cases where the absorption is small (<10 percent), one is quite justified in using the approximation that

$$\eta = \eta_0 e^{-\sum_i \sigma_i \rho_i l_i}, \tag{7}$$

especially when some appropriately average value for l_i is chosen.

In the real world one seldom deals with spectra containing the response function of only a single monochromatic gamma ray, and therefore the experimenter must normally face the problem of unscrambling complex spectra in order to extract the contributions of individual lines. Such an extraction requires a knowledge of the response functions of the detector for each of these gamma rays. These response functions need not be measured directly for every energy but can be obtained via interpolation from a set of response functions measured in the identical geometry (including shielding) with either a set of radioactive sources or a set of convenient, isolated, clean nuclear resonances. Such a set of resonances might include:

$E_\gamma = 0.432$ MeV	$^{10}B(p,\alpha_1)^7Be$	$E_p = 1.533$ MeV
$E_\gamma = 1.274$ MeV	$^{19}F(\alpha,p_1)^{22}Ne$	$E_\alpha = 2.360$ MeV
$E_\gamma = 1.633$ MeV	$^{23}Na(p,\alpha_1)^{20}Ne$	$E_p = 1.254$ MeV
$E_\gamma = 1.980$ MeV	$^{18}O(p,p_1)^{18}O$	$E_p = 2.768$ MeV
$E_\gamma = 2.367$ MeV	$^{12}C(p,\gamma)^{13}N$	$E_p = 0.459$ MeV
$E_\gamma = 3.51$ MeV	$^{12}C(p,\gamma)^{13}N$	$E_p = 1.698$ MeV
$E_\gamma = 4.439$ MeV	$^{15}N(p,\alpha_1)^{12}C$	$E_p = 0.898$ MeV

(In all these cases, as in all experimental gamma-ray measurements, the accurate subtraction of background from the raw data is important. This background will normally include the ambient room background, the background associated with the operation of the accelerator, and the background due to other nuclear reactions taking place in the target. In the case of narrow resonances, backgrounds can be measured by running

just above or just below the resonant energy. Where this is not possible because the resonance is either not narrow or not well isolated from other resonances, the background can be measured at the resonant energy by substituting a chemically similar target in which, however, the particular element or isotope of interest is absent.)

Once these response functions have been measured, for the purposes of comparison and interpolation, it seems most advantageous to normalize the full-energy-peak heights and plot the response curves as a function of $(E-E_\gamma)$ so that all the pronounced features such as the Compton edge and the single-escape and double-escape peaks are aligned. In this way, the interpolations are much more smoothly varying as a function of E_γ than if the response curves were simply plotted as a function of E. With this smooth, monotonic variation the interpolation can be readily carried out point by point as a function of $(E-E_\gamma)$ to generate the response curves at intermediate energies. Once the individual response functions have been obtained, response functions due to the coincidence summing of cascading gamma rays can be generated as

$$\mathbf{N}_{\gamma_1+\gamma_2}(E)=\sum_{E_i=0}^{E}\mathbf{N}_{\gamma_1}(E_i)\cdot\mathbf{N}_{\gamma_2}(E-E_i). \tag{8}$$

Generating the appropriate response functions is clearly the sort of tedious work that computers can handle very quickly and easily. Now having obtained all the appropriate response functions, the next step is to combine them all by varying the relative intensities of each in a simultaneous, point-by-point, least-squares fit to the interesting portion of the experimental spectrum as described by Salmon.[59] For example, for a case with four response functions (A, B, C, and D) at the ith point or channel in the experimental spectrum (K) we can write

$$K_i=\alpha A_i+\beta B_i+\gamma C_i+\delta D_i+\epsilon_i, \tag{9}$$

where α, β, γ, and δ are the relative intensities of the four response functions. One then minimizes the sum of the squares of the errors

$$\begin{aligned} R&=\sum_i \epsilon_i^2 \\ &=\sum_i (K_i-\alpha A_i-\beta B_i-\gamma C_i-\delta D_i)^2 \end{aligned} \tag{10}$$

by differentiating R with respect to α, β, γ, and δ, setting the equations each equal to zero, and then inverting the resulting matrix.

Parker and Kavanagh[51,60] present an example of the steps involved in such analysis (including the generation and interpolation of response

functions and the least-squares fitting of these to the experimental spectrum) in Figures 19 and 20.

Similar work has been done in the compilation of response functions for Ge(Li) detectors.[61,62] However, because of the high resolution of Ge(Li) detectors and because the structures in their response functions are so widely separated, the normal procedure with these detectors seems to be to ignore the Compton continua and concentrate only on the peaks in measuring the energies and intensities of the transitions. For this purpose, peak-finding and peak-fitting programs have been developed which, given a raw spectrum, will locate all the single peaks and doublets, subtract a linear or exponential background, and then fit the peaks with Gaussians (double Gaussians in the case of doublets), determining their centroids, widths, and areas.[63,64]

Finally, some mention should be made concerning the effects of neu-

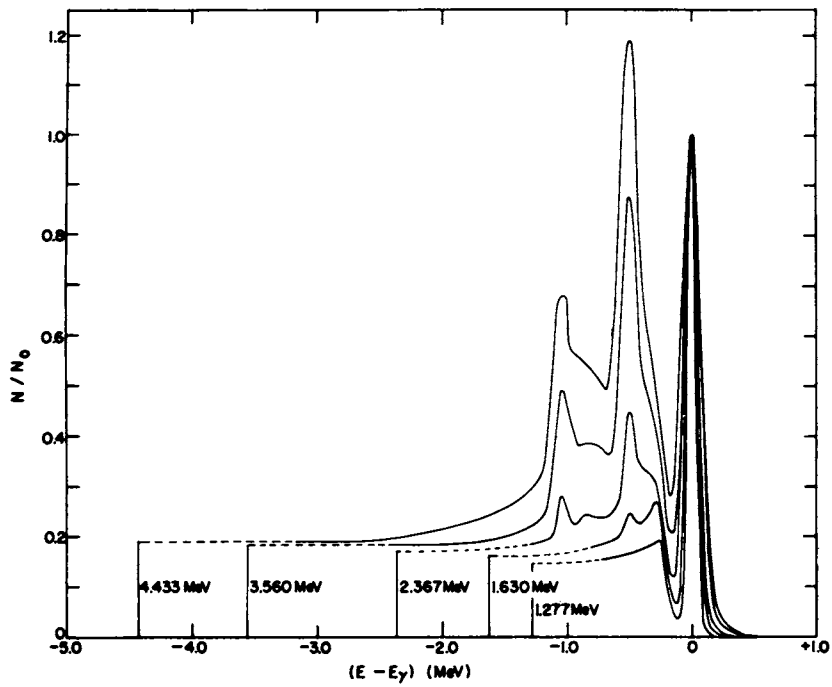

FIGURE 19. The line-shape response calibration of a 3 in. × 3 in. NaI(Tl) crystal as measured experimentally using various nuclear reactions to produce the monoenergetic gamma rays. The gamma-ray energy is indicated at the low-energy end of each function. From such a calibration, it is possible to interpolate the line-shape response at any intermediate energy.

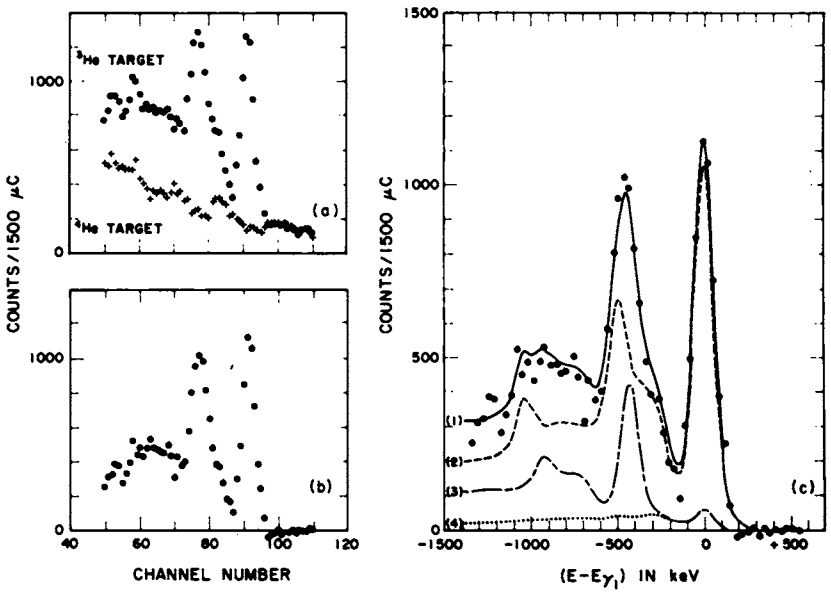

FIGURE 20. Graphical representation of the data reduction and analysis for the case of the $^3He(\alpha,\gamma)^7Be$ reaction at $E_{cm} = 1248$ keV. (a) The dots represent the raw NaI(Tl) spectrum obtained using ^3He as the target gas, while the crosses represent the raw spectrum obtained under identical conditions using ^4He in the target chamber. (b) The dots represent the net $^3He(\alpha,\gamma)^7Be$ gamma-ray spectrum obtained by subtracting the ^4He spectrum from the ^3He spectrum in (a). (c) The net experimental $^3He(\alpha,\gamma)^7Be$ spectrum is represented by the dots. Curve (1) is the least-squares fit to the net spectrum obtained by varying the normalizations of curves (2) and (3), where (2) is the response function for the crossover transition and (3) is the response function for the cascade transition including the effects of coincident summing. Curve (4) is just the contribution of such summing to the cascade response function.

trons on NaI(Tl) and Ge(Li) detectors. For NaI(Tl) crystals, the primary effect is the (n,γ) activation of the NaI to form ^{24}Na and ^{128}I. This activation immediately produces ($E_n + 7$ MeV) worth of gamma rays in the crystal from the capture radiation and produces delayed activities from the beta decay of the ^{128}I ($t_{\frac{1}{2}} = 25$ min, $E = 2.12$ MeV) and the ^{24}Na ($t_{\frac{1}{2}} = 15$ h, $E = 5.51$ MeV). Both of these processes can represent serious background problems for low-yield measurements because they occur inside the crystal and therefore are detected with high efficiency. This is one of the reasons that so much emphasis was put on the necessity of keeping carbon [with the $^{13}C(\alpha,n)^{16}O$ reaction] off targets being used for (α,γ) studies. For Ge(Li) detectors there are two effects, (a) contribu-

tions to the gamma-ray spectrum due to (n,n') inelastic scattering and (b) radiation damage of the device itself. Chasman *et al.*[65] have identified and discussed in detail the lines arising both from inelastic neutron scattering in the cryostat materials (Al, Cu, etc.) and from inelastic scattering in the various Ge isotopes in the crystal. The radiation damage effects in the Ge(Li) detectors take the same form of charge trapping at damage sites in the crystal lattice as we noted earlier for silicon, charged-particle detectors. Kraner *et al.*[66] have carried out an extensive study of these effects and find that the most pronounced changes occur in a degradation of the rise-time characteristics and in a broadening of the pulse-height resolution. These effects seem to have a threshold at an integrated dosage of $\approx 10^{10}$ N/cm^2, below which no damage is really evident and above which the damage rapidly increases so that, for instance, at an integrated dosage of 10^{11} N/cm^2 a 5-keV detector has deteriorated to a resolution of 15 keV. These authors, however, also cite at least one case in which a badly damaged detector was restored to its preirradiation condition by a process of redrifting and re-etching.

ELECTRONICS

In sharp contrast to the situation as recently as 10 years ago when most specialized laboratory electronics was homemade, today an experimenter can satisfy virtually all his requirements using readily available commercial units. Furthermore, beginning with the adoption, in 1964, of the NIM (Nuclear Instrument Modules) standard specifications, most of these units, which are available for a wide variety of functions from a number of different companies, are fully compatible in terms of power requirements, signal levels, and logic levels, so that modules from different manufacturers can often be used interchangeably without interface problems. Rather than present a listing of the vast range of such modules that are available, we will simply note here that they include such diverse items as preamplifiers, main amplifiers, single-channel analyzers, coincidence circuits, digital stablizers, and particle identifiers. For a more complete description of what is available the catalogs of such companies as ORTEC, Canberra, Hamner, EG&G, and Lecroy should be consulted.

Beyond the signal-processing logic units and amplifiers considered above, there comes the question of multichannel pulse-height analysis. For most problems of the sort considered in this report, analyzers with 400 or 512 channels, of the type which have been standard for several years, should suffice. The more recent models, featuring larger memories

and faster pulse conversion, are generally not essential, although they do increase the data-handling capability. Two general exceptions to the adequacy of the smaller analyzers are (a) a program of precision spectroscopy using high-resolution Ge(Li) detectors for which one of the more contemporary 4096-channel analyzers would be highly desirable, if not necessary, in order to take advantage of the detector's resolution and (b) a program of coincidence studies utilizing two-dimensional analysis, in which case one of the modern 64×64 or 128×128 2-d analyzers would be desirable. Some of the manufacturers from whom these types of analyzers are presently available include Hewlett-Packard, Intertechnique, Northern Scientific, Nuclear Data, and Victoreen.

Total Cross-Section Measurements

In many cases in nuclear astrophysics experiments, the required information involves the determination of total cross sections. For instance, in a measurement of the rate of the $^{13}C(p,\gamma)^{14}N$ reaction as part of the CNO cycle, it is not of any particular importance to know whether the capture occurs directly to the ^{14}N ground state or via a cascade of gamma rays through the excited states of ^{14}N; what is important to know is how many $^{14}N_{g.s}$ nuclei are eventually formed. This total cross-section information must normally be collected first from an integration over the angular distribution of each of the reaction products and then from a summation over the contributions of all the various, relevant decay channels. In cases where only a very few decay channels are involved, these integration and summation techniques are feasible but cumbersome. However, for cases, such as the $^{27}Al(p,\gamma)^{28}Si$ reaction discussed in Chapter 1, where the number of decay channels is more than just a very few, this method becomes so cumbersome as to be no longer practical, and other means must be found.

One technique, which can be feasible whenever the residual nucleus is unstable, involves simply using the specific, residual radioactivity (together with the usual lifetime and efficiency corrections) as a measure of the total cross section, as in the case of the $^{7}Be(p,\gamma)^{8}B$ reaction[67,68] or the $^{14}N(\alpha,\gamma)^{18}F$ reaction.[69] For measuring very small cross sections this technique has additional advantages in terms of measuring the delayed activity at times or places removed from the intense, prompt, beam-induced radiations and oftentimes in better geometry or with better shielding than would have been practical at the target chamber location.

A second technique which has been used for measuring total gamma-

ray cross sections involves the use of a Moxon-Rae detector.[70,71] These detectors consist of a thick, low-z (e.g., graphite) gamma-to-electron converter together with a thin ($\approx$0.020-in.) plastic scintillator for detecting the electrons, and on the basis of this these detectors have an efficiency which is a linear function of the gamma-ray energy. The efficiency for "detecting" a gamma-ray cascade is simply the sum of the efficiencies for detecting each of the members of the cascade (provided your geometry is good enough to eliminate the problem of summing due to the coincident detection of two or more members of the cascade). Therefore, the Moxon-Rae detector, whose efficiency is a linear function of gamma-ray energy, has the *same* efficiency for detecting each of the different cascades from a particular initial state, regardless of the number of gamma rays involved or their individual energies, i.e., since

$$E_{\text{cascade}} = \sum_i E_{\gamma_i} = E_{\gamma\ 0} \text{ and } \eta_i \propto E_{\gamma_i}$$

$$\therefore \eta_{\text{cascade}} = \sum_i \eta_i = \eta_0. \tag{11}$$

The thin plastic scintillators used in these detectors have the further advantages that their small volume makes them insensitive to direct gamma-ray or neutron detection and that their fast response times ($\approx$2 nsec) enable them to be used for (n,γ) experiments with pulsed-beam and time-of-flight techniques to separate the (n,γ) events from the intense prompt radiation produced by the primary beam in the target being used to generate the neutrons.

Other alternatives for obtaining total cross-section information include the use of large, well-type detectors to surround the target as completely as possible, thereby integrating over any angular distribution effects, or the sum-geometry technique of Lyons *et al.*,[72] which utilizes two large NaI(Tl) crystals to surround the target and, with their outputs summed, to act like a large, well-type crystal. In analyzing the spectra (including a large summing contribution) obtained in this way, Lyons *et al.*[72] have found empirically that for a discriminator setting of $\approx 0.33 \times E_{\gamma 0}$ the efficiencies for detecting cascades involving one, two, or three gamma rays are very nearly the same, $\pm$5 percent, allowing one to ignore the problem of branching ratios as well as the problem of angular distributions for such detectors.

In experimental nuclear astrophysics, the problems associated with determining *absolute, total* cross sections are almost always compounded by the fact that these cross sections must be measured at energies far below the Coulomb barrier where the interesting yields become vanishingly

small. These low yields make the reduction or elimination of backgrounds one of the most serious problems in experimental nuclear astrophysics, especially for gamma-ray experiments where the large volume of the detectors make them much more sensitive to ambient background radiations such as cosmic rays, ^{40}K, ^{65}Zn, ThC″, and the radiation associated with the operation of the accelerator.

The brute-force way of handling this problem involves the use of massive shielding around the detector, but in this case one must be aware of possible spectrum changes caused by the scattering of radiation into the detector by this shielding as discussed earlier for gamma-ray experiments. Other fairly obvious procedures include the use of high-intensity beams, the detection of delayed activities as discussed earlier in this section, and the placing of the detector as close as possible to the target. (In most cases the angular resolution gained by "good" geometry is not relevant to the astrophysical interest in the reaction.) In this "poor" geometry, however, added care must be taken to define accurately and maintain the position of the beam on the target relative to the detector since a small absolute change in this position can represent an important relative change at such close distances and thus result in a substantial change in the detector efficiency.

Additional precautions relevant to background reduction should include target purity and the cleanliness of the vacuum system as related, for example, to carbon contamination and the $^{13}C(\alpha,n)^{16}O$ reaction discussed earlier. For low-yield experiments attention must also be given to the problems of ion-source cleanliness. A good electrostatic or magnetic-beam analyzer will normally remove any contaminating component from the beam before it reaches the target; however, the additional background produced by the elimination of this contaminant beam (for instance, deuterons) on a set of defining slits or apertures can be devastating to a low-yield reaction such as (α,γ). For this reason, before starting such an experiment it may often be necessary to run the ion source for a day or more simply to cook out any residual gases from the previous operations.

Finally, once the background level has been reduced as much as practical, for low-yield experiments it is just as important to obtain accurate measurements of the various components of the remaining background as it is to obtain measurements of the radiations from the reaction of interest. As noted earlier, the techniques for these background measurements include the use of data obtained at energies very slightly removed from narrow resonances and the use of "dummy" targets which are chemically similar to the "real" targets but in which the element or isotope of interest is absent or at least significantly reduced.

BIBLIOGRAPHY

Two books that contain a good deal of generally useful miscellaneous information are:

1960 Nuclear Data Tables—Part 3, J. B. Marion, ed. (Nat. Acad. Sci.–Nat. Res. Council, Washington, D.C., 1960).

Nuclear Research with Low Energy Accelerators, J. B. Marion and D. M. Van Patter, eds. (Academic Press Inc., New York, 1967). (Abbreviated NRLEA in the references below.)

REFERENCES

1. L. F. Chase, Jr., NRLEA, p. 445 (1967).
2. K. Bethge, K. Meier-Ewert, K. Pfeiffer, and R. Bock, Phys. Lett. *24B*, 663 (1967).
3. S. K. Allison and M. Kamegai, Rev. Sci. Instrum. *32*, 1090 (1961).
4. R. R. Carlson, NRLEA, p. 475 (1967).
5. K. O. Nielsen, Nucl. Instrum. Methods *1*, 289 (1957).
6. R. E. Warren, J. L. Powell, and R. G. Herb, Rev. Sci. Instrum. *18*, 559 (1947).
7. W. A. Fowler, C. C. Lauritsen, and T. Lauritsen, Rev. Sci. Instrum. *18*, 818 (1947).
8. J. B. Marion, Rev. Mod. Phys. *38*, 660 (1966).
9. R. B. Walton, J. D. Clement, and F. Boreli, Phys. Rev. *107*, 1065 (1957).
10. C. N. Davids, Astrophys. J. *151*, 775 (1968).
11. R. H. Spear, J. D. Larson, and J. D. Pearson, Nucl. Phys. *41*, 353 (1963); J. D. Pearson and R. H. Spear, Nucl. Phys. *54*, 434 (1964); and J. D. Larson and R. H. Spear, Nucl. Phys. *56*, 497 (1964).
12. A. Adams, M. H. Shapiro, C. A. Barnes, and E. G. Adelberger, Bull. Amer. Phys. Soc. *13*, 698 (1968).
13. S. H. Maxman, Nucl. Instrum. Methods *50*, 53 (1967).
14. L. Yaffe, Ann. Rev. Nucl. Sci. *12*, 153 (1962).
15. M. L. Smith, ed., *Proceedings of the Seminar on the Preparation and Standardization of Isotopic Targets and Foils*, AERE-R 5097 (Harwell, England, 1965).
16. G. T. J. Arnison, AWRE 0-32/67 (Aldermaston, England, 1967).
17. L. Holland, *Vacuum Deposition of Thin Films* (John Wiley & Sons, Inc., New York, 1956).
18. F. A. Lowenheim, *Modern Electropolating* (John Wiley & Sons, Inc., New York, 1963).
19. E. A. Silverstein, S. R. Salisbury, G. Hardie, and L. D. Oppliger, Phys. Rev. *124*, 868 (1961).
20. H. C. Winkler and M. R. Dwarakanath, Bull. Amer. Phys. Soc. *12*, 16 (1967).
21. H. C. Winkler, Rev. Sci. Instrum. *35*, 1599 (1964).
22. W. Whaling, Handbuch der Physik *34*, 193 (1958); D. Demirlioglu and W. Whaling, Calif. Institute of Technol. Rep. (unpublished, 1962).
23. C. F. Williamson, J. P. Boujot, and J. Picard, CEA-R 3042 (Centre d'Etudes Nucleaires de Saclay, 1966).

24. L. C. Northcliffe, Phys. Rev. *120*, 1744 (1960); Ann. Rev. Nucl. Sci. *13*, 67 (1963).
25. L. P. Robertson, B. L. White, and K. L. Erdman, Rev. Sci. Instrum. *32*, 1405 (1961).
26. A. B. Brown, C. W. Snyder, W. A. Fowler, and C. C. Lauritsen, Phys. Rev. *82*, 159 (1951).
27. H. A. Enge, M. A. Wahlig, and I. Aanderaa, Rev. Sci. Instrum. *28*, 145 (1957).
28. P. D. Barnes, D. Biegelson, J. R. Comfort, and R. O. Stephen, WNSL Internal Report #25, Yale University (unpublished, 1965).
29. H. M. Loebenstein, D. W. Mingay, and C. S. Zaidins, Nucl. Instrum. Methods *33*, 175 (1965).
30. C. S. Zaidins, Calif. Institute of Technol. Tech. Rep. (unpublished, 1962).
31. G. L. Miller, W. M. Gibson, and P. F. Donovan, Ann. Rev. Nucl. Sci. *12*, 189 (1962); and W. M. Gibson, G. L. Miller, and P. F. Donovan, in *Alpha, Beta and Gamma Ray Spectroscopy*, K. Siegbahn, ed. (North-Holland Publishing Co., Amsterdam, 1965), p. 345.
32. G. Fabri, J. Karolyi, and V. Svelto, Nucl. Instrum. Methods *50*, 50 (1967).
33. G. Andersson-Lindstroem, Nucl. Instrum. Methods *56*, 309 (1967).
34. A. O. Hanson and J. L. McKibben, Phys. Rev. *72*, 673 (1947).
35. G. B. Bishop, Nucl. Instrum. Methods *62*, 247 (1968).
36. M. Birk, G. Goldring, and P. Hillman, Nucl. Instrum. Methods *21*, 197 (1963).
37. R. G. Miller and R. W. Kavanagh, Nucl. Instrum. Methods *48*, 13 (1967).
38. S. E. Arnell, R. Hardell, A. Hasselgren, L. Johnson, and O. Skeppstedt, Nucl. Instrum. Methods *54*, 165 (1967).
39. D. M. Van Patter, NRLEA, p. 99 (1967).
40. C. Chasman, K. W. Jones, R. A. Ristinen, and D. E. Alburger, Phys. Rev. *159*, 830 (1967).
41. D. E. Alburger and E. K. Warburton, Phys. Rev. *152*, 914 (1966).
42. D. C. Hensley, Private communication.
43. D. C. Hensley, Astrophys. J. *147*, 818 (1967).
44. S. L. Blatt, D. B. Nichols, R. G. Arns, J. D. Goss, H. J. Hausman, Bull. Amer. Phys. Soc. *13*, 173 (1968).
45. M. E. Rose, Phys. Rev. *91*, 610 (1953).
46. G. W. Grodstein, NBS Circular #583 (1957).
47. R. L. Heath, AEC Rep. IDO-16880 (1964).
48. C. D. Zerby and H. S. Moran, Nucl. Instrum. Methods *14*, 115 (1961).
49. F. C. Young, H. T. Heaton, G. W. Phillips, P. Forsyth, and J. B. Marion, Bull. Amer. Phys. Soc. *10*, 54 (1965) and private communication.
50. BNL Van de Graaff Group, private communication.
51. P. D. Parker, Ph.D. Thesis, Calif. Institute of Technol. (unpublished, 1963).
52. G. Christaller, Nucl. Instrum. Methods *50*, 173 (1967).
53. G. T. Ewan and A. J. Tavendale, Can. J. Phys. *42*, 2286 (1964).
54. R. L. Heath and J. E. Cline, AEC Rep. IDO-17222 (1967).
55. J. M. Freeman and J. G. Jenkin, Nucl. Instrum. Methods *43*, 269 (1966).
56. W. R. Kane and M. A. Mariscotti, Nucl. Instrum. Methods *56*, 189 (1967).
57. D. P. Donnelly, H. W. Baer, J. J. Reidy, and M. L. Wiedenbeck, Nucl. Instrum. Methods *57*, 219 (1967).
58. E. F. Plechaty and J. R. Terrall, UCRL-50178 (1966).
59. L. Salmon, Nucl. Instrum. Methods *14*, 193 (1961).

60. P. D. Parker and R. W. Kavanagh, Phys. Rev. *131*, 2578 (1963).
61. J. Kopecky, W. Ratynski, and E. Warming, Nucl. Instrum. Methods *50*, 333 (1967).
62. B. J. Allen, J. R. Bird, and S. Engstrom, Nucl. Instrum. Methods *53*, 61 (1967).
63. M. A. Mariscotti, Nucl. Instrum. Methods *50*, 309 (1967).
64. R. G. Helmer, R. L. Heath, M. Putnam, and D. H. Gipson, Nucl. Instrum. Methods *57*, 46 (1967).
65. C. Chasman, K. W. Jones, and R. A. Ristinen, Nucl. Instrum. Methods *37*, 1 (1965).
66. H. W. Kraner, C. Chasman, and K. W. Jones, Nucl. Instrum. Methods *62*, 173 (1968).
67. R. W. Kavanagh, Nucl. Phys. *15*, 411 (1960).
68. P. D. Parker, Phys. Rev. *150*, 851 (1966).
69. P. D. Parker, Phys. Rev. *173*, 1021 (1968).
70. M. C. Moxon and E. R. Rae, Nucl. Instrum. Methods *24*, 445 (1963).
71. R. L. Macklin, J. H. Gibbons, and T. Inada, Nucl. Phys. *43*, 353 (1963).
72. P. Lyons, J. Toevs, and D. G. Sargood (to be published).

CHAPTER 3

Table of Reactions and Bibliography

In this chapter, we provide a selected list of reactions of interest to nuclear astrophysics. These are presented as a guide to charged-particle reactions for which thermonuclear cross sections have a known practical application. The list is long because nature has provided a large number of astronomical settings of interest. Most other reactions do not seem at present to have specific thermonuclear interest. Reactions between ^{14}N and ^{3}He, for example, are not listed because there seems to be no important thermal environment wherein both nuclei have significant abundances at temperatures where they can interact. Needless to say, the assemblers of this table are not omniscient, so the table must not be regarded as definitive or complete. Future research will no doubt point to applications not envisioned today.

Adjacent to each reaction is the particular known application and the temperature near which the value of $\langle \sigma v \rangle$ is of interest for that application. Selected references to the reaction and its application are listed by number. The references are of two types:

1. General information concerning the context of the astronomical interest,
2. Laboratory studies of that reaction which have been made with the astrophysical problem in mind.

Not all experimental studies of each reaction are listed, because the bibliographies of the later studies usually cite the earlier ones. It is assumed that the reader will, as a matter of course, consult the compilations of nuclear data listed in reference 15 of Chapter 1. The nuclear studies are listed adjacent to the astrophysical reaction on which they bear,

rather than adjacent to the auxiliary reactions exploited to obtain relevant information. For example, the reference to $^{12}C(^{6}Li,d)^{16}O$ occurs at $^{12}C(\alpha,\gamma)^{16}O$.

The table lists primarily charged-particle reactions of importance in the epochs of thermal fusion in stars. These are the most clearly understood and most urgently needed applications. There are two lists that have been omitted completely, however, and one that is only partial. We have not listed most of the neutron-induced (primarily radiative capture) reactions because of the length of that list; however, several (n,γ) and (n,p) reactions of importance to the network of carbon burning have been included because of their special significance. Some of the (n,p) reactions on radioactive targets may be studied by their inverse reactions. The references cited in Chapter 1 under Neutron Reactions (page 30) must be studied to extract the neutron cross sections needed for the synthesis of the heavy elements. In addition to the heavy-element synthesis, the neutron reactions with all stable light nuclei are of importance in explosive synthesis in big and little bangs. We also have not listed the charged-particle reactions of interest to explosive nucleosynthesis for targets $Z \geq 6$. They include all exothermic reactions with protons, neutrons, and alpha particles, but the question of the relative importance of these reactions is not entirely clear. The potential investigator should study reference 47 of Chapter 1. Another host of reactions occur during silicon burning, but the importance of many of them is reduced by the tendency toward equilibration with the inverse reaction. Accordingly, we have selected several reactions whose absolute rates during silicon burning appear in a preliminary survey to be of special interest.

We suggest that laboratory work could usefully be undertaken on most of the reactions listed below. By simultaneously studying the astrophysical situation, many modestly equipped laboratories could, we believe, contribute to this exciting field of research.

Reactions Relevant for Nuclear Astrophysics

REACTION	APPLICATION (TEMPERATURE)	REFERENCE
$^{1}H(p,\beta^{+}\nu)^{2}D$	hydrogen burning ($1<T_6<20$)	1,2,3
$^{2}D(p,\gamma)^{3}He$	surface convection ($0.1<T_6<5$)	1,2,4,23,25
	explosive nucl. ($T_9<5$)	8
$^{2}D(d,p)^{3}T$	explosive nucl. ($T_9<10$)	8
$^{3}T(p,\gamma)^{4}He$	explosive nucl. ($T_9<10$)	8
$^{3}T(\alpha,\gamma)^{7}Li$	explosive nucl. ($T_9<10$)	8,24

REACTION	APPLICATION (TEMPERATURE)	REFERENCE
$^{3}He(p,\beta^{+}\nu)^{4}He$	hydrogen burning ($1<T_6<20$)	2
$^{3}He(d,p)^{4}He$	early hydrogen burning (probably unimportant)	2
$^{3}He(\tau,\gamma)^{6}Be$	explosive nucleosynthesis ($T_9<5$)	8
	hydrogen burning	27
$^{3}He(\tau,2p)^{4}He$	hydrogen burning, ν astron. ($5<T_6<20$)	1,2,4,5,6,9
$^{3}He(\alpha,\gamma)^{7}Be$	hydrogen burning, ν astron. ($5<T_6<20$)	1,2,4,25,26
	explosive nucl. ($T_9<10$)	8
$^{4}He(d,\gamma)^{6}Li$	explosive nucl.	8
$^{4}He(\alpha,\alpha)^{4}He$	helium burning	28,29
$^{6}Li(p,\gamma)^{7}Be$	explosive nucl.	8
$^{6}Li(p,\alpha)^{3}He$	surface convection ($T_6<2$),	10
	explosive nucl. ($T_9<5$)	7,8
$^{6}Li(\alpha,\gamma)^{10}B$	explosive nucl. ($T_9<4$)	8
$^{7}Li(p,\alpha)^{4}He$	hydrogen burning ($5<T_6<20$)	1,2,7
	surface convection ($T_6<2$)	10
	explosive nucl. ($T_9<5$)	8
$^{7}Li(\alpha,\gamma)^{11}B$	explosive nucl. ($T_9<3$)	8
$^{7}Be(p,\gamma)^{8}B$	hydrogen burning, ν astron. ($5<T_6<20$)	1,2,4,7,12
	explosive nucl. ($T_9<10$)	8
$^{7}Be(\alpha,\gamma)^{11}C$	explosive nucl. ($T_9<2$)	8
$^{8}Be(\alpha)^{4}He$	helium burning	28,29
$^{8}Be(\alpha,\gamma)^{12}C$	helium burning, 3α ($0.1<T_9<10$)	7,11
$^{9}Be(p,\gamma)^{10}B$	explosive nucl. ($T_9<10$)	8
$^{9}Be(p,\alpha)^{6}Li$	explosive nucl. ($T_9<10$), surface convection	8,10
$^{9}Be(p,d)^{8}Be$	explosive nucl. ($T_9<10$)	8
$^{9}Be(\alpha,n)^{12}C$	explosive nucl. ($T_9<10$)	8,35
$^{10}Be(p,\gamma)^{11}B$	explosive nucl.	8
$^{10}Be(p,\alpha)^{7}Li$	explosive nucl.	8
$^{10}Be(\alpha,n)^{13}C$	explosive nucl.	8
$^{10}Be(p,\gamma)^{11}C$	explosive ($5<T_9<10$)	8
$^{10}B(p,\alpha)^{7}Be$	explosive ($T_9<5$), surface convection	8,10
$^{10}B(\alpha,n)^{13}N$	explosive	8
$^{10}B(\alpha,p)^{13}C$	explosive	8
$^{11}B(p,\gamma)^{12}C$	explosive ($T_9<10$), surface convection	8,10

REACTION	APPLICATION (TEMPERATURE)	REFERENCE
$^{11}B(p,\alpha)^{8}Be$	explosive ($T_9<10$), surface convection	8,10
$^{11}B(\alpha,n)^{14}N$	explosive ($T_9<10$), surface convection	8
$^{11}B(\alpha,p)^{14}C$	explosive ($T_9<10$), surface convection	8
(NOTE: From this point onward the reactions of interest for explosive nucleosynthesis are omitted from this list. Reference 8 involves almost every exothermic reaction involving light nuclei and p,n,α.)		
$^{12}C(p,\gamma)^{13}N$	CNO ($T_6<100$)	1,7,13,30
	carbon burning ($0.6<T_9<5$)	14
$^{13}C(n,\gamma)^{13}C$	carbon burning	14
$^{13}N(p,\gamma)^{14}O$	CNO ($T_6>100$)	7,13
$^{13}C(p,\gamma)^{14}N$	CNO ($T_6<100$)	1,7,13,31
	carbon burning ($0.6<T_9<5$)	14
$^{14}N(p,\gamma)^{15}O$	CNO ($T_6<100$)	1,7,13,15,32
$^{15}N(p,\gamma)^{16}O$	CNO	1,7,13,33
$^{15}N(p,\alpha)^{12}C$	CNO	1,7,13
$^{16}O(p,\gamma)^{17}F$	CNO	1,7,13,34
	carbon and oxygen burning ($T_9<5$)	14
$^{16}O(n,\gamma)^{17}O$	carbon burning ($1<T_9<5$)	14
$^{17}O(p,\alpha)^{14}N$	CNO, carbon and oxygen burning	1,7,13,14
$^{12}C(\alpha,\gamma)^{16}O$	helium burning ($1<T_8<5$)	1,7,16,42
	carbon burning ($0.6<T_9<5$)	7,14,42
	silicon burning ($3<T_9<6$)	7,17,42
$^{13}C(\alpha,n)^{16}O$	helium burning ($0.7<T_8<3$), n's	1,7,18,35
	carbon burning ($0.6<T_9<5$)	14,35
	thermal instability and mixing	21,22
$^{13}N(\alpha,p)^{16}O$	carbon burning ($1<T_9<5$)	14
$^{13}N(n,p)^{13}C$	carbon burning ($1<T_9<5$)	14
$^{14}N(\alpha,\gamma)^{18}F$	helium burning ($0.7<T_8<2$)	7,19,37
	carbon burning ($T_9<5$)	14
$^{16}O(\alpha,\gamma)^{20}Ne$	helium burning ($1<T_8<5$)	1,7,16
	carbon and oxygen burning ($1<T_9<5$)	14
	silicon burning ($3<T_9<6$)	17
$^{16}O(n,\gamma)^{17}O$	carbon and oxygen burning ($1<T_9<5$)	14
$^{17}O(\alpha,n)^{20}Ne$	helium burning, n's	1,7,18
	carbon and oxygen burning ($1<T_9<5$)	14

REACTION	APPLICATION (TEMPERATURE)	REFERENCE
$^{20}Ne(\alpha,\gamma)^{24}Mg$	helium burning ($1<T_8<5$)	1,7,16
	carbon and oxygen burning ($1<T_9<5$)	14
	silicon burning ($3<T_9<6$)	17
$^{18}O(p,\alpha)^{15}N$	helium burning with mixing ($0.6<T_8<2$)	21
	carbon burning	14
$^{18}O(\alpha,\gamma)^{22}Ne$	helium burning ($1<T_8<3$)	1,7,18,19
$^{18}O(\alpha,n)^{21}Ne$	helium burning ($T_8\geq 2$), n's	18,19
$^{18}F(n,p)^{18}O$	carbon burning ($1<T_9<5$)	14
$^{21}Ne(\alpha,n)^{24}Mg$	helium burning, n's ($1<T_8<3$)	1,7,18
	carbon and oxygen burning ($T_9<5$)	14
$^{22}Ne(\alpha,n)^{25}Mg$	helium burning, n's ($T_8\leq 3$)	1,7,18,19,20
	carbon and oxygen burning ($T_9<5$)	14
$^{22}Ne(\alpha,\gamma)^{26}Mg$	helium burning ($1<T_8<3$)	18
	carbon and oxygen burning	14
$^{20}Ne(p,\gamma)^{21}Na$	NeNa cycle ($20<T_6<100$)	36
	carbon and oxygen burning ($T_9<5$)	14
$^{21}Na(n,p)^{21}Ne$	carbon and oxygen burning ($T_9<5$)	14
$^{21}Ne(p,\gamma)^{22}Na$	NeNa cycle ($20<T_6<100$)	36
	carbon and oxygen burning ($T_9<5$)	14
$^{22}Na(n,p)^{22}Ne$	carbon and oxygen burning ($T_9<5$)	14
$^{22}Ne(p,\gamma)^{23}Na$	NeNa cycle ($20<T_6<100$)	36
	carbon and oxygen burning ($T_9<5$)	14
$^{23}Na(p,\alpha)^{20}Ne$ and $^{23}Na(p,\gamma)^{24}Mg$	NeNa cycle ($20<T_6<100$)	36,38
	carbon and oxygen burning ($T_9<5$)	14,38
	silicon burning ($T_9<6$)	17,38,39
$^{23}Na(n,\gamma)^{24}Mg$	carbon burning ($T_9<5$)	14
$^{23}Na(\alpha,p)^{26}Mg$	carbon burning ($T_9<5$)	14
$^{24}Na(p,n)^{24}Mg$	carbon burning ($T_9<5$)	14
$^{23}Mg(n,p)^{23}Na$	carbon burning ($T_9<5$)	14
$^{24}Mg(\alpha,\gamma)^{28}Si$	carbon and oxygen burning ($1<T_9<5$)	14
	silicon burning ($3<T_9<6$)	17,39,40
$^{24}Mg(n,\gamma)^{25}Mg$	carbon and oxygen burning ($1<T_9<5$)	14
	s-process ($0.1<T_9<2$)	41
$^{24}Mg(p,\gamma)^{25}Al$	carbon and oxygen burning ($1<T_9<5$)	14
$^{25}Mg(p,\gamma)^{26}Al$	carbon and oxygen burning ($1<T_9<5$)	14

REACTION	APPLICATION (TEMPERATURE)	REFERENCE
$^{25}Mg(\alpha,n)^{28}Si$	carbon and oxygen burning ($1<T_9<5$)	14
$^{25}Mg(n,\gamma)^{26}Mg$	carbon and oxygen burning ($1<T_9<5$)	14
	s-process ($0.1<T_9<2$)	41
$^{26}Mg(p,\gamma)^{27}Al$	carbon and oxygen burning ($1<T_9<5$)	14
$^{25}Al(n,p)^{25}Mg$	carbon and oxygen burning ($1<T_9<5$)	14
$^{26}Al(n,p)^{26}Mg$	carbon and oxygen burning ($1<T_9<5$)	14
$^{27}Al(p,\gamma)^{28}Si$	carbon and oxygen burning ($1<T_9<5$)	14
	silicon burning ($3<T_9<6$)	17,39,43
$^{12}C(^{12}C,\alpha)^{20}Ne$ $^{12}C(^{12}C,p)^{23}Na$ $^{12}C(^{12}C,n)^{23}Mg$	carbon burning ($0.6<T_9<7$)	14,44,45
$^{16}O(^{12}C,\alpha)^{24}Mg$ $^{16}O(^{12}C,p)^{27}Al$ $^{16}O(^{12}C,n)^{27}Si$	explosive carbon burning ($2<T_9<7$)	14,44,46
$^{16}O(^{16}O,\alpha)^{28}Si$ $^{16}O(^{16}O,p)^{31}P$ $^{16}O(^{16}O,n)^{31}S$	oxygen burning ($2<T_9<7$)	43
$^{16}O(^{16}O,^{8}Be)^{24}Mg$	oxygen burning ($2<T_9<7$)	43,47
$^{28}Si(\alpha,\gamma)^{32}S$	oxygen burning ($1<T_9<5$)	43
	silicon burning ($2<T_9<6$)	17,39
$^{28}Si(p,\gamma)^{29}P$	oxygen burning ($1<T_9<5$)	43
	silicon burning ($2<T_9<6$)	17,39
$^{29}Si(\alpha,n)^{32}S$	oxygen burning ($1<T_9<5$)	43
$^{29}Si(p,\gamma)^{30}P$	oxygen burning ($1<T_9<5$)	43
$^{30}Si(\alpha,\gamma)^{34}S$ $^{30}Si(\alpha,n)^{33}S$	oxygen burning ($1<T_9<5$)	43
$^{30}Si(p,\gamma)^{31}P$	oxygen burning ($1<T_9<5$)	43
$^{31}P(p,\alpha)^{28}Si$	oxygen burning ($1<T_9<5$)	43
$^{31}P(p,\gamma)^{32}S$	silicon burning ($2<T_9<6$)	17,39
$^{31}P(\alpha,p)^{34}S$	oxygen burning ($1<T_9<5$)	43
	silicon burning ($2<T_9<6$)	17,39
$^{32}P(p,n)^{32}S$	oxygen burning ($1<T_9<5$)	43
$^{31}S(n,p)^{31}P$	oxygen burning ($1<T_9<5$)	43
$^{32}S(\alpha,\gamma)^{36}A$	oxygen burning ($1<T_9<5$)	43
	silicon burning ($2<T_9<6$)	17,39

REACTION	APPLICATION (TEMPERATURE)	REFERENCE
$^{32}S(p,\gamma)^{33}Cl$	oxygen burning ($1<T_9<5$)	43
	silicon burning ($2<T_9<6$)	17,39
$^{32}S(n,\gamma)^{33}S$	oxygen burning ($1<T_9<5$)	43
	s-process ($0.1<T_9<3$)	41
$^{33}S(p,\gamma)^{34}Cl$	oxygen burning ($1<T_9<5$)	43
$^{33}S(n,\gamma)^{34}S$	oxygen burning ($1<T_9<5$)	43
	s-process ($0.1<T_9<3$)	41
$^{34}S(p,\gamma)^{35}Cl$	oxygen burning ($1<T_9<5$)	43
$^{35}Cl(p,\gamma)^{36}A$	oxygen burning ($1<T_9<5$)	43
	silicon burning ($2<T_9<6$)	17,39
$^{36}A(\alpha,\gamma)^{40}Ca$	oxygen burning ($1<T_9<5$)	43
	silicon burning ($2<T_9<6$)	17,39
$^{40}Ca(\alpha,\gamma)^{44}Ti$	silicon burning ($2<T_9<6$)	17,39
$^{44}Ti(\alpha,p)^{47}V$	silicon burning ($2<T_9<6$)	39,48
$^{44}Ti(n,\gamma)^{45}Ti$	silicon burning ($2<T_9<6$)	39,48
$^{42}Ca(\alpha,p)^{45}Sc$	silicon burning ($2<T_9<6$)	39,48

References and Notes

1. D. D. Clayton, *Principles of Stellar Evolution and Nucleosynthesis* (McGraw-Hill Book Co., Inc., New York, 1968).
2. P. D. Parker, J. N. Bahcall, and W. A. Fowler, Astrophys. J. *139*, 602 (1964).
3. J. N. Bahcall and R. M. May, Astrophys. J. *152*, L17 (1968).
4. T. A. Tombrello, "Astrophysical Problems," in *Nuclear Research with Low-Energy Accelerators*, J. B. Marion and D. M. Van Patter, eds. (Academic Press Inc., New York, 1967).
5. R. M. May and D. D. Clayton, *Astrophys. J.* (Sept. 1968).
6. H. C. Winkler and M. R. Dwarakanath (to be published); A. D. Bacher and T. A. Tombrello, Phys. Rev. (to be published); E. W. Blackmore and J. B. Warren, Can. J. Phys., *46*, 233 (1968).
7. W. A. Fowler, G. R. Caughlan, and B. A. Zimmerman, Ann. Rev. Astron. Astrophys. *5*, 525 (1967).
8. R. V. Wagoner, W. A. Fowler, and F. Hoyle, Astrophys. J. *148*, 3 (1967); R. V. Wagoner, "Synthesis of Elements within Exploding Objects," Astrophys. J. (to be published.)
9. I. Iben, Jr., Astrophys. J., *147*, 624 (1967).
10. W. A. Fowler, J. L. Greenstein, and F. Hoyle, Geophys. J. Roy. Astron. Soc. *6*, 148 (1962), see Section 11, p. 185.
11. P. A. Seeger and R. W. Kavanagh, Nucl. Phys. *46*, 577 (1963).
12. P. D. Parker, Astrophys. J. *145*, 960 (1966); Phys. Rev. *150*, 851 (1966); T. A. Tombrello, Nucl. Phys. *71*, 459 (1965).

13. G. R. Caughlan and W. A. Fowler, Astrophys. J. *136,* 453 (1962); *139,* 1180 (1964).
14. H. Reeves and E. E. Salpeter, Phys. Rev. *116,* 1505 (1959); W. D. Arnett and J. W. Truran, Astrophys. J. (to be published) contains a thorough list of carbon-burning reactions; see also ref. 44.
15. D. C. Hensley, Astrophys. J. *147,* 818 (1967); D. E. Alburger and E. K. Warburton, Phys. Rev. *152,* 914 (1966).
16. W. Deinzer and E. E. Salpeter, Astrophys. J. *140,* 499 (1964).
17. D. Bodansky, D. D. Clayton, and W. A. Fowler, Astrophys. J. Suppl., No. 148 (1968).
18. H. Reeves, Astrophys. J. *146,* 447 (1966).
19. I. Iben, Jr., Astrophys. J. *143,* 483 (1966).
20. J. Peters, Astrophys. J. *154,* 225 (1968).
21. R. H. Sanders, Astrophys. J. *150,* 971 (1968).
22. G. R. Caughlan and W. A. Fowler, Astrophys. J. *139,* 1180 (1964).
23. G. M. Griffiths, M. Lal, and C. D. Scarfe, Can. J. Phys. *41,* 724 (1963).
24. G. M. Griffiths, R. A. Morrow, P J. Riley, and J. B. Warren, Can. J. Phys. *39,* 1397 (1961).
25. T. A. Tombrello and P. D. Parker, Phys. Rev. *131,* 2582 (1963).
26. P. D. Parker and R. W. Kavanagh, Phys. Rev. *131,* 2578 (1963).
27. W. D. Harrison, W. E. Stephens, T. A. Tombrello, and H. Winkler, Phys. Rev. *160,* 752 (1967).
28. J. Benn, E. B. Dally, H. H. Muller, R. E. Pixley, H. H. Staub, and H. Winkler, Phys. Lett. *20,* 43 (1966).
29. W. Reichart, H. H. Staub, H. Stüssi, and F. Zamboni, Phys. Lett. *20,* 40 (1966).
30. R. N. Hall and W. A. Fowler, Phys. Rev. *77,* 197 (1950); J. D. Seagrave, Phys. Rev. *84,* 1219 (1951); D. F. Hebbard and J. L. Vogl, Nucl. Phys. *21,* 652 (1960).
31. J. D. Seagrave, Phys. Rev. *85,* 197 (1952); D. F. Hebbard and J. L. Vogl, Nucl. Phys. *21,* 652 (1960); R. E. Brown, Astrophys. J. *137,* 338 (1963); D. D. Clayton, Phys. Rev. *128,* 2254 (1962).
32. D. F. Hebbard and G. M. Bailey, Nucl. Phys. *49,* 666 (1963); D. F. Hebbard and B. Povh, Nucl. Phys. *13,* 642 (1959); D. C. Hensley, Astrophys. J. *147,* 818 (1967); W. A. S. Lamb and R. E. Hester, Phys. Rev. *108,* 1304 (1957).
33. D. F. Hebbard, Nucl. Phys. *15,* 289 (1960).
34. J. J. Domingo, Nucl. Phys. *61,* 39 (1965); R. F. Christy and I. Duck, Nucl. Phys. *24,* 89 (1961); R. E. Hester, R. E. Pixley, and W. A. S. Lamb, Phys. Rev. *111,* 1604 (1958).
35. S. N. Davids, Astrophys. J. *151,* 775 (1968).
36. J. B. Marion and W. A. Fowler, Astrophys. J. *125,* 221 (1957); S. Hinds, H. Marchant, and R. Middleton, Nucl. Phys. *51,* 427 (1964).
37. P. D. Parker, "The $^{14}N(\alpha,\gamma)^{18}F$ Reaction" (to be published).
38. R. Fisher and W. Whaling, Phys. Rev. *131,* 1723 (1963).
39. J. W. Truran, A. G. W. Cameron, and A. Gilbert, Can. J. Phys. *44,* 563 (1966).
40. P. Lyons, J. Toevs, and D. G. Sargood (to be published).
41. Reference 52 of Chapter 1.
42. J. D. Larsen and R. H. Spear, Nucl. Phys. *56,* 497 (1964).

43. No really adequate discussion of oxygen burning exists in the literature, but the nature of the problem is very similar to that of carbon burning so the reader may draw his own analogs to reference 14. Above $T_9 = 3$ the problem has similarities to silicon burning as described in references 17 and 39.
44. W. D. Arnett, Nature *219*, 1344 (1968).
45. J. R. Patterson, H. Winkler, and C. S. Zaidins, "Experimental Investigation of the Stellar Nuclear Reaction $^{12}C + {}^{12}C$ at Low Energies," Astrophys. J. (to be published); E. Almquist, D. A. Bromley, and J. A. Kuehner, Phys. Rev. Lett. *4*, 515 (1960); E. Almquist, J. A. Keuhner, D. McPherson, and E. W. Vogt, Phys. Rev. *136*, B84 (1964).
46. It has not been established whether these reactions are ever important. Although they cannot be significant in stars in hydrostatic equilibrium, they may be of significance when the carbon is largely exhausted in a superheated gas following explosive ignition. Despite this uncertainty, experimental information is desirable.
47. Because of the Coulomb barrier in the final channel this reaction is probably unimportant. There exists the possibility, however, that the ^8Be transfer may occur at larger interaction radii than does the compound nucleus formation between $^{16}O + {}^{16}O$, in which case this reaction could assume importance.
48. The special importance of these reactions is described in Section VII of reference 17.

Part II

ATOMIC PHYSICS

One need hardly emphasize to physicists the central role that atomic spectroscopy has played in the development of modern physics. However, it seems that the very success with which precise spectroscopic data have been acquired and interpreted has tended to obscure two important facts. Little is known about the structures of multiply ionized particles or about the mean lives of excited electronic levels in atoms and ions.

The present discussion of beam-foil spectroscopy (BFS) deals with a relatively new technique which makes possible a concerted attack on the foregoing features of atomic constitution. Simple both in conception and execution, this technique enables the small laboratory to make substantial contributions to areas of physics which, though of basic importance, were previously beyond the capabilities of even the most sophisticated experimenters. In addition, still other kinds of research, having no direct connection with either of the above problems, have evolved with the help of the beam-foil method. One example is the observation of Stark-induced interference in the quasi-degenerate states of hydrogenic systems. Many other fascinating BFS topics remain to be exploited.

Our discussion has been prepared in two chapters. The first (Chapter 4) presents an overview of beam-foil spectroscopy and attempts to give practical advice on conducting a variety of experiments. In order to stress the instrumental simplicity of some of the work, there is included guidance on how to succeed in BFS without really analyzing.

The second (Chapter 5) concentrates on the vital subject of lifetime measurements. It is perhaps this phase of BFS, more than any other, which has attracted the attention of a number of laboratories. Among other things, the lifetime data promote the close collaboration of experimental and theoretical atomic physicists, astrophysicists, and plasma specialists. Indeed, the interdisciplinary nature of BFS is one of its most intriguing aspects; we hope that this report will lead other laboratories to include BFS research in their activities.

CHAPTER 4

Beam-Foil Spectroscopy

Beam-foil spectroscopy (BFS) has proved to be a simple, but powerful, method for the study of the level structures of monatomic ions. In this method,[1] particles of some element of interest are accelerated, magnetically analyzed, and admitted into an evacuated target chamber (Figure 21). The target is a foil of carbon or beryllium with a thickness of 500 to 1000 Å. The particles pass through the foil, undergo interactions therein, and emerge radiating light (Figure 22). The light comes from the particle beams and *not* from the foil. Spectroscopic analysis of that light is the principal subject of BFS. An example is shown in Figure 23.

An important emerging field, BFS brings the techniques of nuclear physics to bear on problems of central importance in atomic physics and provides important guides[2,3] to recent calculations on the role of configuration interaction in level decay times. Physicists concerned with applications will find BFS particularly useful in astrophysics, plasma research, and certain aspects of solid-state physics. To the academic physicists, BFS has the appeal that students learn both nuclear and atomic

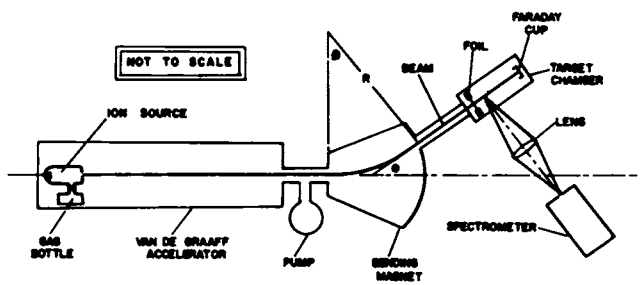

FIGURE 21. Schematic arrangement of BFS experiment.

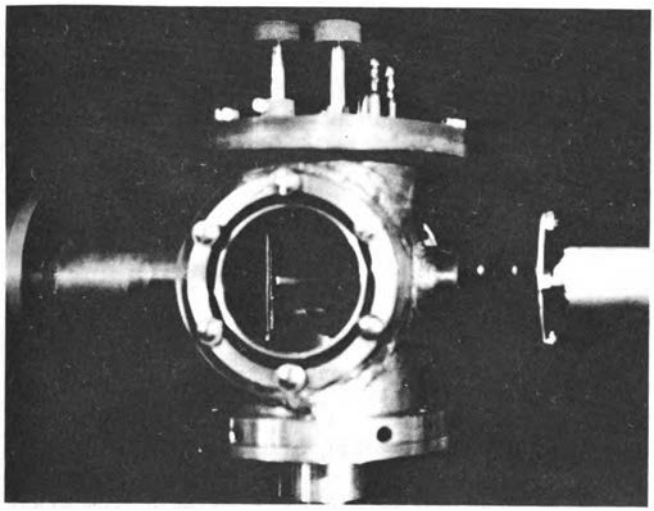

FIGURE 22. A beam of nitrogen, with an energy of 2 MeV, moves from left to right. On passing through a carbon foil (thickness $\sim$10 μg/cm^2), the nitrogen ions radiate light.

physics as well as instrumentation. Since the experiments can often be carried out by a single person, the student receives individual training in the traditional sense.

At a time when research budgets are being severely reduced, it is important that available facilities be used productively at minimum cost. While operating costs per man are relatively independent of the nature of an on-site laboratory research project, capital costs do vary widely. A total capital expenditure of about $75,000 is needed for the establishment of a well-instrumented BFS laboratory; if an accelerator is already avail-

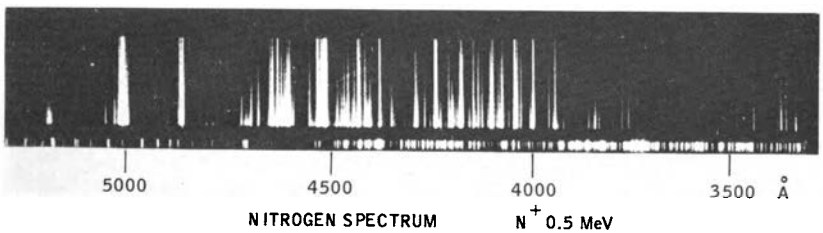

FIGURE 23. Intensity-wavelength distribution from a 0.5-MeV nitrogen beam. The beam is moving upwards and is spectroscopically analyzed with a stigmatic grating spectrograph with a reciprocal dispersion of 35 Å/mm (in second order). The long streaks of various lengths are the lines of interest. The short lines are from a comparison lamp (Fe–Ne).

able, the investment can be substantially reduced. This estimate assumes that the accelerator is a 2-MV electrostatic accelerator. However, much good work can be done with 100-keV machines, which require an even smaller initial outlay. Other equipment needed for BFS will be described later. Figure 24 illustrates the 2-MeV Van de Graaff Laboratory at the University of Arizona.

Summary of Experiments in Beam-Foil Spectroscopy

We begin with a summary of the kinds of experiments to which BFS is devoted.

WAVELENGTH-INTENSITY DISTRIBUTIONS

Basic to all BFS studies is the determination of the spectra of the emitted light.[4–12] Such data show which levels have been excited. With BFS tech-

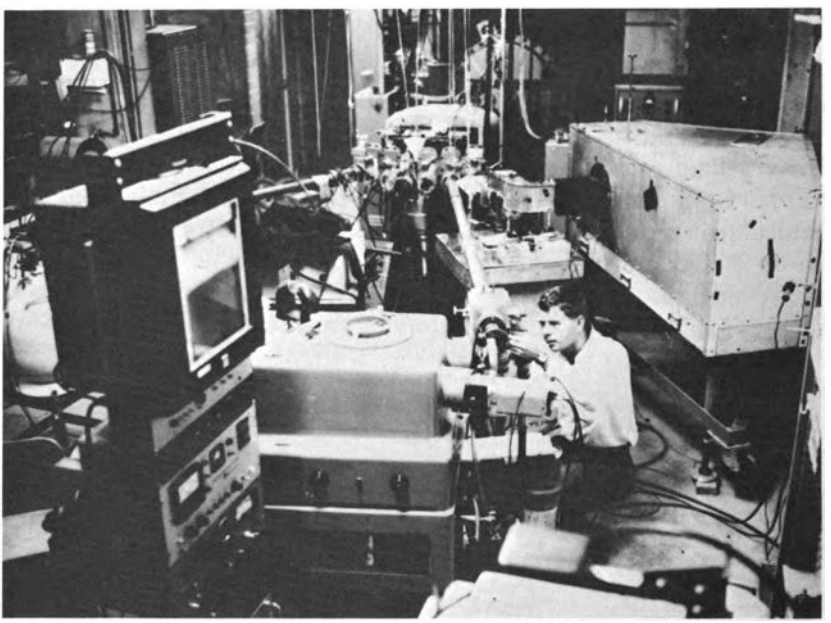

FIGURE 24. Photograph of University of Arizona 2-MeV Van de Graaff Laboratory. Professor W. S. Bickel is seen working on the target chamber for a McPherson, 1-m, vacuum uv, normal-incidence spectrometer. The irregular pentagonal box at the right houses the Meinel $f/0.8$ spectrograph. The beam-analyzing magnet can be seen behind the array of beam pipes. This laboratory, in which the accelerator is also housed, is rectangular, 30 ft wide $\times$ 50 ft long.

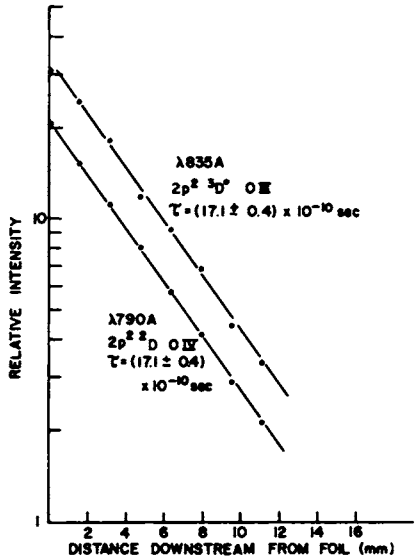

FIGURE 25. Data for the determination of the mean lives of the $2p^3\,{}^4D^\circ$ level in O III and the $2p^3\,{}^2D$ level in O IV. Note the short wavelengths of the detected radiations (from reference 20).

niques spectral lines have been generated which have never before been reported in the literature. These lines indicate the existence of hitherto unsuspected energy levels in monatomic systems.

MEAN LIVES

The place at which the excitations occur is well-defined, since the foil is thin. If a spectral line is isolated, either with a spectrograph or an interference filter, its intensity indicates the number of particles in a particular excited state. As the excited particles move downstream, the intensity of each line declines. Because the particle speeds are constant, the variation of intensity with distance is the same as the variation of intensity with time, and the former thus measures the time-dependence of the population of the decaying state. Simply stated, this means that measurements on the intensity of a spectral line versus distance can be directly interpreted in terms of the mean life of the parent state. Moreover, these measurements can be made for levels in highly ionized emitters and even where the associated radiations lie in the extreme ultraviolet; thus information can be obtained which few other methods can supply.[13–24] A typical result is shown in Figure 25.

CHARGE DISTRIBUTIONS

Generally speaking, the particles are accelerated as singly charged ions. However, they emerge from the foil with a spread of charges, the exact proportions in each charge state depending on the energy and nuclear charge of the incident beam. It is, of course, important to ascertain to which charge state an observed spectral line should be assigned. This can easily be done[25,28] by passing the beam through a transverse electric field, which separates the paths followed by particles in different charge states. The spectrum of the individual components can then be studied. An example of such splitting is shown in Figure 26.

It is sometimes of interest to know the charge distributions even without reference to spectroscopy. The electrostatic deflection method is an excellent way of determining those distributions. One result appears in Figure 27. Charge-state (and stopping-power) measurements are discussed also in Chapter 6.

SOLID-STATE EFFECTS

It seems likely that the light generated in a beam of given element and energy will show some dependence on the nature of the foil. If the ionization-excitation distributions depend on a collision between the incident particle and an electron in the foil, the degree to which the electron is bound may affect the results of the collision. Although the ion energy is

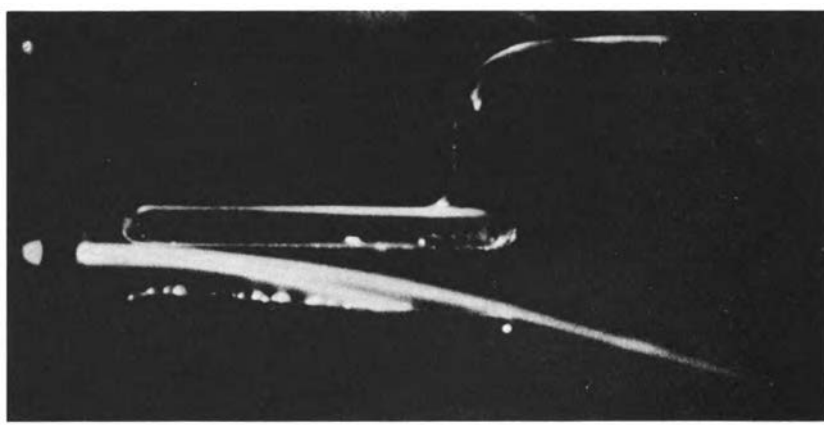

FIGURE 26. A nitrogen beam, with an energy of 1 MeV, passes from left to right through a transverse electric field of 70 kV/cm. The light radiated from N^+ and N^{2+} ions is readily identified. Note that each of these sources is absolutely free from any chemical or other contamination (from reference 25).

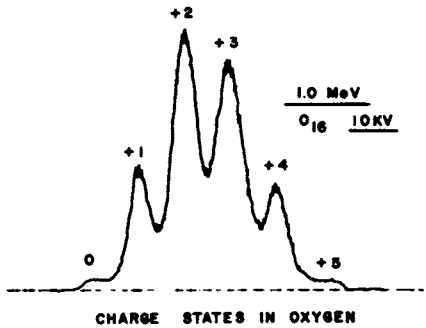

FIGURE 27. Charge distribution observed when O^+ ions, with an energy of 1.0 MeV, passed through a carbon foil. An electrostatic deflecting system similar to that of Figure 26 was used, but the field was much smaller. The voltage applied to the deflecting plates was 10 kV.

large in the laboratory system, the energy in the center of mass of a system consisting of the ion and an electron is rather small:

$$E_{\text{cm}} = \frac{m_e}{M_{\text{ion}} + m_e} E_{\text{ion}}. \tag{1}$$

Thus a 1-MeV oxygen ion corresponds to only 34 eV, so that electron-binding effects are apt to be substantial. The investigator might look for such effects by comparing foils made of metals and insulators (say, Be and B).

In addition, there could well be significant differences between amorphous and crystalline foils. For crystalline targets, channeling effects may appear in the light. Very few experiments along these lines have been done, and a wide-open field awaits the interested physicist.

GENERAL EQUIPMENT

In discussing how a BFS experiment is set up, it is convenient to begin with the ion source and follow the particles from there into the target chamber. It is assumed that the operation of the accelerator needs no discussion except for some features of the ion source.

THE ION SOURCE

A conventional electrostatic accelerator contains an rf ion source in which virtually any gas can be ionized, and from which ions can be extracted. The University of Arizona laboratory has accelerated H, D,

^{3}He, ^{4}He, C (as CH_4 and CO_2), N, O, F (as SF_6), Ne, Si (as SiH_4), S (as SF_6), Ar, Kr, and Xe. Beams of 0.5 μA or greater are obtained from the foregoing gases. In addition, the University of Arizona laboratory has accelerated Al and Fe by using Ar in a source but making the extraction canal of the metals mentioned. Here the extracted beams are $\sim 10^{-2}$ μA. Others have accelerated B and Cl (as BCl_3). (Nongaseous elements—Li, Na, K, Fe—have been extracted from other types of ion sources.) Thus a great variety of elements is available even though only the most common type of ion source is at hand. If the element to be studied can be used in gaseous form, perhaps as one component of a chemical molecule, the acceleration is easy to achieve.

BEAM ANALYSIS

The first real difficulty occurs when the beam comes out of the accelerator. The beam usually contains numerous elements in diverse chemical forms. Even hydrogen may appear as H^+, HH^+, and HHH^+; oxygen is often present as a contaminant, both as O^+ and O_2^+. When CO_2 is accelerated, C^+, O^+, CO^+, O_2^+, and CO_2^+ may be obtained at the very least. Sometimes, other combinations like H_2O^+ or NO^+ occur in sizable amounts.

It is obviously helpful to be able to select from the beam that particular part which is of interest in a proposed experiment. The Arizona group makes the selection with a magnetic analyzer. While such devices are common enough in accelerator laboratories, the use of heavy molecules demands a magnet of more than ordinary bending power. With the Arizona (horizontal) 2-MV Van de Graaff, the magnet has exit ports at 0°, $\pm 6.5°$, $\pm 15°$, and $\pm 25°$. At 25°, the mass-energy product* is 20, which means that the maximum energy that can be given to an ^{16}O beam at that angle is 1.25 MeV. On the other hand, the University of Arizona's (vertical) 6-MV Van de Graaff has been equipped with a magnet with a mass-energy product of 600 at 90°. Thus, the accelerator can be used at full energy for particles up to mass 100. The point is that the analyzing magnet should be powerful even if the accelerator has relatively low energy. For a 2-MV machine, a magnet with a mass-energy product of 50 or more at 30° is recommended. Of course, a smaller magnet can still be very useful, as has been demonstrated.

For a good magnet, the magnet current can be used as a reliable indi-

* The mass-energy product is ME/Z^2, where M is the particle mass (in atomic units), E is the particle energy (in MeV), and Z is the particle charge. Thus $MEP = 20$ means singly charged neon (mass 20) can be deflected at energies up to 1 MeV.

cator of the mass being deflected, but it is more satisfactory to measure the field itself. A proton moment gaussmeter is satisfactory for this purpose, but it is expensive (about $5000). The Arizona group has used a Rawson-Lush rotating-coil gaussmeter which costs about $1000. This instrument has the handicap that it cannot be on all the time because a rocker arm wears out and replacing it is a nuisance. Arizona also has a Varian temperature-compensated, Hall-effect gaussmeter which costs about $2500. It has the advantage over a proton moment gaussmeter of working at very small fields as well as at large fields and it is said to be good to $\pm 0.1\%$.

PARTICLE ENERGIES

The choice of particle energy is affected by several considerations. For example, the higher the energy, the higher the average charge of the foil-transmitted particles. Roughly speaking, the energy levels of highly ionized particles are more widely spaced than in particles of small net charge. Thus an increasing particle energy tends to put more of the radiation in the short-wavelength region, perhaps even in the vacuum ultraviolet or x-ray spectral ranges. On the other hand, some highly stripped ions (like Fe^{+14}) also yield visible light, and it is often interesting to look for long-wavelength emanations from very highly ionized particles.

For low-Z elements, like H and He, operation at energies above 300 keV and 1 MeV, respectively, leads primarily to fully stripped nuclei which have no interest to the spectroscopist. It is not uncommon to want to run at an energy below that for which the accelerator works well. In such cases, one can accelerate a strategically chosen molecule for the incident particle. Thus, an rf ion source, when a bit dirty, emits about one third of its ion output as H_3^+ when hydrogen is being used. Therefore, the acceleration of H_3^+ at voltage V yields atomic hydrogen projectiles each with energy $\frac{1}{3}$ eV. By using deuterium, the projectile velocity can be reduced by another factor of $2\frac{1}{2}$.

The foregoing examples can be extended, with some experimental complications, as follows. If CH_4^+ is accelerated, the hydrogen energy is 1/16 eV, where V is the operating voltage. By accelerating CO_2^+, the carbon and oxygen energies are 12/44 and 16/44, respectively, of the energy of the molecule.

It might be thought that intensity data could be better acquired for low particle speeds than for high speeds, since the particles then spend more time in front of the spectrograph slit. In reality, however, little control over the velocity may be possible, because the state of interest may not

be excited if the particle velocity is far from some particular value. The "best energy" to use in an experiment is that at which the observed intensity of the line(s) of interest is a maximum. Therefore, the "best energy" depends critically on the experiment under consideration, and no general value can be specified.

TARGETS

Carbon targets can be purchased from Oak Ridge or from Yissum Research Development Company, Administration Building, Hebrew University, Jerusalem, Israel. They can also be made by the experimenter. The Arizona group makes its own targets in order to have the capability of trying different materials. The method is best described by Dearnaley.[27] Maxman[28] also has a very helpful paper on target preparation.

A vacuum evaporator is needed to make a target. New microscope slides are coated with liquid soap or detergent, dried, and then polished with Kimwipes or soft cloths until the coating appears to have been completely removed. Pointed spectroscopic carbon rods, $\frac{3}{16}$ or $\frac{1}{4}$ in. in diameter, are held in contact by a light spring. The slides are mounted some 4–10 in. away from the juncture of the rods. At a pressure of $\sim 10^{-6}$ Torr, current sent through the rods causes the carbon to evaporate. A little experience is needed to find the best time and current factors for the desired thicknesses.

Carbon is the preferred target material because carbon foils are easy to make, relatively strong mechanically, and have a low enough Z to keep the Rutherford scattering small. However, the Arizona group has used Be and B as well. No systematic study has been made of the relative merits of different foil materials.

After evaporation, the slide is scratched into areas approximately $\frac{1}{2}$ in. $\times \frac{1}{2}$ in. and dipped into water. Individual pieces of carbon float freely away from the slide. The Arizona target holders have a $\frac{1}{4}$-in.-diameter hole in a $\frac{1}{32}$-in.-thick metal plate (Al, Cu, brass, and stainless steel all work well). A carbon piece is picked up on a holder and the target is ready for use.

Target life is a sensitive function of the element being accelerated, the particle energy, and the particle beam intensity. A carbon foil will withstand many hours of bombardment by 5 μA of 500-keV neon. In general, foil life increases as the particle energy is raised. At 4 MeV, beams of 1–2 μA of oxygen and neon have not destroyed the foils even after several days of bombardment.

The cause of foil breakage is not known, but it appears that it is not due to heating. For one thing, the pinholes and tears which develop do

not look like they are due to a heated foil. A group at Livermore has found that foil life is greatly increased if the foil is surrounded by a low-pressure gas. Bashkin has argued, in unpublished work, that foil damage arises from electrostatic forces due to the ejection of electrons from the target. Slight statistical fluctuations in the rate of electron ejection could prevent the instantaneous return of charge neutrality of the foil and thereby induce rupturing. When the foil is in a gas, there is always a ready supply of electrons present at every point of the foil surface so that the likelihood of foil breakage is reduced. It would be helpful to have reliable data on foil breakage.

Target foils also thicken as they are bombarded, and it is necessary occasionally to take this change into account in analyzing the data. The thickening comes from the deposition of carbon from the general hydrocarbon vapor which forms a component of the residual gas in the target chamber. The better the vacuum, the less the increase in target thickness.

TARGET CHAMBERS

Details of a typical target chamber are illustrated in Figure 28. This chamber is used for the wavelength range above 1800 Å. The windows are of quartz. A vacuum spectrograph can easily be coupled to such a chamber. The ambient pressure in the chamber is $<10^{-6}$ Torr.

The chamber may be used as shown when wavelengths are to be measured and also when lifetimes are to be determined from photographic data. However, photoelectric recording of lifetime data requires movement of either the foil or the detecting system. Both kinds of motion have been used, the choice depending primarily on the distances which must be traversed. When the foil is moved, it is also useful to move the

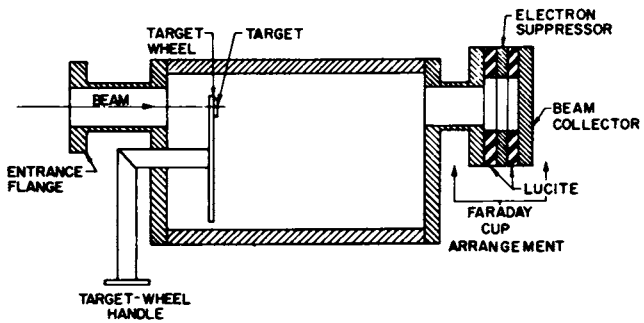

FIGURE 28. A typical target chamber.

Faraday cup to keep a constant separation of the particle collector and the target.

As is well known by nuclear physicists, the Faraday cup must not receive or lose electrons if there is to be a proper measure of the number of incident particles. One way of avoiding the electron problem is to bias a metal ring negative by ~300 V with respect to ground. The ring is between the target and the cup (see Figure 28) and must be so located that it cannot be struck by the beam.

SPECTROGRAPHS AND SPECTROMETERS

THE MEINEL SPECTROGRAPH The Meinel spectrograph (Figure 29) is a modified version of a Czerny-Turner spectrograph. The main modification is that a Schmidt camera replaces the usual second mirror. The

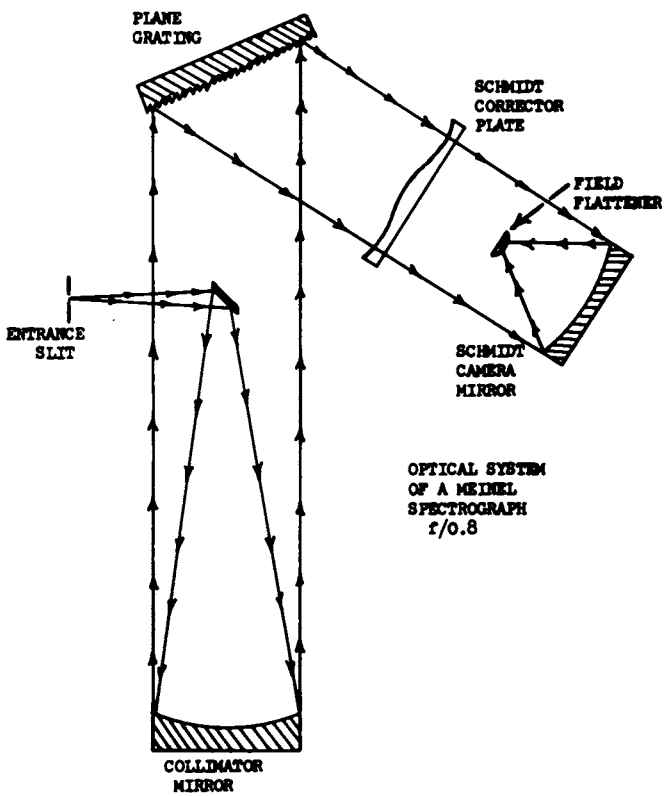

FIGURE 29. The Meinel spectrograph.

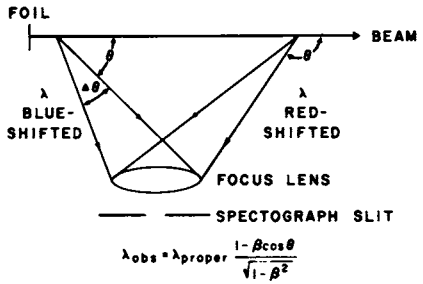

FIGURE 30. The origin of Doppler broadening in the beam-foil source. Note that the spectral lines will appear increasingly redder as the emitters move downstream from the foil. This effect can be seen in the slant of the lines in Figure 23.

camera is very fast—the Arizona instrument has $f/0.8$ and a 9-in.-diameter corrector lens. The focal length is short, which is mechanically convenient. In addition, the fold in the incident light path puts all elements on-axis, thereby reducing the aberrations of the off-axis Czerny-Turner arrangement.

The Meinel spectrograph is stigmatic, a most important property for BFS. This means that whatever intensity variation is present in the source lines is faithfully recorded on the detector plates. This, in principle, permits accurate determinations of wavelengths, relative line intensities, and mean lives. Moreover, information on perhaps 100 levels can be obtained in a single exposure. Of course, the measurements are beset by all the well-known difficulties of transforming plate densities into intensities. However, there is a special problem which arises from the high speed of the emitters.

In the situation illustrated in Figure 30 there is substantial, and continuously variable, line broadening because of the Doppler effect. One consequence is that the lines recorded with the Meinel spectrograph have widths of several angstrom units. Moreover, the on-axis system was achieved at the expense of various central obstructions, including the folding mirror and the plate holder. This introduces vignetting,[29] and a line which should have the shape shown in Figure 31(a) actually looks like that of Figure 31(b).

Clearly, the line broadening can be reduced by reducing the entrance aperture in the direction parallel to the particle beam, and the line-doubling effect can be eliminated by putting the aperture off-axis. An interesting fact is that these changes in geometry *do not affect the photographic speed of the camera,* and the line density on the plate is the same as when the full aperture is used. This improvement in line shape does

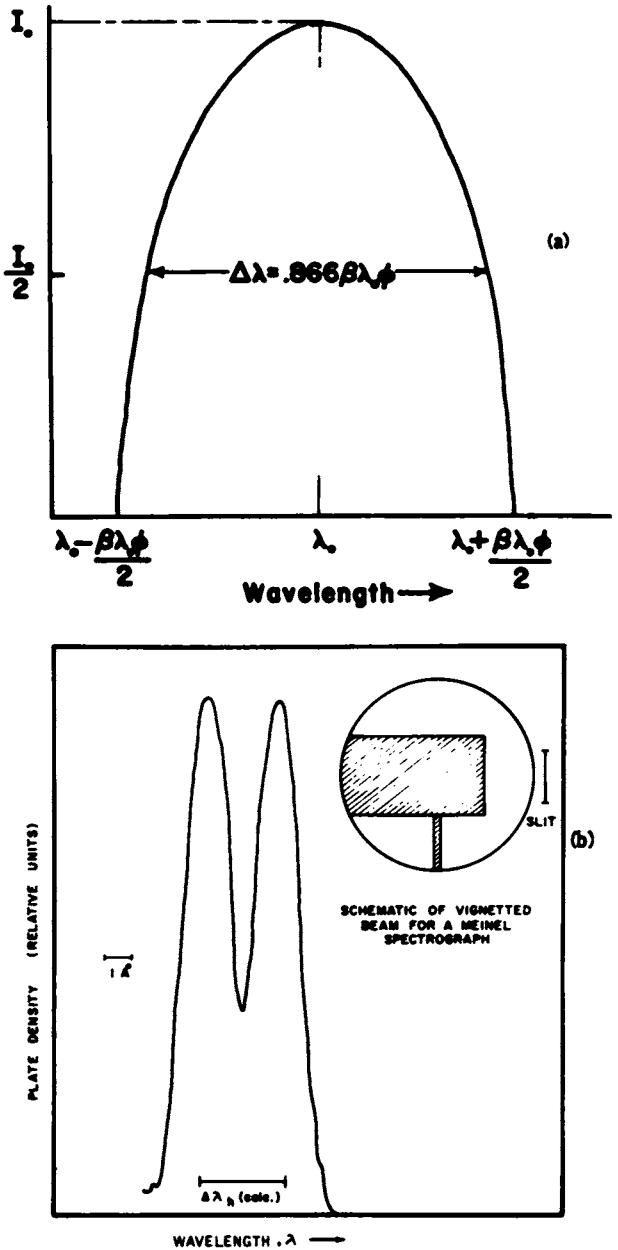

FIGURE 31. (a) Line shape as seen over angle $90 \pm \varphi$ to radiating beam direction. (b) Vignetted line shape due to central obstructions in Meinel spectrograph.

not occur without complications. Since the collimator is not completely filled, resolution is sacrificed—fortunately, this is not enough to be bothersome in practice. Various aspects of the vignetting problem are treated elsewhere.[30]

The Meinel spectrograph when built with uv quartz transmitting elements has a nominal wavelength range which extends upwards from 1800 Å. For the Arizona instrument, the reciprocal dispersion is 35 Å/mm in second order, and the wavelength range on the plate is ~1000 Å. The large number of reflecting surfaces causes a serious loss of light for wavelengths below 3000 Å, and no data have been obtained below 2500 Å with the Meinel. Wavelength calibration is achieved by focusing the light from a standard lamp (Fe–Ne is often used) on the slit through the same optical system as the beam light sees. A good measuring machine is needed to get wavelengths off the plate. A densitometer is also necessary for the determination of intensity variations either from line to line or along the length of a line.

There are two real drawbacks to the Meinel spectrograph. Insofar as is known, it is not commercially available but must be homebuilt, and it is also expensive. For the Arizona instrument, the grating cost alone is $3600. The Schmidt camera is also costly. Of course, the substitution of glass for uv quartz would reduce the expense considerably and would still give one a very good instrument. With glass, the short-wavelength cutoff is around 3300 Å, but many hundreds of spectral lines with wavelengths longer than 3300 Å can be detected. There is a great deal of work that can be done using glass optics.

THE PERKIN-ELMER SPECTROMETER Another instrument used by the Arizona group for wavelengths above 1800 Å is made by Perkin-Elmer Corporation (model No. 210-B) and has the immediate advantage over the Meinel of being available for purchase. Moreover, it employs photoelectric, rather than photographic, recording. By using available gratings, it is possible to work up into a wavelength region about 1 μ, although difficult order-sorting and detection problems must be faced. A 1440 line/mm grating permitting work primarily in first, second, and third orders is a good choice. With a photomultiplier like an EMR 541F, the detectable wavelengths lie between 2000 and 4000 Å, while a 1P21 permits extension of the range from 4000 to 8000 Å. Also, the 1P21 cuts out any second- or higher-order lines so that the observed lines are all in first order. This simplifies the order-sorting problem. Although the collimator is an off-axis paraboloid, the aberrations are small.

Various photomultipliers can be used depending on the wavelength

range to be studied. It is well worthwhile to obtain tubes which have low noise because the signals are rather weak.

With this instrument, as with all the photoelectric devices to be described, the entrance slit is illuminated with light from a short slice of the beam. Motorized rotation of grating provides a wavelength scan which can be calibrated by comparison with a standard source. A typical result is given in Figure 32. These data were obtained with ~ 1 μA of Ne at 4 MeV. The effective resolution can be gauged from Figure 32. The spectrometer, which is small in size and weight, has been mounted on a track, and lifetime data have been obtained[81] with it.

SEYA-NAMIOKA SPECTROMETER This device (Figure 33) was obtained from McPherson Instrument Company at a cost of about $15,000. It has a 0.5-m focal-length grating. It is a vacuum instrument and allows one to work between 300 Å and $\sim$5000 Å. A handicap is bad astigmatism. The device was set up so that the entrance slit viewed a short slice of the beam. With photoelectric recording, it was natural to make intensity measurements, and, in fact, lifetime work was done with that spectrometer.[18,15]

NORMAL INCIDENCE SPECTROGRAPH In the interest of somewhat higher speed and resolution, the Arizona group replaced the Seya-Namioka with a 1.0-m normal-incidence spectrograph which was bought from McPherson for about $26,500. It is used in much the same way as the S-N was, but it cuts out sharply at 500 Å on the short-wavelength side.

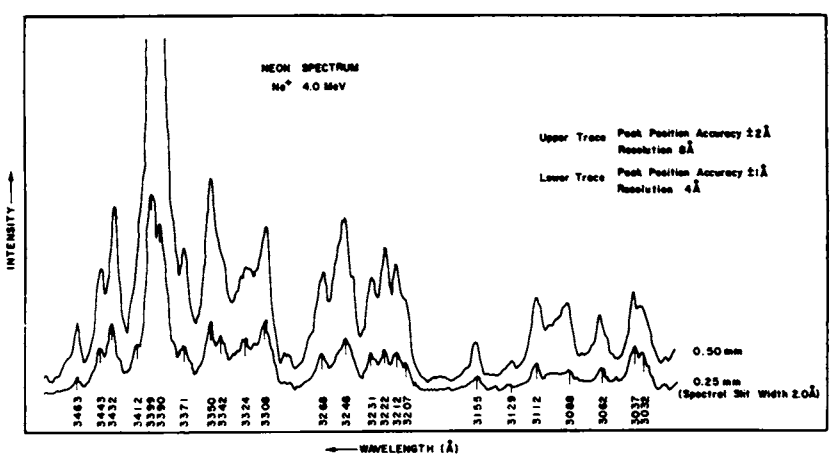

FIGURE 32. Neon lines as obtained from a 2-MeV neon beam analyzed with the Perkin-Elmer spectrograph. The figure incorrectly gives the energy as 4 MeV.

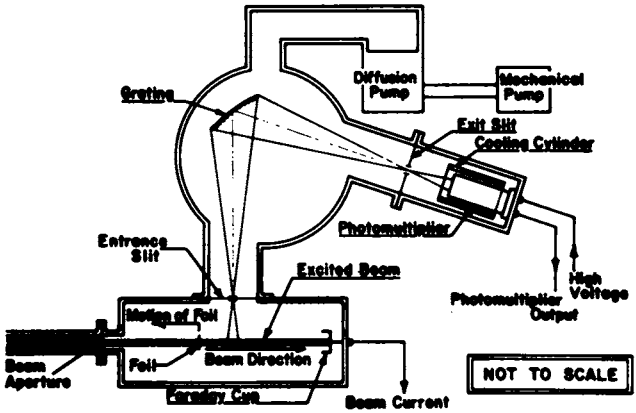

FIGURE 33. A Seya-Namioka vacuum spectrograph.

The aberrations are considerably smaller with this instrument than with the S-N.

Either of the last two instruments discussed above can be recommended as good vacuum instruments for BFS, especially for lifetime work.

GRAZING INCIDENCE SPECTROGRAPH With such a unit, it is possible to work with radiations as short as 100 Å. The wavelength range between 100 and 1200 Å is most interesting, in part because of possible relevance to the radiations in the solar corona and in part because of the new calculations of oscillator strengths for transitions of short wavelength. However, the instrumentation required is probably the most expensive of all. The units built at the Air Force Cambridge Research Laboratory,[4,17,18,21] are estimated to cost approximately $40,000. There is at least one commercial system, offered by McPherson, for approximately $30,000, but the Arizona group has not had any experience with it.

OTHER SPECTRAL INSTRUMENTS Sometimes, as in the case of the spectra from hydrogen and helium, a spectral line can be isolated with an interference filter and the light detected with a simple photomultiplier. Special tubes exist which are suitable for the detection of Lyman-α (1216 Å in H and dropping as Z^{-2} for other hydrogenic ions). Many important experiments can be carried out with such minimal equipment. For research on the interference of the fine-structure levels of hydrogenic systems, a low-energy accelerator ($\sim$100 keV) and a simple detecting arrangement are ideal.

The soft x-ray region can be examined with an x-ray spectrometer.

AUXILIARY APPARATUS The comparison of yields from different targets, for different bombardment times, or for changes in particle energy, requires some kind of beam monitor. The basic unit of reference is, naturally, the number of particles passing through the foil, but subsidiary reference units may be used in certain circumstances. A discussion of the several common monitoring techniques may be found elsewhere.[30] The following briefly describes the kinds of instruments needed for monitoring.

Since the beam is charged, the number of particles can be found by counting the total charge collected in the Faraday cup. This is done with a current integrator circuit, of which there are many varieties. The Arizona laboratory uses Elcor Model A309B current integrators. They cost approximately $1800 and are subject to annoying drifts and calibration errors. In proper condition, they are good to $\pm 1\%$.

There is a minor problem in measuring the absolute number of incident particles because of the charge distribution that develops when the particles go through the target. The charge distribution depends on the three familiar BFS parameters: the element being accelerated, the particle energy, and the nature of the foil. Hence, the charge distribution should actually be determined for every run that is made. This appears to be an awkward demand. A simple response can be made, as follows:

Let the beam current when the foil is out be I_o and the beam current when the foil is in be I_i. The number of particles entering the target chamber in time t is then,

$$N_o = \frac{Q_o}{e} = \frac{1}{e}\int_0^t I_o dt, \tag{2}$$

where e is the electronic charge. Then, as long as the incident particle current is reasonably steady,

$$Q_o = \frac{I_o}{I_i}\int_0^t I_i dt \tag{3}$$

and N_o is known. I_o, I_i, and $\int_0^t I_i dt$ should be measured for every run.

It is often satisfactory to monitor the light output itself. This may be accomplished with a photomultiplier which detects the integrated light intensity or with a filter–photomultiplier arrangement which accepts a narrow wavelength band. In either case, power supplies, amplifiers, and a digital recording unit are essential. A current integrator may be used as the recorder.

The foregoing treatment of photoelectric instruments has assumed that the tube current is of interest. However, pulse-counting is an alternative detection method which is often preferable. This is particularly so when

the light level is low, for in this situation the current integrator may introduce significant noise which is avoided with photon counting. The procedures to be followed for photon counting in such a case are detailed elsewhere.[32]

It was mentioned earlier that photographic recording necessitates use of a measuring machine and a densitometer. The Arizona group has access to a modified Hilger-Watts-Engis microdensitometer (courtesy Steward Observatory of the University of Arizona) and a Grant profile comparator (courtesy Kitt Peak National Observatory). Each of these is expensive (approximately $20,000 and $40,000, respectively). Collaboration among laboratories might be a fruitful way of reducing the investment any one group has to make.

Results and Further Research

WAVELENGTH-INTENSITY DISTRIBUTIONS

The data taken on nitrogen,[9] using the Meinel spectrograph, are shown in Figure 34. The figure is a densitometer tracing across the base of the photographic plate, the lines on which are shown in Figure 23. Comparison of the observed wavelengths with those in the literature permitted identification of a number of transition arrays. These appear along the line labeled A. At B are levels the decays of which were not detected, while at C are probable contaminants which were seen when N_2^+ (mass 28) was accelerated, the problem being that CO, also of mass 28, could have been present in the incident beam. (The contaminant lines vanished when the incident beam was N^+, with mass 14.) Three interesting features may be mentioned.

First, two of the prominent lines, designated by their wavelengths, cannot be reconciled with any known lines in any stage of ionization of nitrogen. In fact, no known level pairs can be connected by the new lines even if selection rules are disregarded. The wavelength uncertainty is conservatively estimated to be ± 1 Å, but the new lines are at least 3 Å away from any known lines.

The occurrence of previously unknown lines is a surprisingly common result of BFS. In nitrogen, the Arizona group has seen a dozen such lines. Sodium[10] has exhibited over 80 (of ~90 total lines seen), iron[12] has given ~150 (out of ~200), and other elements (oxygen,[5] neon,[33] sulfur,[34] for example), have also shown new lines. It is of obvious importance to catalog as many of these lines as possible and to calculate the level structures that are responsible for them.

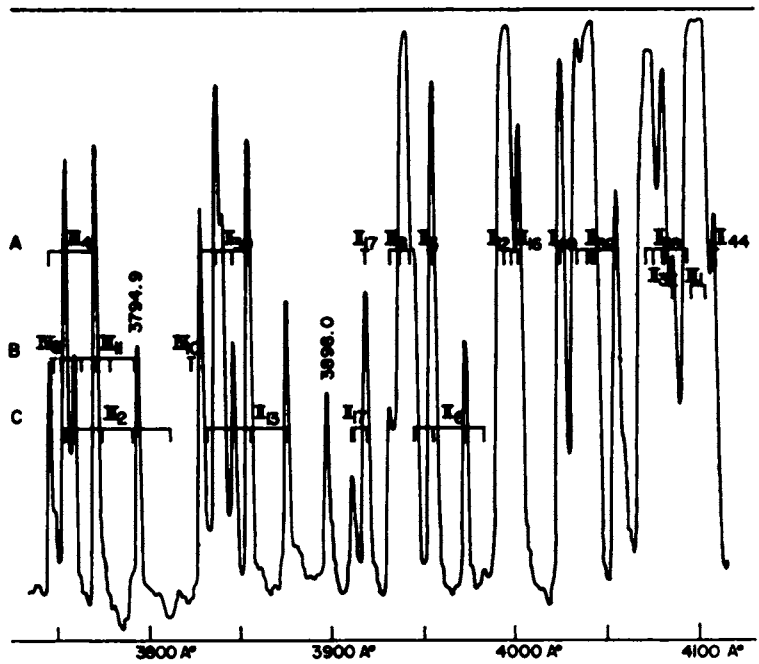

FIGURE 34. Densitometer tracing across the base of the lines shown in Figure 23.

The possible application of the new lines to the understanding of quasars should not be overlooked. Quasars are characterized by the appearance of spectral lines (in either emission or absorption) which cannot be directly recognized as the result of known transitions in any elements. However, the assumption that the quasars are receding from us at high speed causes a large red shift to be introduced into each spectral line. It is asserted[35] that a proper choice of red shift permits the association of the observed lines with well-known ones. Indeed, this association is used to deduce the speed of recession.

The beam-foil technique also gives hitherto unseen spectral lines, and it does not seem beyond all possibility that the quasar lines, like those in the beam-foil source, are due not to excessive red shifts but to unfamiliar excitation and/or de-excitation mechanisms in the astronomical object. In order to assess the possible connection between the beam-foil and quasar lines, it would be necessary to extend present knowledge of the new beam-foil lines. It must be kept in mind that some red shift is certain

to be present in the quasars so that a systematic effort to match the quasar and beam-foil lines would require using the red shift as a free parameter.

Second, the lines show a wide range of relative intensities. Since those intensities are related to the relative populations of the decaying levels and to the relative Einstein A-coefficients, it is possible to examine such matters as the level distributions produced in the beam-foil interaction and the validity of the one-electron approximation in describing level properties. Clearly, these points should be investigated as a function of the incident particle energy.

Third, there is a marked dependence,[5,12] not indicated in Figure 34, of the relative line intensities on particle energy. In comparing yields at one energy with those at another, account must be taken of the change in time for which the particles are viewed by the spectrograph. Only a few experiments of this nature have been published. Wavelength experiments have so far been carried out for restricted wavelength ranges for H, He, B, C, N, O, F, Ne, Na, Al, S, Ar, K, Fe, Kr, and Xe. Those experiments for the most part were conducted at a few bombarding energies below 2 MeV. Much work remains to be done.

Some qualitative answers may be given to the question of why the beam-foil source should contain spectral lines not seen in other sources. One important feature of the beam-foil source is that the excitation occurs in a time which is very short on an atomic time scale. Thus it takes $\sim 10^{-14}$ sec for the particles to pass through the foil and perhaps 10^{-16} sec to pass by a single foil atom. Under this condition, the uncertainty principle alone precludes the formation of well-defined energy levels. (For $\Delta t \sim 10^{-16}$ sec, the energy spread is ~ 10 eV.) Moreover, the possibility exists for the escalation of a particle in an excited state into a still higher level before the particle leaves the foil. These conditions simply do not exist in other kinds of sources.

Another point is that the decay of the excited systems takes place in a good vacuum in contrast to the situation in, say, a gaseous discharge. Therefore, a high cross section for collisional de-excitation could cause the "new" states to vanish nonradiatively in a discharge whereas they must radiate in the beam-foil source.

LIFETIMES

The variation in the line lengths in Figure 23 is a direct consequence of the finite lifetimes of the decaying levels. Indeed, Figure 23 displays more lifetime data than all of physics produced prior to the development of BFS. Since many of the excited levels occur in highly ionized species,

their mean lives are of particular interest, and the authors are not aware of any alternative technique for measuring them.

Only a few mean-life determinations have actually been reported to date, so there is great opportunity to add to a significant area of physics by working on mean lives. Moreover, the results are of immediate importance to astrophysics,[35–37] since the stellar abundances depend crucially on the (generally unknown) mean lives. For astrophysics, the interest is usually in the neutral or singly ionized species, although studies of the solar corona involve much higher stages of ionization.

Associated with, and somewhat easier than, the mean-life experiments are those on the branching ratios of excited states, that is to say, measurements of the relative intensities of the various spectral lines which a single level can emit. Little work has as yet been done on this problem.

Among the elements of especial interest are the rare earths. An ion source suitable for these elements would have to be built, but the rewards would more than compensate for that developmental effort.

CHARGE DISTRIBUTIONS

It is a curious fact that the charge distributions which have been measured directly differ substantially from those which can be inferred from BFS. A particular discrepancy is in the proportion of neutral particles in the foil-transmitted beam. The direct measurements show that a substantial fraction of the beam is neutral when the incident energy is low. On the other hand, BFS data fail to reveal any neutral emitters except for hydrogen and helium.

In this circumstance, it is desirable to repeat and extend experiments on the directly measured charge distributions as a function of particle energy and element. In the arrangement used to obtain Figure 27, the particle beam was separated into its several charge components by an electrostatic field. The components were detected with a Faraday cup or a tungsten-wire, secondary-electron emitter. Slightly better results could be obtained with a position-sensitive detector, although such detectors do not last very long with heavy ion beams. CsI crystals mounted on a photomultiplier also could be used. The "channeltron" (sold by Mallard) is another possibility.

Experiments of this kind are not hard to do, and they avoid all the complexities of spectroscopy. Nonetheless, they are of real importance to BFS and to other phases of physics, so they deserve careful attention. Some useful references are by Hall[38] and Phillips.[39] This is another area in which low-energy accelerators would be of particular utility.

EXTERNAL FIELDS

The charge-distribution experiments illustrate an attractive characteristic of BFS. Since the target chamber is at room temperature and ground electrical potential, external fields may easily be applied to the particles. Two different kinds of experiments have been done with such a field. In one, interference of the fine-structure states of hydrogen and He^+ was demonstrated[40,41] and compared with theory.[42] In the other, strong fields were applied[25,26] (as in charge distributions) to permit spectroscopic observations on emitters of net charge. This permits unambiguous and correct assignment of the ionization state from which each of the spectral lines originates. It is this latter type of experiment which is particularly recommended.

It should be recognized that these are the only known experiments ever carried out in which the charge of the emitter could be determined without any question whatsoever. This information is especially valuable in the analysis of the new spectral lines, and all those lines in nitrogen have been charge-identified by this technique. Of the various ways in which the split beams can be viewed, the one used in the first charge-splitting experiment[25] has the advantage that the charge analysis can be done satisfactorily even with a low-dispersion spectrograph. If the spectrograph looks in the plane of the split beams,[26] it is possible to detect the charge appropriate to emitters of very short mean life, but high dispersion is required.

Since few charge-determination experiments have been done, this represents another area in which virtually every element and bombarding energy can be studied productively.

It should be noted that only dc fields have so far been applied to the radiating beam. Undoubtedly, many experiments will be conducted using varying fields in a number of frequency ranges. Somewhat related experiments, involving the illumination of the particle beam with laser light or electrons, will also occur to the atomic physicist.

SOLID-STATE EFFECTS

It is reasonable to expect that the nature and thickness of the exciter foil play some role in the ionization-excitation distribution imparted to a given incident beam. However, few studies have been made of that role. It has been shown[43] that the intensity of the light is a function of foil thickness. It is also known that molecular and atomic hydrogen ions of the same speed do not experience the same interaction in a foil. On the

other hand, so simple a matter as the substitution of one element for another as the foil has not received serious attention.

Another matter which bears study is whether surface layers of strategically selected elements (like Li or Na) might substantially alter —perhaps enhance—the excitation distribution, although the ionization distribution may not be sensitive to such layers.[89] It is further apparent that the phenomenon of channeling ought to be looked at with BFS. While it is known that the foil-transmitted beam contains numerous electrons, the number–energy distribution has not been measured. It should be done for a variety of target foils.

Another intriguing experiment is to examine the spectral distribution when the foil is held at various temperatures. For example, cooling a semiconductor to make it behave more like an insulator, or heating it to put more electrons in the conduction band, might affect the resultant light output. If so, the light could serve as a tool for the study of the band structures of thin foils.

Experiments along the lines suggested in this chapter are rather uncomplicated, the principal difficulty being the assurance that the several targets all have the same absolute thickness. Probably the best way of checking the thickness is in terms of the energy loss suffered by alpha particles which are sent through the foils. This would entail use of a solid-state particle detector and a multichannel analyzer.

CAPITAL COSTS

A rough estimate of the capital investment which a sizable BFS program would require appears below. It will occur to the reader that a modest initial outlay will enable him to carry out many good experiments. The following list is in no sense the minimum; it covers the needs for a major effort.

	$ thousands
2-MV electrostatic accelerator	40
Beam-analyzing magnet	15
Spectrograph	15
Microdensitometer } Not needed for photoelectric	20
Comparator } recording of data	40
Phase-sensitive detector	2
Power supplies, photomultipliers, amplifiers, recorders, etc.	10
Current integrator	2

Because of the variation in available apparatus from laboratory to laboratory, it is unrealistic simply to add the foregoing numbers to get a total.

REFERENCES

1. S. Bashkin, A. B. Meinel, P. R. Malmberg, and S. G. Tilford, Phys. Lett. *10,* 63 (1964).
2. W. Wiese, Paper No. 18 in *Proceedings of the Conference on Beam-Foil Spectroscopy,* S. Bashkin, ed. (Gordon and Breach, New York, 1968).
3. R. Garstang, Paper No. 19 in reference 2.
4. S. Bashkin, L. Heroux, and J. Shaw, Phys. Lett. *13,* 229 (1964).
5. S. Bashkin, D. Fink, P. R. Malmberg, A. B. Meinel, and S. G. Tilford, J. Opt. Soc. Amer. *56,* 1064 (1966).
6. S. Bashkin, R. K. Wangsness, and L. Heroux, Phys. Rev. *151,* 87 (1966).
7. S. Bashkin, W. S. Bickel, H. D. Dieselman, and J. B. Schroeder, J. Opt. Soc. Amer. *57,* 1395 (1967).
8. A. Denis, J. Desesquelles, M. Dufay, and M. Poulizac, C.R. Acad. Sci. Paris *266,* 64 (1968).
9. U. Fink, G. N. McIntire, and S. Bashkin, J. Opt. Soc. Amer. *58,* 475 (1968).
10. L. Brown, W. K. Ford, Jr., V. Rubin, W. Trächslin, and W. Brandt, Paper No. 2 in reference 2.
11. M. Luther and A. Robeson, Paper No. 3 in reference 2.
12. W. Whaling, R. B. King, and P. L. Smith, Paper No. 24 in reference 2.
13. K. Berkner, W. S. Cooper III, S. N. Kaplan, and R. V. Pyle, Phys. Lett. *16,* 35 (1965).
14. A. S. Goodman and D. J. Donahue, Phys. Rev. *141,* 1 (1964).
15. W. S. Bickel and S. Bashkin, Phys. Lett. *20,* 488 (1966).
16. W. S. Bickel and A. S. Goodman, Phys. Rev. *148,* 1 (1966).
17. L. Heroux, Phys. Rev. *153,* 156 (1967).
18. L. Heroux, Phys. Rev. *161,* 47 (1967).
19. J. A. Jordan, G. S. Bakken, and R. E. Yager, J. Opt. Soc. Amer. *57,* 530 (1967).
20. W. S. Bickel, Phys. Rev. *162,* 7 (1967).
21. L. Heroux, Paper No. 11 in reference 2.
22. W. S. Bickel, Paper No. 12 in reference 2.
23. J. Desesquelles and M. Dufay, Paper No. 16 in reference 2.
24. E. L. Chupp, L. W. Dotchin, and D. J. Pegg, Paper No. 17 in reference 2.
25. P. R. Malmberg, S. Bashkin, and S. G. Tilford, Phys. Rev. Lett. *15,* 98 (1965).
26. U. Fink, J. Opt. Soc. Amer. *58,* 937 (1968).
27. G. Dearnaley, Rev. Sci. Instrum. *31,* 197 (1960).
28. S. H. Maxman, Nucl. Instrum. Methods *50,* 53 (1967).
29. L. C. Marquet, J. Opt. Soc. Amer. *57,* 878 (1967).
30. S. Bashkin, Appl. Opt. *7,* (Dec. 1968).
31. B. Curnutte, W. S. Bickel, R. Girardeau, and S. Bashkin, Phys. Lett. *27A,* 680 (1968).
32. L. Heroux, Appl. Opt. *7* (Dec. 1968).

33. B. K. Curnutte (unpublished).
34. S. Bashkin, W. S. Bickel, and B. Curnutte (unpublished).
35. See, e.g., C. R. Lynds, Paper No. 26 in reference 2.
36. L. H. Aller, Paper No. 21 in reference 2.
37. P. Swings and J. P. Swings, Paper No. 25 in reference 2.
38. T. Hall, Phys. Rev. *79*, 504 (1950).
39. J. A. Phillips, Phys. Rev. *97*, 404 (1955).
40. S. Bashkin, W. S. Bickel, D. Fink, and R. K. Wangsness, Phys. Rev. Lett. *15*, 284 (1965).
41. W. S. Bickel and S. Bashkin, Phys. Rev. *162*, 12 (1967).
42. R. K. Wangsness, Phys. Rev. *149*, 60 (1966).
43. W. S. Bickel, J. Opt. Soc. Amer. *58*, 213 (1968).

BIBLIOGRAPHY

Other publications known to us that deal with beam-foil spectroscopy are:

L. Kay, Phys. Lett. *5*, 36 (1963).
S. Bashkin, Nucl. Instrum. Methods *28*, 88 (1964).
S. Bashkin and A. B. Meinel, Astrophys. J. *139*, 413 (1964).
L. Kay, Proc. Phys. Soc. (London) *85*, 163 (1965).
S. Bashkin, Science *148*, 1047 (1965).
S. Bashkin and P. R. Malmberg, Proc. Phys. Soc. (London) *87*, 589 (1966).
L. Kay, Proc. Phys. Soc. (London) *87*, 591 (1966).
S. Bashkin and G. Beauchemin, Can. J. Phys. *44*, 1603 (1966).
J. L. Kohl, Phys. Lett. *24A*, 125 (1967).
S. Bashkin and K. S. Burton, J. Opt. Soc. Amer. *57*, 282 (1967).
W. S. Bickel, Appl. Opt. *6*, 1309 (1967).
A. Denis, C.R. Acad. Sci. Paris *266*, 1016 (1968).
W. S. Bickel, R. Girardeau, and S. Bashkin, Phys. Lett. *28A*, 154 (1968).
E. L. Chupp, L. W. Dotchin, and D. J. Pegg, Phys. Rev. *175*, 44 (1968).
S. Bashkin, Appl. Opt. *7*, 2341 (1968).
W. S. Bickel, Appl. Opt. *7*, 2367 (1968).
U. Fink, Appl. Opt. *7*, 2373 (1968).
L. Heroux, Appl. Opt. *7*, 2351 (1968).
W. L. Wiese, App. Opt. *7*, 2361 (1968).

CHAPTER 5

Atomic Lifetime Measurements

The beam-foil spectroscopy technique described in the preceding chapter provides a new and powerful tool for the measurement of atomic lifetimes, a problem of longstanding interest to physicists and especially astrophysicists. The ions emerging from the foil move with constant and nearly uniform velocity, and the lifetime of the radiating states can be determined by simply measuring the decrease in the transition rate or brightness downstream from the foil. Beam velocities are typically 10^7 to 10^9 cm/sec, so that lifetimes in the range 10^{-10} to 10^{-7} sec are accessible; these are typical lifetimes for dipole optical transitions. This method of lifetime measurement has one uniquely attractive feature: it is the only method applicable to highly charged ions.[1] In the following sections we take up the experimental method as it has been developed so far, its instrumentation and analysis, with special attention to those techniques, instruments, and references that are likely to be unfamiliar in accelerator laboratories, and conclude with a discussion of some measurements that are needed now.

Experimental Method

Consider an ion emerging with velocity v from the foil at $z=0$ in an excited state ψ_i. This state will decay in time, and in space, since $z=vt$:

$$|\psi_i|^2 \propto e^{-t/\tau_i} = e^{-z/v\tau_i}. \tag{1}$$

If N_i atoms emerge from the foil at $z=0$ in excited state ψ_i, the number surviving at a distance z behind the foil is $N_i(z)=N_i(0)e^{-z/v\tau_i}$, and the transition rate from ψ_i to any lower state ψ_j is proportional to $N_i(z)$. We

neglect for the moment transitions from higher states which repopulate ψ_i. To measure the lifetime τ_i one need measure only the z dependence of the radiation λ_{ij} emitted from a segment Δz of the glowing beam. Only one decay channel or wavelength λ_{ij} need be observed, and two wavelengths that blend need not be resolved so long as they come from the same upper state. Some sort of spectral analysis is necessary in order to isolate one wavelength λ_{ij} in the light emitted by the beam.

INSTRUMENTATION

Three methods of spectroscopic analysis have been used in the published lifetime measurements: spectrometers (or monochromators), narrow-band interference filters, and spectrographs. The first two employ photoelectric detectors which have the great advantage of a response linear in the photon flux. The spectrograph uses a photographic plate, a nonlinear detector difficult to use for quantitative flux measurements. On the other hand, the spectrograph has the advantages of spatial resolution and multichannel capability, recording many transitions at one time.[2] The foremost consideration in evaluating alternative instruments is the very low intensity of the light source, the fundamental limitation on the applicability of this method of lifetime measurement.

INTERFERENCE FILTERS

Interference filters have distinct advantages for those measurements to which they are applicable at all, i.e., wavelengths greater than 2000 Å and well separated from neighboring lines. With the optical system pictured in Figure 35, the beam image falls on the photocathode, and the segment Δz is defined by a mask on the face of the phototube. Note that the filter is placed in the parallel beam between the two lenses because the pass wavelength is a function of the angle of incidence. The pass wavelength can be tuned, decreased from its nominal value by as much as 2 percent, by tilting the filter. The acceptance angle is defined by the collimating lens, which need not be achromatic, and can be made quite large, limited only by the restriction that the Doppler broadening should be no greater than the passband of the filter. References 3 and 4 describe lifetime measurements made with an interference filter as the resolving element.

The counting rate for any detection system is proportional to the entrance aperture and the path length Δz that can be observed, and both of these factors impair the resolution and broaden the passband of the

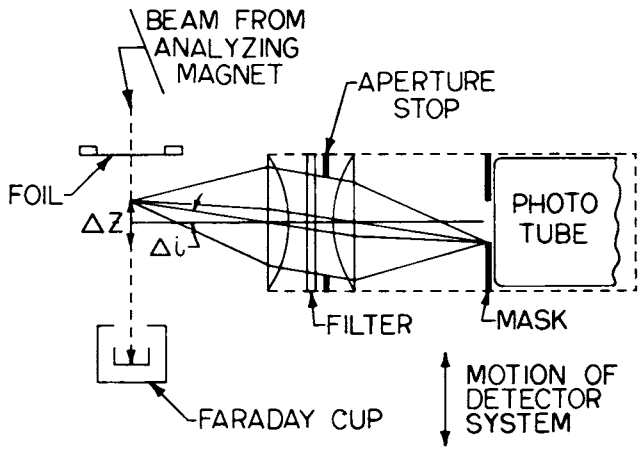

FIGURE 35. Typical experimental geometry for lifetime measurements with a filter to isolate a specific transition. The beam segment observed, Δz, is defined by the mask on the face of the photomultiplier tube. The angle of incidence, i, varies from center to ends of Δz. Aperture stop reduces scattered light from rays passing through outer edges of collimator lens.

detector. However, the filter is less sensitive to the variation in the angle of incidence Δi resulting from Δz than is the spectrometer or spectrograph. For the filter the transmitted wavelength λ varies with angle of incidence[5] as $d\lambda/di \propto -(\sin i)(\cos i)\lambda$, whereas for the diffracting instruments the corresponding quantity is $d\lambda/di \propto (\cos i)\lambda$. The factor $\sin i$ at small angles of incidence means that the filter can see a larger field of view without materially broadening the passband. This feature is especially attractive in measurements of long-lived transitions which are inherently weak because the decays are spread over a long path. Although this broad field of view and its compact size make the filter attractive for some measurements, it should be kept in mind that the filter alone is not sufficient: some other instrument is needed to ascertain that no other lines lie within the passband of the filter.

Narrow-passband interference filters are produced by many different suppliers[6] with a broad range of combinations of the significant parameters: center wavelength, passband width, peak transmission, and background or parasitic transmission. The pass wavelength varies from 2000 Å far into the infrared; passband widths vary from about 10 Å FWHM to several hundred angstroms. Peak transmission is typically 30 percent for filters incorporating metal films and 80 percent or more for the multilayer dielectric filters, which are available only for wavelengths of 4000 Å or longer.[5] Most suppliers evaporate to order; some[7]

also publish dated lists of surplus filters in stock which are much cheaper than the same filter when produced on order. Prices range from $30 to $300 for standard items.

THE SPECTROMETER

The spectrometer (or monochromator with photoelectric detector) is the most broadly useful and widely used resolving instrument for lifetime measurements. It can be used for wavelengths in the vacuum ultraviolet,[8] far beyond the cut-off of an interference filter, and it has been used to measure the lifetime of transitions separated by only 4 Å,[9] lines that cannot be resolved with present-day interference filters. The same instrument can be used to scan the spectrum prior to the lifetime measurement in order to see which decay channels are strongest and free from interference.

This high resolution is not attained without a corresponding reduction in aperture and counting rate, a serious concession in view of the weak source strength. A typical 1-m focal-length spectrometer with unity magnification and a grating of 1000 grooves/mm has an instrumental line-width or passband of 10 Å for a 1-mm entrance slit, and this line-width is proportional to the slit width. For reasons that will be made clear below, the long dimension of the slit must be placed normal to the beam direction so that the slit width defines the length of the beam segment Δz that can be observed. To achieve a passband less than 10 Å, the beam segment is limited to less than 1 mm, with consequent limitation on the counting rate. Furthermore, the acceptance aperture of commercial spectrometers is smaller than can be readily realized with a filter; $f/3.6$ is the fastest aperture ratio commercially available.

In scanning the spectrum with a spectrometer, a factor of 10 increase in counting rate can often be realized by orienting the entrance slit parallel to the beam, but this arrangement is not suitable for lifetime measurements. The beam undergoes small-angle scattering in the foil and diverges as it moves downstream; the light source expands and becomes less dense downstream from the foil. It is essential that the slit and the aperture of the spectrometer accept photons from all parts of this enlarged source. Otherwise, one would observe a decrease in the photon flux downstream from the foil that reflects acceptance geometry instead of the lifetime of the decay. For this reason the slit jaws are set parallel to the beam, and the slit width defines the beam segment Δz that is observed.

For wavelengths greater than 2000 Å, a lens can be used to focus an image of the glowing beam on the entrance slit of the spectrometer,

as in reference 10; for measurements in the ultraviolet, the slits are located close to the glowing beam with no lens in between as in Figure 36.[8]

For several reasons mentioned above, the counting rate obtained with the spectrometer is low, and it will often be desirable to count single photons with a photomultiplier tube cooled to reduce background. Morton[11] gives a helpful review of single-photon counting and of the causes and cure of background pulses from photomultiplier tubes. For the uv wavelength region, a variety of windowless photoelectric detectors and phototubes with special windows are available commercially.[12]

Both the spectrometer and the filter system require point-by-point measurements along the beam, and some means must be provided to allow for fluctuations of the beam current which could introduce variations from point to point that have nothing to do with atomic lifetimes. This normalization is usually provided by a detector at a fixed location, preferably near the foil where the beam is brightest, and the movable detector counts for that period during which the fixed detector is accumulating a preset number of photons. Ideally, the fixed detector would be sensitive only to the particular wavelength counted in the movable detector, although in most of the measurements reported so far, the monitor has been an unfiltered photomultiplier. Alternatively, the beam current can be integrated in a cup downstream from the foil. This latter method assumes that the charge-state distribution and the distribu-

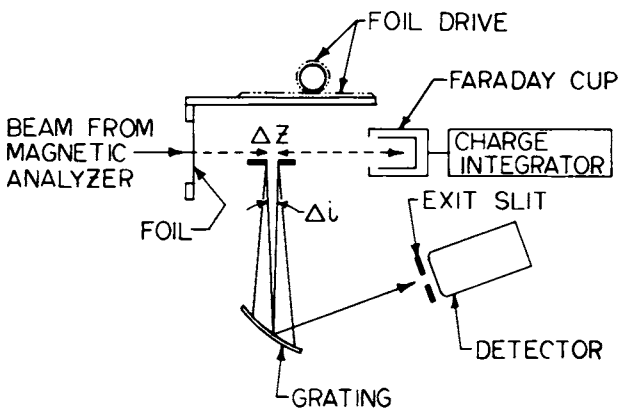

FIGURE 36. Typical experimental geometry for lifetime measurements with a monochromator. No lenses or windows are used, and this geometry is used for measurements in the vacuum ultraviolet. Full widths of the entrance slit contribute to the passband of the monochromator. In the figure, the jaws of both slits are normal to the plane of the paper.

tion of excited states remain constant in spite of the changes taking place in the foil during bombardment. Furthermore, the integration of heavy-ion beams introduces difficulties not present with proton and alpha-particle beams.[13] Beam-current normalization is therefore less direct than monitoring the light emission at a fixed location, but it has been used successfully in several experiments.[8,9,14]

SPECTROGRAPHS

Photographs of the glowing beam made with a spectrograph (see Figure 23, page 79) furnish striking evidence of the finite life of atomic states and immediately suggest the use of a spectrograph for lifetime measurements. The spectrograph has several advantages to recommend it: it collects data at a rate many orders of magnitude faster than the spectrometer or filter, since all wavelengths and all positions along the beam are recorded simultaneously. Furthermore, beam fluctuations cannot affect the measurements, and the beam need not be monitored precisely as in point-by-point measurements. Data can be accumulated over several days if desirable. Unfortunately, these impressive advantages are offset by the difficulty of quantitative photometry with photographic plates. Photographic plates have low efficiency and, more serious, are nonlinear in integrated photon flux density and nonlinear in time. Since the photographic emulsion responds to flux per unit area incident on the emulsion, and since the ion-beam radiation is usually very weak, the spectrograph must have a large aperture, a short-focal-length camera, and consequently, low dispersion. Furthermore, fast emulsions with their inevitable coarse grain must be employed.[15] The small-scale spectrograms and the coarse grain add materially to the imprecisions of photographic photometry. However, for accurate measurements of wavelengths which are necessary if the numerous previously unobserved lines appearing in ion-beam spectra are to be classified, conventional spectrographic methods using photographic plates may have the advantage.

Lifetime measurements require the photography of an extended source, and the spectrograph must be free from astigmatism and vignetting. The spectrograph is oriented so that the beam, or an image of the beam, falls along the position of the entrance slit, and the entrance slit is then removed. Two experiments have been reported in which lifetimes have been derived from photographs: Fink *et al.*[16] have made measurements on nitrogen beams with a fast Meinel spectrograph, and Brown and his colleagues[17] have made measurements on a sodium beam with a spectrograph employing an image tube in the focal plane of the spectrograph. In neither of these experiments was the photometry

sufficiently precise to permit correction for the cascading transitions, to which we will return below. There is a great need for a linear detection scheme that will permit the spectrograph to realize its tremendous data-collecting and data-storing potential.

Data Analysis: Cascading

The population $N_i(z)$ of the state ψ_i not only decreases by radiative decay but is augmented by transitions into state ψ_i from higher states ψ_x:

$$\frac{dN_i}{dt} = -\sum_j A_{ij}N_i + \sum_x A_{xi}N_x, \tag{2}$$

where A_{ij} is the spontaneous transition probability from state ψ_i to state ψ_j, and $\sum_j A_{ij} = 1/\tau_i$. If the population $N_x(t)$ of an upper state decays with lifetime τ_x, $N_x(t) = N_x(o)\ \exp(-t/\tau_x)$, then the population of the state ψ_i becomes

$$N_i(z) = N_i(o)e^{-z/v\tau_i} + \sum_x A_{xi}N_x(o)\left(\frac{e^{-z/v\tau_x} - e^{-z/v\tau_i}}{1/\tau_i - 1/\tau_x}\right). \tag{3}$$

Further terms will be added to this sum (a) if the upper states themselves are repopulated by transitions from still higher levels, and (b) if the passband of the detector includes wavelengths for additional transitions of different lifetime. This latter possibility has been observed frequently,[3,4] but the first one has not yet been identified.

The observed decay curve $I(z,\Delta z)$ is proportional to the number of photons λ_{ij} emitted in the interval z to $z+\Delta z$:

$$I(z,\Delta z) \propto \int_z^{z+\Delta z} \frac{A_{ij}}{v} N_i(z)dz = A_{ij}\tau_i N_i(o)e^{-z/v\tau_i}(e^{-\Delta z/v\tau_i} - 1)$$

$$+ A_{ij}\sum_x \frac{A_{xi}N_x(o)}{1/\tau_i - 1/\tau_x}[\tau_x e^{-z/v\tau_x}(e^{-\Delta z/v\tau_x} - 1) - \tau_i e^{-z/v\tau_i}(e^{-\Delta z/v\tau_i} - 1)]. \tag{4}$$

In general, the shape of the decay curve depends on Δz, but in two common cases Δz appears only as a multiplicative factor.

1. If Δz is small compared to $v\tau_i$ and $v\tau_x$, the exponentials in Δz can be expanded to yield the approximation $I(z,\Delta z) \propto (A_{ij}/v)\ \Delta z\ N_i(z)$. This expression for small Δz can be rewritten $I(z,\Delta z) \propto (A_{ij}/\sum_j A_{ij})$ $(\Delta z/v\tau_i)\ N_i(z)$. The factor $\Delta z/v\tau_i$ reduces the yield for long-lived states

in a spectrum scan and must be taken into account when comparing the relative observed yield of different transitions to extract the branching ratio $(A_{ij}/\sum_j A_{ij})$, as has been emphasized by Heroux.[8]

2. When cascading, represented by the second term in $I(z,\Delta z)$, is negligible, the shape of the decay curve is independent of Δz no matter how large $\Delta z/v\tau$ is.

The decomposition of the sum of exponentials $I(z,\Delta z)$ to yield τ_i, and in addition as many values for the τ_x, $N_i(o)$, and $N_x(o)$ as possible, is the basic problem in the analysis of beam-foil lifetime measurements, and it is clearly a formidable one. Information about the initial populations will provide the clues to understanding the excitation mechanism, which in turn will enable one to estimate initial populations and design experiments with minimum interference from cascading transitions. Several authors have developed computer programs for this calculation, and at least two programs have been made available for use by others.[18,19] Jordan *et al.*[3] have been able to extract as many as four terms from their measurement on He II with an uncertainty which they estimate at 6 percent. Every author who has attempted this analysis stresses the necessity for accuracy in the decay-curve measurements if the sum is to be decomposed at all. It is this necessity for precision that would seem to favor a counting experiment, with good statistics, over a photographic measurement of the decay curve.

Machine computation has been widely used, but simple graphic methods are often adequate. Heroux[8] describes fully an example of graphical analysis of a N IV decay curve, from which he extracts two exponential terms plus a constant background. His analysis also illustrates the advantages of measuring several decay curves for other transitions from upper states which can cascade into lower states of interest; a system of interrelated transitions can often be unraveled when a single transition cannot.

Fortunately, many decay curves show only a simple single exponential decay. This situation occurs when:

1. $A_{xi}N_x(o) \approx 0$: higher states are weakly populated or do not decay into the state ψ_i. For example, if ψ_i is so highly excited that higher ψ_x decay by autoionization.

2. $\tau_x/\tau_i \ll 1$, in which case all cascading is crowded in close to the foil and is negligible throughout the main range of the decay curve. Initial slope may be positive in this case.

3. $\tau_x/\tau_i \gg 1$, in which case $I(z,\Delta z)$ can be written, assuming $\Delta z/v\tau$ small for simplicity,

$$I(z,\Delta z) = \frac{A_{ij}}{\Sigma A_{ij}} \frac{\Delta z}{v\tau_i} N_i(o) e^{-z/v\tau_i} + \sum_x \frac{A_{xi}}{\Sigma A_{xi}} \frac{\tau_i}{\tau_x} N_x(o) (e^{-z/v\tau_x} - e^{-z/v\tau_i}) \quad (5)$$

and the second term will be negligible when $\tau_x/\tau_i \gg 1$.

When a single exponential is observed, the identification of this τ_i with the upper state in the observed transitions, instead of a higher cascading state, is usually based on appeal to theoretical estimates or on measurements of the decay for the higher states.

The analysis of the decay curves requires a knowledge of the beam velocity, which is usually determined by subtracting the estimated energy loss in the foil from the known initial beam energy. Velocity determinations by Doppler shift have not been reported. Foil thickness can be determined by weighing a known area, and the energy loss can be computed from the experimental measurements summarized by Northcliffe,[20] or for ion energies less than 20 keV/AMU, the theoretical expressions of Lindhard *et al.*[21] may be used. Northcliffe's summary also includes information on equilibrium charge-state distributions which is useful in choosing a beam energy for maximum yield of the particular ion desired. Since $I(z,\Delta z) \propto 1/v$, it may be advantageous to use a beam energy below that at which the desired ion fraction is maximum.

Ion Sources

Most of the beam-foil spectroscopy experiments in the literature have made use of the conventional rf ion source, and the choice of ions studied so far has been limited to those that can be produced from an rf ion source with gaseous feedstock. The rf source will be familiar to most readers of this report and will not be discussed further.

Ion sources for solid materials are less common. Lithium sources have been described[22] for use in nuclear research but are not at present available commercially. For other solid materials, the ion sources developed originally for atomic scattering are compact and well-suited to installation in the terminal of an electrostatic accelerator. In all these sources, the solid is heated to a temperature at which its vapor pressure is about 1 μ, and the vapor is then ionized by electron impact as in a conventional diode source. All these sources can be used interchangeably for gases or solids.

Magnuson *et al.*[23] have described a source that produces tens of micro-

amperes of Al^+, Zn^+, Cu^+, Ag^+, and Fe^+ and operates at a maximum temperature of 1600°C. Maximum power consumption is about 1 kW, and a dielectric liquid is circulated between the high-voltage terminal and a heat exchanger at ground potential to carry away the heat. The paper also includes a review of other types of ion sources for solid materials.

Fite and his colleagues[24] have described a smaller modification of the Magnuson source that uses less power and is air-cooled. As used by Fite, this source delivers only nanoamperes of current (U^+, Sr^+, Ba^+, Te^+, Be^+), but it should be able to deliver larger currents by enlarging the extraction aperture and increasing the electron arc current. As long as carbon foils are used to strip and excite the beam, beam currents larger than a few microamperes are not useful, especially for high-Z ions.

The sources designed for use with isotope separators[25] deliver very large currents of practically all elements, but they are rarely small enough to fit in the terminal of an accelerator, and they are often designed to produce molecular rather than atomic ions. The source designed for the Copenhagen isotope separator is compact enough to fit in an accelerator and is now available commercially.[26] Similar in principal to the sources mentioned above, it is carefully designed for high efficiency and currents approaching a milliampere. With 900 W of heater power, the furnace reaches 1100°C. To produce beams of refractory elements, compounds of higher vapor pressure are used, and the manufacturer claims that 80 percent of the beam is $(atom)^+$ with molecular feedstock.

Some Needed Lifetime Measurements

The interest in atomic lifetimes stems from their use in analyzing the composition of stars, the interstellar medium, and terrestrial plasmas. The measurements that one would list as most needed depend upon the particular application and interest. Garstang[27] has discussed astrophysical needs that can be attacked by the beam-foil method. To quote from his paper:

> Ions which are worthy of study include almost all stages of ionization of C, N, O, Ne, Na, Mg, Si, S, Ca, Fe, Ni. . . . If asked to pick out one group that would be more useful than any others, I think I would say that one should select all stages of ionization of iron, and try to determine the transition probabilities of the lines connecting the ground configuration with the first three or four excited configurations, and the transition probabilities for the lines connecting these excited configurations. I think I would give second priority to various lines of silicon, and after that to the stronger lines of carbon, nitrogen, and oxygen. . . . Further work is badly needed on the transition probabilities of lines involving highly excited states of important

elements, particularly Fe I and other transition group elements. . . . Another area of importance for traditional spectroscopy is in the lines of the rare earths. . . .

Garstang also lists specific transitions that are important in judging the validity of various approximations used in theoretical calculations. He also notes the increasing interest in the far ultraviolet spectrum.

Bahcall[28] has compiled a list of 114 lines of particular importance in the interpretation of quasar absorption spectra for which reliable transition probabilities are needed. Of the 114 lines, 101 are in the uv wavelength range between 900 and 1900 Å.

Aller[29] tabulates and assesses the reliability of f-values used in the determination of the abundance of all elements observed in the sun: nearly half of these f-values he judges "doubtful" or "poor," nearly two thirds of them are estimated theoretically, since experimental measurements are not available. Aller's book includes a complete discussion of abundance measurements in stars and nebulae and a good review of the availability of the atomic transition probabilities needed for this analysis.

Glennon and Wiese[30] have compiled a bibliography of the literature on transition probabilities, both theory and experiment, that is indispensible to those interested in this field. In addition to the primary literature on particular values, they list review articles, critical summaries, and compilations. They summarize the over-all availability of atomic transition probabilities as follows:

From the compilation it may be seen that for a few of the 92 natural elements no material is available. For many other elements data exist only for the neutral atom and the first stage of ionization. Furthermore, the number of transitions treated is often quite small, and sometimes only the transition probability for the resonance line or for forbidden transitions are available.

Wiese and his co-workers at the National Bureau of Standards are making a critical compilation of all measured and calculated values of atomic transition probabilities. Their review of the region $Z=1$–10 has been published,[31] and work on higher values of Z is in progress. Their critical comparison of different values makes use of the fact that transition probabilities between corresponding levels in an isoelectronic sequence follows a smooth functional dependence on Z, $f(Z)$, just as the term values do. They are thus able to compare measured or calculated lifetimes for a particular transition in one ion with the corresponding lifetime in other ions. On the basis of their survey of the first ten elements, they find that measurements of transitions between low-lying levels would be useful from the point of view of establishing the shape

of the function $f(Z)$ for complex configurations. The following transitions are especially important, since theoretical treatments have not as yet been successful for these cases because of strong configuration interaction:

$2s^2\ 2p\ ^2P - 2s^2\ 3s\ ^2S$ transition in B I (2497 Å), C II (858 Å), N III (452 Å), O IV (279 Å), and Ne V (174 Å)
$2s^2\ 3s\ ^2S - 2s^2\ 3p\ ^2P$ transition in B I (11661 Å), C II (6579 Å), N III (4099 Å), O IV (3066 Å)
$2s^2\ 2p\ ^2P - 2s\ 2p^2\ ^2P$ transition in B I (1378Å), C II (904 Å), N III (685 Å), O IV (554 Å)
$2s^2\ 2p\ ^2P - 2s\ 2p^2\ ^2S$ transition in B I (1537 Å), C II (1036 Å), N III (764 Å), O IV (609 Å)
$2s^2\ 2p^2\ ^3P - 2s\ 2p^3\ ^3P$ transition in C I (1329 Å), N II (916 Å), and O III (703 Å)

It should be noted that most of these wavelengths lie in the far ultraviolet. Note also that nearly all the beams needed for these measurements can be produced with an rf ion source. As Wiese extends his analysis to higher values of Z, he will certainly be able to point out further measurements that are critical in guiding and assisting the theoretical calculation and resolving discrepancies.

References and Notes

1. For a review of other methods of measuring atomic transition probabilities, see E. W. Foster, Rep. Progr. Phys. *27*, 469 (1964).
2. See A. Girard and P. Jacquinot, "Principles of Instrumental Methods in Spectroscopy," in *Advanced Optical Techniques*, A. C. S. Van Heel, ed. (John Wiley & Sons, Inc., New York, 1967), Chap. 3, for a discussion of the relative merits of spectrometers and spectrographs.
3. J. A. Jordan, Jr., G. S. Bakken, and R. E. Yager, J. Opt. Soc. Amer. *57*, 530 (1967).
4. A. S. Goodman and D. J. Donahue, Phys. Rev. *141*, 1 (1966).
5. Those not familiar with this relatively new optical device will find a brief introductory discussion in the *AIP Handbook of Physics*, pp. 6–133, and a thorough treatment in F. Ables, "Optics of Thin Films," in *Advanced Optical Techniques*, A. C. S. Van Heel, ed. (John Wiley & Sons, Inc., New York, 1967), Chap. 7.
6. The Optical Industry and Systems Directory, Seven North Street, Pittsfield, Massachusetts 01201, is an annual publication listing suppliers of interference filters as well as other optical components.
7. Bausch & Lomb, Inc., Rochester, New York 14602; Optical Coating Laboratory Inc., P. O. Box 1599, 2789 Griffen Ave., Santa Rosa, California 95403; Baird-Atomic, Inc., 33 University Rd., Cambridge, Massachusetts 02138.

8. L. Heroux, Phys. Rev. *153,* 156 (1967).
9. A. Denis, J. Desesquelles, M. Dufay, and M. C. Poulizac, C. R. Acad. Sci. Paris *265,* 471 (1967).
10. S. Bashkin, D. Fink, P. R. Malmberg, A. B. Meinel, and S. G. Tilford, J. Opt. Soc. Amer. *56,* 1064 (1966).
11. G. A. Morton, Appl. Opt. *7,* 1 (1968).
12. J. A. R. Sampson, *Techniques of Vacuum Ultraviolet Spectroscopy* (John Wiley & Sons, Inc., New York, 1967).
13. H. M. Loebenstein, D. W. Mingay, H. Winkler, and C. S. Zaidins, Nucl. Phys. *91,* 481 (1967).
14. K. Berkner, W. S. Cooper III, S. N. Kaplan, and R. V. Pyle, Phys. Lett. *16,* 35 (1965).
15. The Eastman Kodak Co. has recently put on the market plates which are especially sensitive under conditions of very low intensities and long exposure times. Two emulsions, Type Ia-O (blue sensitive) and Ia-E (panchromatic), are available. See Kodak Bulletin P-9, "Plates and Films for Science and Industry" (1967).
16. U. Fink, G. N. McIntire, and S. Bashkin, J. Opt. Soc. Amer. *58,* 475 (1968).
17. L. Brown, W. K. Ford, V. Rubin, W. Traichslen, and W. Brandt, *Proceedings of the Beam Foil Spectroscopy Conftrence, University of Arizona,* 1967 (Gordon and Breach, New York, 1968).
18. F. Grard, University of California Radiation Laboratory Rep. UCRL 10153, TID-4500, 17th ed. (unpublished).
19. P. R. Rogers, MIT Laboratory for Nuclear Science Tech. Rep. No. 76 (1962) (unpublished).
20. L. C. Northcliffe, Ann. Rev. Nucl. Sci. *13,* 67 (1963).
21. J. Lindhard, M. Scharff, and H. E. Schiott, Kgl. Dan. Vidensk. Selsk. Mat. Fys. Medd. *33,* No. 14 (1963).
22. E. Norbeck, Phys. Rev. *105,* 204 (1957).
23. G. P. Magnuson, C. E. Carlston, P. Mahadevan, and A. R. Comeaux, Rev. Sci. Instrum. *36,* 136 (1965).
24. Layton, Stebbings, Brackman, Fite, Ott, Carlston, Comeaux, Magnuson, and Mahadevan (unpublished). May be obtained by writing W. L. Fite, Physics Department, University of Pittsburgh. Also Fite, Layton, and Stebbings, "Experimental Studies of Heavy Ion Exchange in Air," Air Force Weapons Laboratory Tech. Rep. No. AFWL-TR-65-181 (GA-6738), General Atomics Division, General Dynamics Corporation, Dec. 9, 1965 (unpublished).
25. The first nine papers in Vol. 38 of Nucl. Instrum. Methods (1965) describe recent ion sources for mass separator use.
26. K. O. Nielsen, Nucl. Instrum. Methods *1,* 289 (1957). An improved version of this source is available from Physicon Company, P. O. Box 232, Boston, Massachusetts 02114.
27. R. H. Garstang in *Proceedings of the Beam Foil Spectroscopy Conference, University of Arizona,* 1967 (Gordon and Breach, New York, 1968).
28. J. N. Bahcall, Astrophys. J. (1968) (in press).
29. L. H. Aller, *The Abundance of the Elements* (Interscience Publishers, Inc., New York, 1961).
30. B. M. Glennon and W. L. Wiese, NBS Misc. Publ. No. 278 (1966).
31. W. L. Wiese, M. W. Smith, and B. M. Glennon, *Atomic Transition Probabilities,* Vol. 1. *Hydrogen Through Neon,* NSRDS-NBS 4 (1966).

Part III

SOLID-STATE PHYSICS

Overlap between the fields of nuclear physics and solid-state physics has grown rapidly in recent years, as solid-state physicists have increasingly recognized the usefulness of nuclear particles as probes of the properties of solids and as nuclear physicists have increasingly recognized the importance of solid-state effects in their targets and particle detectors. This overlap of interest is discussed in this part of the report on the uses of low-energy accelerators from the standpoint of the solid-state physicist.

A division has been made into five major sections. The first (Chapter 6) deals with general questions of energy loss and penetration of particles with energies in the keV to MeV range into amorphous and crystalline solids. This subject, perhaps surprisingly, is not closed, but presents a number of stimulating and challenging unresolved problems. The second section (Chapter 7) treats a very new subject, actually an extremely important outgrowth of the material in Chapter 6: the application of the anisotropic penetration of particles in crystalline solids ("channeling") to studies of crystal orientation, lattice damage, and foreign atom location. This field is relatively simple to enter from the experimental standpoint and is wide open to studies in the enormous variety of crystalline solids of current solid-state interest.

The third section (Chapter 8), on ion implantation, has technological overtones added to a diversity of solid-state problems. There are many intriguing questions associated with the possibilities of tailoring solid-state materials by adding atoms dynamically—implanting them—rather than by the more conventional doping-during-growth or diffusion-doping techniques. The problems of where the atoms go and of the rather massive lattice damage associated with implantation are issues of major current interest and importance.

Next, Chapter 9, which deals with interactions of nuclear moments with solid-state environments, involves a sophisticated area of common scientific interest to nuclear and solid-state physicists. By measuring the interaction of magnetic fields and electric field gradients in solids with the magnetic dipole moments and electric quadrupole moments of nuclei one can study either the fields or the moments. In the case of implanted atoms, hyperfine interaction studies offer some particularly intriguing possibilities. The experiments in this area, however, are generally quite complex. The final section (Chapter 10), on materials analysis, deals with one of the oldest applications of nuclear reactions to the study of solids. However, it offers almost unlimited opportunity for introduction of clever ideas and new approaches by which more sensitivity or more specificity in the analysis of solid-state materials may be obtained.

The material presented in this part is by no means exhaustive but will hopefully provide a glimpse into fields ripe for the harvest by people with access to the tools of the nuclear physicist and with insight into the physics of the solid state.

CHAPTER 6

Penetration and Energy Loss

Studies of the penetration and energy-loss behavior of accelerated atomic particles in the keV to MeV energy region provide a fruitful field of investigation in that they span the gap between ordinary atomic collisions (involving eV or sub-eV atoms), on the one hand, and the much higher-energy events of nuclear physics, on the other. Such particles have sufficient kinetic energy to penetrate deeply into the inner electronic shells of the target atoms, thereby producing much higher levels of electronic excitation than those observed in ordinary atomic collisions. As a result, a very broad range of excitation processes can occur, some of which would be otherwise nonobservable. For example, as discussed in Chapter 4, a completely new branch of atomic spectroscopy has recently evolved (beam-foil spectroscopy) in which, by measuring the emission spectra from a beam of highly excited ions (obtained by passing them through a thin carbon foil) it is possible to study the population and lifetime of many atomic energy levels. Equally valuable information about the interaction of energetic atomic beams with matter can be obtained by studying the emission of electrons or of characteristic inner shell x rays as the beam traverses a solid, by measuring the range or rate of energy loss of the particles in the beam, or (in single crystals) from scattering studies.

Investigations of energy loss and penetration behavior not only are a means of studying the basic atomic collision processes involved, but they also provide necessary information for many of the recent solid-state applications of small accelerators: range and energy-loss data are required, for example, in the ion implantation and hyperfine interaction studies described in Chapters 8 and 9.

Except for a few low-Z projectiles such as H^+ and He^+, experimental work in the penetration field was almost nonexistent until about a

decade ago. The main reason for this lack of interest was the lack of suitable heavy ion accelerators. Recent improvements in ion-source techniques, however, now make it possible to obtain suitable beams of a wide variety of ions at energies from a few keV up to several MeV—using either an electrostatic accelerator or, at lower energies, an "isotope separator" of the Scandinavian type. Already, a considerable amount of data have been accumulated and indicate that penetration behavior is far more complex than was originally anticipated, and that much more experimental work will be required. Several completely unexpected effects have been observed; some of these have opened up whole series of new and interesting experiments. Two such examples are the channeling phenomenon, viz., the existence of a strong directional dependence for various penetration effects in single crystals; and the existence of a pronounced *oscillatory* dependence of stopping power on the atomic number of the projectile. Both these effects still require a great deal of further study and therefore represent promising areas for research with small accelerators. In addition, the channeling phenomenon also provides a useful tool for studying certain properties of crystalline matter; these will be discussed separately in Chapters 7 and 8.

The published literature in the penetration field is quite extensive. References 1 and 2 are useful reviews of some of the earlier work; an up-to-date review of the channeling studies is given in references 3 and 4. Areas of current research interest have been well covered by several recent conferences; their proceedings[5–7] therefore provide a valuable starting point.

Because of the dominance of channeling effects in single crystals, it is convenient to divide penetration studies into two categories: (a) amorphous targets and (b) single crystals. Much basic data is still needed in both categories. However, with the current widespread interest in channeling and its applications, single-crystal studies appear to offer the more exciting area for research with small accelerators. Measurements in polycrystalline targets should generally be placed in Category (a); however, the penetration usually also exhibits a significant "channeled" component (cf., for example, Figure 7 in reference 8) due to a small fraction of the crystallites in the bombarded area being aligned with the incident beam direction.

Amorphous Targets

Status of the Physics

A comprehensive theoretical treatment of the penetration of heavy ions in amorphous targets has been given by Lindhard *et al.*[9,10] There are

two basic types of energy loss processes involved: nuclear (or elastic) collisions, in which the Coulomb repulsion between the screened nuclear charges causes energy to be transferred from the projectile to an entire target *atom,* and electronic (or inelastic) collisions, in which kinetic energy is converted into electronic excitation. The first type involves large energy losses per collision and significant angular deflection of the beam; the second type involves much smaller energy losses and negligible deflection. For most purposes, these two processes can be treated as though they were quite independent of each another, although, of course, this is not strictly true. Figure 37 illustrates their predicted energy dependence, expressed in terms of the "universal" energy and distance parameters (ϵ and ρ) introduced by Lindhard to minimize the atomic number dependence. Nuclear stopping is more important at low energies, reaching a maximum at $\epsilon \sim 0.4$, but for ϵ values greater than ~ 2 electronic stopping is predominant, since it continues to increase linearly with velocity. At much higher energies than those depicted in Figure 37, the electronic stopping also reaches a maximum

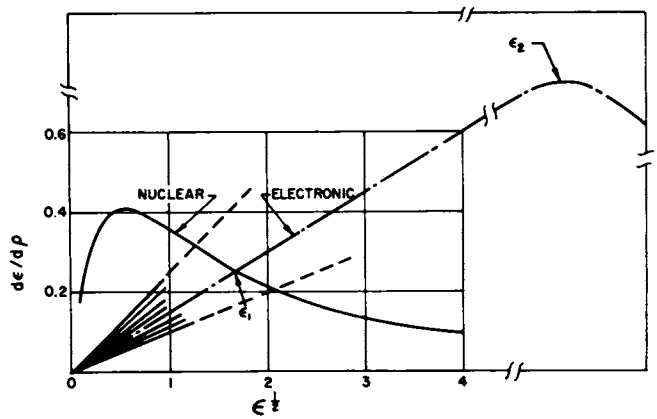

FIGURE 37. The rate of energy loss ($d\epsilon/d\rho$) due to (a) nuclear collisions; (b) electronic interactions. The universal energy and distance parameters, ϵ and ρ, introduced by Lindhard, are defined as follows:

$$\epsilon = E(\text{keV}) \times \frac{32.52 A_2}{Z_1 Z_2 (Z_1^{\frac{2}{3}} + Z_2^{\frac{2}{3}})^{\frac{1}{2}} (A_1 + A_2)},$$

$$\rho = R(\mu\text{g cm}^{-2}) \times \frac{166.5 A_1}{(Z_1^{\frac{2}{3}} + Z_2^{\frac{2}{3}})(A_1 + A_2)^2},$$

where R is the range, E is the energy, Z_1, Z_2 are the atomic numbers, and A_1, A_2 are the masses of the projectile and target atoms, respectively. For electronic stopping, a weak dependence on atomic number remains, even after converting into ρ-ϵ units. Hence, a family of curves (one for each combination of Z_1 and Z_2) is obtained; the majority of cases fall within the dotted lines.

and eventually falls off as E^{-1}. This high-energy region is the familiar "Bethe formula" region, which has been investigated extensively for many years. Typical values of the energy at which this maximum in $(\partial\epsilon/\partial\rho)$ occurs and also of the transition point ($\epsilon\sim 2$) between nuclear and electronic stopping are given in Table 4.

In the predominantly nuclear-stopping region (i.e., $\epsilon<2$), the available experimental data agree rather well with Lindhard's universal curve (see, for example, reference 11) and, although more data would be desirable, the physics seems to be rather well in hand. At higher energies, however, where electronic stopping predominates, the picture becomes much less satisfactory. The measured values of $(\partial\epsilon/\partial\rho)$ still agree *roughly* with those predicted by theory, but in many cases[12,13] they deviate significantly from the expected $E^{\frac{1}{2}}$ dependence. In addition, they exhibit a strong oscillatory dependence on Z_1, the atomic number of the incident ion, whereas the theory predicts only a weak and monotonous increase. The cause of these discrepancies has not yet been established, and evidently much more experimental work is needed. Fortunately, for most of the heavy ions, this is the energy region for which the small accelerators covered by this report are ideally suited.

EXPERIMENTAL TECHNIQUES AND AREAS FOR STUDY

There are at least four basic types of experiments: (in order of increasing difficulty) ranges, energy-loss measurements, specific interactions, and single-collision studies.

RANGES This is probably the simplest type of experiment, particularly if the accelerator facilities are capable of handling radioactive projectiles. A thick amorphous (or polycrystalline) target is bombarded with a beam of monoenergetic ions, and the depth (i.e., "range") distribution of

TABLE 4 Characteristic Energies, E_1 and E_2, for Some Typical Ions in Tungsten

ION	TRANSITION ENERGY, E_1, CORRESPONDING TO $\epsilon \sim 2$ (MeV)	ENERGY, E_2, OF MAXIMUM ELECTRONIC STOPPING (MeV)
^{4}He	0.04	0.5
^{16}O	0.2	13
^{39}K	0.5	100
^{129}Xe	2.5	1300

the embedded atoms is then measured. Sometimes this can be accomplished *in situ* by using a suitable proton or He^+ beam to determine the depth distribution of the embedded foreign atoms, as in recent experiments of Powers *et al.*[14] The more common procedure is to remove a series of thin, uniform layers from the surface of the bombarded target and to measure the number of injected atoms contained in each. If these atoms are radioactive, the number contained in each layer is of course particularly easy to establish. Several reliable mechanical and chemical techniques for removing sufficiently thin, uniform layers from a large variety of targets are now available (see, for example, references 8 and 15–18). The rate of energy loss, i.e., the stopping power, dE/dx (or $d\epsilon/d\rho$), can be derived by taking the reciprocal slope of a series of such range measurements as a function of energy.

ENERGY-LOSS MEASUREMENTS A more direct method for obtaining the stopping power (dE/dx) is to measure the energy loss ΔE for a beam as it traverses a thin amorphous film of thickness Δx. This method has the difficulty of requiring rather thin, self-supporting films—typically, a few hundred angstroms—but techniques for preparing these are now fairly widely available. A reasonably precise instrument for measuring the beam energy before and after it has traversed the film is also required. This may be an electrostatic or magnetic analyzer. Measurements of this type have provided the most extensive investigation so far of the oscillatory Z_1-dependence of electronic stopping power.[13] Many similar measurements are still required.

Such measurements provide not only the stopping power but also the charge-state distribution of the emitted beam. This latter quantity is obviously related in some way to the electronic interactions that have occurred in the foil and at the surface of emergence and may possibly provide further insight into the nature of the Z_1-oscillations.

Stopping power measurements can also be made in gases[19] by using a differentially pumped gas cell in place of the thin film.

SPECIFIC INTERACTIONS Instead of measuring the over-all electronic stopping power, more detailed information about the nature of specific electronic interactions can be obtained by observing the various characteristic radiations (e.g., light, x rays, or electrons) emitted by the highly excited ions and target atoms as they subsequently de-excite. One highly developed aspect of this is beam-foil spectroscopy, in which delayed photon emission from the excited ions in the transmitted beam enables the lifetimes of the atomic states involved to be measured. This is described in detail in Chapter 4 of this report. The lifetimes for de-excita-

tion by electron and/or x-ray emission are much shorter than those for emission of optical photons, and the decay will in fact occur before the particle has moved more than a few angstroms from the collision site. Consequently, it is no longer possible to use the beam-foil technique of observing the actual lifetimes. Nevertheless, yield measurements can provide a great deal of useful information on the importance of specific electronic interactions. For example, Khan[20] has recently initiated a series of x-ray yield measurements for various heavy ions penetrating thin carbon and aluminum targets. The yields are readily observable, even at beam energies below 1 MeV, and exhibit strong fluctuations with atomic number of projectile and target.

SINGLE-COLLISION STUDIES The "ideal" stopping-power experiment is one in which each particle undergoes no more than a single collision, since in this experiment it is then possible (in principle), by means of coincidence techniques, to measure all the pertinent parameters: e.g., the charge state and energy of both the projectile and the struck atom, the scattering angle, and the various radiations emitted. Single-collision experiments of this type have been made for 10–100 keV inert gas ions using a gas scattering chamber equipped with two electrostatic analyzers in coincidence.[21,22] They show that large inelastic losses (up to several hundred eV) are associated with some of the more violent collisions. Extending such measurements to a variety of projectiles and to a wider range of energy could provide extremely valuable information on the nature of the electronic energy losses. However, the techniques involved are quite sophisticated, so that for a new group this is probably not the best *entry* point into the field.

SINGLE-CRYSTAL TARGETS

PHYSICAL BACKGROUND

Whenever a beam of accelerated atomic particles enters a crystal within a certain critical angle ($\psi_{\frac{1}{2}}$) of a major axis (or plane), it then becomes "channeled"; i.e., each time it approaches one of the aligned rows of lattice atoms, the gradually increasing Coulomb repulsion between the projectile and the lattice atoms is sufficient to steer it away again, thereby preventing violent nuclear collisions from occurring. One obvious consequence is that the rate of energy loss is much smaller for a channeled particle, and hence it can penetrate more deeply than in an amorphous target. Nuclear stopping depends much more strongly on

the impact parameter than does electronic stopping; hence, nuclear stopping is more strongly affected by channeling. As a result, the transition to predominantly electronic stopping (Figure 37) occurs at much lower energies for a channeled beam than for one in an amorphous target; for example, with Xe ions in an aligned tungsten crystal, the transition occurs at ~4 keV,[24] whereas in "amorphous" tungsten the corresponding transition energy is ~2.5 MeV (Table 4). Consequently, channeling can be utilized to suppress the nuclear stopping almost entirely, thereby enabling electronic stopping to be investigated over a much wider energy region than would otherwise be possible.

The measured values of $(\partial\epsilon/\partial\rho)$ for channeled ions are usually a factor of 2–5 smaller than the corresponding "amorphous" values, due to the decreased electron density that they encounter. Furthermore, the values exhibit an even stronger oscillatory dependence on Z_1 than those in amorphous targets. Recent experiments in silicon crystals[25] show that peak-to-valley Z_1-oscillations of up to a factor of 10 occur for well-channeled ions, whereas in similar amorphous targets the maximum variation in stopping power is only 30–40 percent. The cause of these large oscillations has not yet been established, although ion size certainly appears to be a significant factor. Obviously, much more experimental (and theoretical) work is desirable in this area.

A comprehensive theoretical treatment of the steering process responsible for channeling has been provided by Lindhard.[23] He has derived relatively simple expressions for the critical angle as a function of E, Z_1, Z_2, and d (the lattice spacing). He has also shown that around each aligned row or plane in the lattice there exists a forbidden region, a tenth to a few tenths of an angstrom in width, into which a channeled beam cannot penetrate. Consequently, the yields of processes requiring closer impacts than ~0.1 Å—processes such as backscattering, inner shell x-ray production, nuclear reactions, and Coulomb excitation —all fall essentially to zero for channeled particles (Figure 38). Such processes are therefore particularly sensitive indicators for studying the conditions necessary to maintain a channeled trajectory.

EXPERIMENTAL TECHNIQUES AND AREAS OF ACTIVE INTEREST

The various types of measurement may be subdivided into three categories: ranges, energy-loss measurements, and close-impact studies. In all three cases, one of the basic problems is to obtain suitable single-crystal targets. The Research Materials Information Center at Oak Ridge maintains a useful card index system through which a satisfactory source of supply can often be found. The more difficult problem,

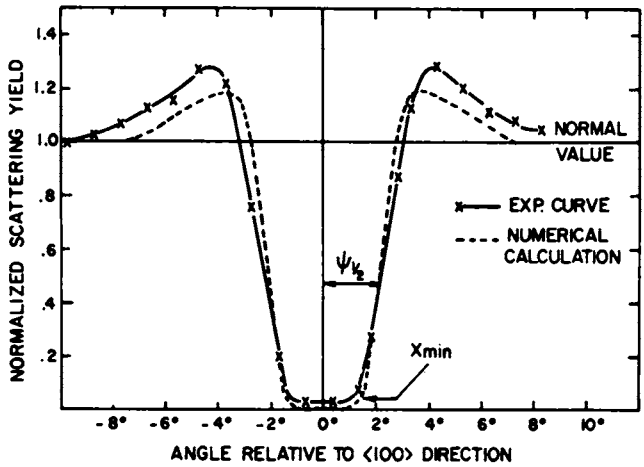

FIGURE 38. The experimental and calculated axial "dip" in Rutherford scattering yield for 480-keV protons incident along a ⟨100⟩ direction in tungsten at 390°K (taken from reference 26, Figure 10).

however, is to obtain a sufficiently clean surface on the crystal so that the beam is not appreciably scattered from the aligned direction as it enters the crystal. In this respect, it should be emphasized that even the thin oxide layer (10–50 Å) that is normally present on most metal surfaces is sufficient to "dechannel" a significant fraction (several percent) of an incident beam. Hence, careful chemical cleaning of the surface and good vacuum conditions in the target chamber are desirable and, in some cases, essential.

RANGES The same techniques are used as in amorphous targets, except that the crystal must first be carefully aligned in order to inject the (radioactive) heavy ions along a channeling direction. This alignment can be accomplished by standard x-ray methods; a simpler and more precise method, however, is to use the channeling behavior of a proton beam[27] from the same accelerator in order to make the alignment *in situ*. For quantitatively significant data, an alignment of $\sim 0.2°$ or better is desirable. One area in which range studies in single crystals are currently in great demand is in the semiconductor field, due to the increasing importance of ion implantation (see Chapter 8). Because of the large Z_1-oscillations in stopping power that have been observed,[25] theoretical estimates or even extrapolations from existing data are not always sufficiently reliable, and it is obviously desirable to have experimental data in as many systems as possible. There is also some

evidence[28] to suggest that for a given projectile, equally large Z_2-oscillations in the stopping power may exist.

ENERGY-LOSS MEASUREMENT Transmission experiments through thin single-crystal films are able to provide much more information about the nature of the channeling process than can be obtained from range measurements. By mounting the crystal on a suitable goniometer (having two or, preferably, three independent axes of rotation), one can observe the energy distribution, the charge-state distribution, and the angular spread of the transmitted beam as a function of crystallographic orientation. In addition, one of the close-impact processes described below under Close-Impact Processes can also be measured simultaneously in order to provide information on, for example, the quality of the crystal and on the rate of dechanneling. The biggest experimental difficulty, of course, is to obtain thin enough films of crystallographic perfection comparable with that attainable in a bulk crystal. The channeling of low-Z projectiles ($^1H^+$, $^2H^+$, He^+) in Si, Ge, Cu, and Au has been investigated rather intensively by means of such transmission studies. In fact, the existence of proton channeling was first demonstrated in this way.[29] A few recent references[30–32] have been selected in order to provide the reader with a convenient entry into the literature.

Transmission studies with heavier projectiles are also of considerable interest, particularly since such large Z_1-oscillations have been seen in the stopping power. However, apart from the pioneering work of Eisen[25] in silicon, transmission measurements with heavy ions are essentially nonexistent. This is evidently another fertile field in which some of the "small-accelerator" groups could make a real contribution.

It should perhaps be emphasized that, for channeled ions (due to the suppression of nuclear stopping), the optimum film thickness for a transmission experiment turns out to be essentially independent of atomic number—provided the energies are below the maxima in the electronic stopping curves (i.e., below E_2 in Table 4). Hence, at 1 MeV, for example, transmission experiments of heavy ions from Li to U can all be made using single-crystal films of approximately the same thickness.

There is another particularly exciting feature of transmission studies that has not yet been fully exploited. Recently, the Oak Ridge group[33] found that in the case of planar channeling they observed as many as five to six different energy-loss groups in the transmitted beam—provided the beam was not *perfectly* aligned with the plane and provided the angular resolution at the detector was considerably smaller than the critical angle for planar channeling. The available evidence suggests that each energy group may be identified with particles having had a discrete

number of planar "bounces"—4, 5, 6, . . . etc.—in traversing the crystal and hence with a well-defined trajectory between the planes. If so, then from such measurements it may eventually be possible to evaluate interatomic potentials as a function of impact parameter. The Oak Ridge experiments used 30–100 MeV Br and I ions from a tandem accelerator and Au crystal films a few thousand angstroms thick. Heavy-ion experiments at 1–2 MeV would require films about a factor of 5 thinner, but this is still within the available thickness range for self-supporting single-crystal films. Similar experiments have recently been reported for H^+ and He^+ in the 1 MeV region[32]; again, several discrete energy-loss groups have been seen.

CLOSE-IMPACT PROCESSES The best way of investigating the steering mechanism responsible for channeling is to measure the yield of any process requiring closer impacts than ~0.1 Å—for example, nuclear reactions,[27] Rutherford backscattering,[34,35] Coulomb excitation, inner shell x-ray production.[36] As shown in Figure 38, such yields are attenuated drastically whenever the beam is aligned within a certain critical angle of a major axis or plane. The observed yield is a *quantitative* measure of the unchanneled fraction of the beam. Hence measurements of this type provide not only the critical angle ($\psi_{\frac{1}{2}}$), but also the fraction (χ_{min}) of the incident beam that has become dechanneled on passing through the crystal surface. Both these quantities can be predicted from Lindhard's theoretical treatment.[23] Several fairly extensive studies of this type have been made,[27,34,35] and in general the agreement with theoretical predictions is rather good. For certain processes, it is possible also to measure the interaction yield (and hence the *un*channeled fraction) as a function of penetration depth into the crystal. For example, in the case of Rurtherford scattering, precise energy analysis of the scattered particles enables the depth dependence of the scattering yield to be observed. In this way, the "dechanneling" rate of an initially aligned beam can be studied; furthermore, by extending the measurements to elevated temperatures, the dechanneling contribution due to enhanced lattice vibrations can also be determined. Depth and temperature studies such as these provide particularly detailed information on channeling behavior. Typical values of the "escape length"—i.e., of the depth within which 50 percent of a channeled beam becomes dechanneled—lie between 10 and 50 μ for the major axial directions, and 1 and 5 μ for the major planes. Very few measurements of this type have yet been made, except in Si and W crystals.[35,37] Recently, Feldman *et al.*[38] have developed a theoretical treatment of dechanneling, which appears to fit

the observed depth and temperature dependences in Si and W reasonably well.

Most of the close-impact studies that have been carried out to date have used low-Z projectiles such as protons or helium ions and any of the large variety of nuclear reactions that they induce. However, even with the limited energy range available to small accelerators, there are many types of close-impact processes that can be used to monitor the channeling behavior. Bergstrom *et al.*[39] have used Rutherford scattering to study the channeling of various ions from ^{1}H to ^{132}Xe in tungsten in the energy region 0.1–2.0 MeV. Similarly, inner shell x-ray production can be used for heavy ions in this energy region, as has recently been demonstrated by Khan.[20]

The existence of such large yield attenuations in the close-impact processes has led to many interesting applications in other solid-state fields; some of these are discussed in Chapters 7 and 8.

REFERENCES

1. D. K. Nichols and V. A. J. Van Lint, Solid State Phys. (1965).
2. B. G. Harvey, Ann. Rev. Nucl. Sci. *10,* 235 (1960).
3. I. Bergstrom and B. Domeij, Nucl. Instrum. Methods *43,* 146 (1966).
4. S. Datz, C. Erginsoy, G. Liebfried, and H. O. Lutz, Ann. Rev. Nucl. Sci. *17,* 129 (1967).
5. International Conference on Atomic Collision and Penetration Studies, Chalk River, Canada (Sept. 18–21, 1967). Published in Can. J. Phys. *46,* 449–782 (1968).
6. International Conference on Solid State Physics Research with Accelerators, Brookhaven, N.Y. (Sept. 25–28, 1967). Published as BNL-50083.
7. International Conference on Electromagnetic Isotope Separators and Their Application, Aarhus, Denmark (June 14–18, 1965). Published as Nucl. Instrum. Methods *38* (1965).
8. M. McCargo, J. A. Davies, and F. Brown, Can. J. Phys. *41,* 1231 (1963).
9. J. Lindhard and M. Scharff, Phys. Rev. *124,* 128 (1961).
10. J. Lindhard, M. Scharff, and H. Schiott, Kgl. Dan. Vidensk. Selsk. Mat. Fys. Medd. *33,* No. 14 (1963).
11. P. Jespersgård and J. A. Davies, Can. J. Phys. *45,* 2983 (1967).
12. J. H. Ormrod, J. R. Macdonald, and H. E. Duckworth, Can. J. Phys. *43,* 275 (1965).
13. B. Fastrup, P. Hvelplund, and C. A. Sautter, Kgl. Dan. Vidensk. Selsk. Mat. Fys. Medd. *35,* No. 10 (1966).
14. D. Powers, W. K. Chu, and P. D. Bourland, Phys. Rev. *165,* 376 (1968).
15. J. A. Davies, J. Friesen, and J. D. McIntyre, Can. J. Chem. *38,* 1526 (1960).
16. J. L. Whitton, J. Appl. Phys. *36,* 3917 (1965).
17. T. Andersen and G. Sorensen, Can. J. Phys. *46,* 483 (1968).

18. H. Lutz and R. Sizmann, Phys. Lett. *5*, 113 (1963).
19. B. Fastrup, A. Borup, and P. Hvelplund, Can. J. Phys. *46*, 489 (1968).
20. J. M. Khan (Lawrence Radiation Lab.), private communication. See also the earlier work of J. M. Khan, D. L. Potter, and R. D. Worley, Phys. Rev. *139*, A1735 (1965), and references therein.
21. G. H. Morgan and E. Everhart, Phys. Rev. *128*, 667 (1962).
22. V. V. Afrosimov and N. V. Fedorenko, Zh. Tekhn. Fiz. *34*, 1624 (1964).
23. J. Lindhard, Kgl. Dan. Vidensk. Selsk. Mat. Fys. Medd. *34*, No. 14 (1965).
24. L. Eriksson, J. A. Davies, and P. Jespersgård, Phys. Rev. *161*, 219 (1967).
25. F. H. Eisen, Can. J. Phys. *46*, 561 (1968).
26. J. U. Andersen, Kgl. Dan. Vidensk. Selsk. Mat. Fys. Medd. *36*, No. 7 (1967).
27. J. U. Andersen, J. A Davies, K. O. Nielsen, and S. L. Andersen, Nucl. Instrum. Methods *38*, 210 (1965).
28. J. L. Whitton, Can. J. Phys. *46*, 581 (1968).
29. G. Dearnaley, IEEE Trans. Nucl. Sci. *NS-11*, 249 (1964).
30. B. R. Appleton, C. E. Erginsoy, and W. M. Gibson, Phys. Rev. *161*, 330 (1967).
31. A. R. Sattler and G. Dearnaley, Phys. Rev. *161*, 244 (1967).
32. W. M. Gibson, J. B. Rasmussen, P. Ambrosius-Olesen, and C. J. Andreen, Can. J. Phys. *46*, 551 (1968).
33. H. O. Lutz, S. Datz, C. D. Moak, and T. S. Noggle, Phys. Rev. Lett. *17*, 285 (1966).
34. E. Bøgh and E. Uggerhøj, Nucl. Instrum. Methods *38*, 216 (1965).
35. J. A. Davies, J. Denhartog, and J. L. Whitton, Phys. Rev. *165*, 345 (1968).
36. J. M. Khan, D. L. Potter, and R. D. Worley, Phys. Rev. *163*, 81 (1967).
37. B. R. Appleton, L. C. Feldman, and W. L. Brown, reference 6, pp. 45–47.
38. L. C. Feldman, B. R. Appleton, and W. L. Brown, reference 6, pp. 58–73.
39. I. Bergström, K. Björkqvist, B. Domeij, G. Elädda, and S. Andersen, Can. J. Phys. *46*, 2679 (1968).

CHAPTER 7

Application of Channeling to Solid-State Studies

In Chapter 6, the recently discovered "channeling effect" was discussed as one of the dominant features of the penetration behavior of atomic beams in crystals. Although many aspects of channeling require further study, the understanding of the steering process involved is now sufficiently well established that the channeling effect can be used as a tool for studying certain properties of crystals. Already several interesting applications have evolved, some of which probably constitute more fruitful areas for future research than that of channeling itself. Three of these will be considered in this section: orientation of crystals, lattice and surface disorder, and location of foreign atoms within the unit cell.

All these applications are based on the fact that interactions with lattice atoms requiring smaller impact parameters than ~ 0.1 Å are completely prohibited for a channeled particle. Consequently, the yields of close-impact processes such as nuclear reactions, backscattering, or x-ray production fall almost to zero for a beam incident in a channeling direction (see, for example, Figure 38 in Chapter 6). Typically, 20–100-fold attenuations in yield are achieved by careful alignment with a major axis, indicating that as much as 95–99 percent of the beam can become channeled. Large attenuations such as these are important in the application of channeling to other fields

Precise Orientation of Crystals

The channeling effect provides a simple method[1–3] for precise orientation of a single crystal For this purpose, wide-angle Rutherford scattering is particularly useful, because it can be applied to any crystal, pro-

vided a proton or helium ion beam of $E \gtrsim 50$ keV is available. With care, an accuracy of 0.02° can be achieved; and an alignment to within 0.1° takes only 10–15 min. One interesting feature of the method is that, by measuring the energy spectrum of the scattered protons, it is possible to study simultaneously the channeling behavior of the beam at different depths beneath the crystal surface. Hence, the method determines the crystal orientation as a function of depth and thus provides information on the mosaic spread along the beam direction. Typical depth resolution with a solid-state detector is about 400 Å; however, this can be improved to ~50 Å by using an electromagnetic analyzer.

An alternative, but closely related, technique for determining the orientation (or even the structure) of a single crystal is to utilize the "blocking" effect: i.e., the directional dependence of the *emission* of atomic particles originating from lattice sites. The rows and planes of atoms deflect (block) all particles initially directed along high symmetry directions so that in an angular distribution outside the crystal there is a deficit of particles in directions parallel to atomic rows and planes. Experimentally wide-angle Rutherford scattering can also be used to observe blocking, but now the beam is brought in along a "random" direction in order to avoid channeling. During the backscattering process, the proton or helium ion penetrates almost to the center of the lattice atom; it can therefore be considered as "originating" from a lattice site. A position-sensitive detector or film is placed 20–30 cm from the crystal (to provide adequate angular resolution), and a "pattern" due to the orientation dependence of the emitted particles is observed. In fact, reversibility arguments[4] and experiment[5] show that the critical angles and attenuation factors for blocking and channeling are identical. Hence, strong attenuations in emission rate are observed along all the major axes and planes, thereby producing a crystallographic projection at the detection surface. One particularly simple detection technique[6] is to use a "track" detector, such as cellulose nitrate, instead of photographic film. In this case, with 1-MeV helium ions, a bombardment of 1–10 μC on the crystal is sufficient to produce a readily visible "track" pattern on the plastic after etching (Figure 39).

Lattice and Surface Disorder

The observation of large attenuations in yield (Figure 38, Chapter 6) suggests that the aligned yield χ_{min} for a close-encounter process can be used to study the extent of lattice disorder. Any atom displaced from its regular lattice site by more than ~0.1 Å is able to interact with the

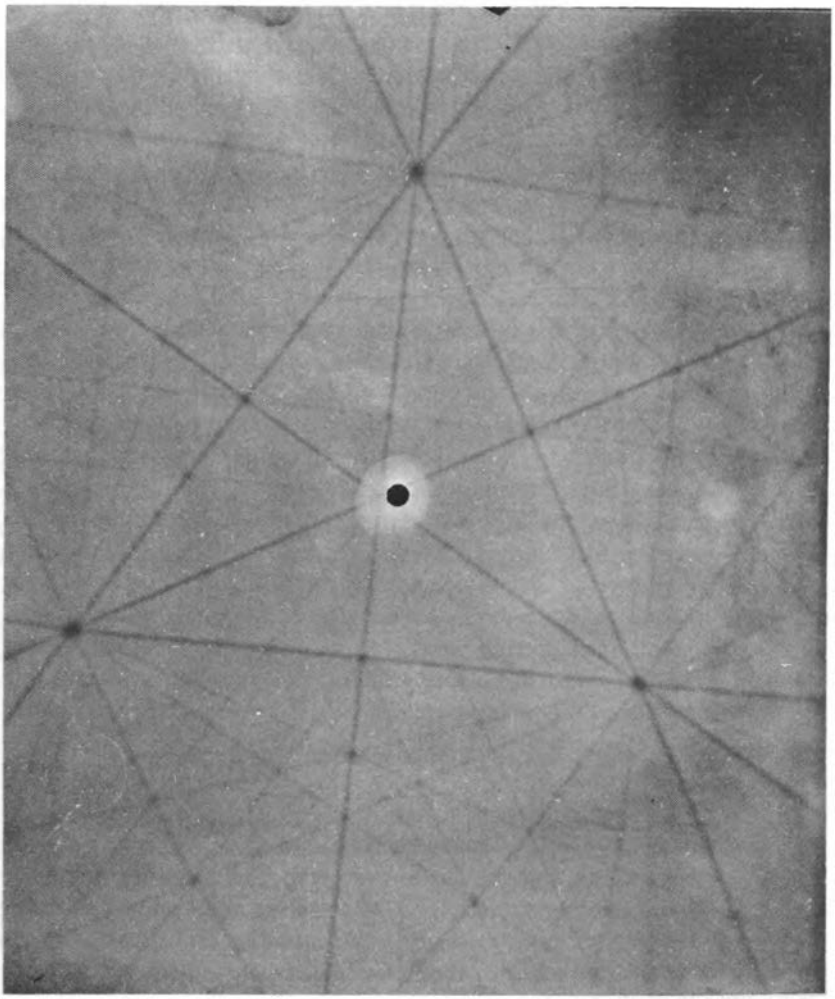

FIGURE 39. Blocking pattern of helium ion "tracks" on a sheet of cellulose nitrate (after etching in 5*N* NaOH at 60°C for 2–3 min), produced by the backscattering of 1.0-MeV He^+ from a {111} surface of GaAs.[6] The central black dot with the bright halo is the aperture through which the incident beam entered the scattering chamber; the apices of the prominent equilateral triangle correspond to the three ⟨110⟩ axes at 34.4° from the central ⟨111⟩ axis. A large number of higher-index axes and planes are clearly visible in the blocking pattern.

channeled beam and therefore contributes to the measured value of χ_{min}. In this way Bøgh[7] has shown that proton channeling is sufficiently sensitive to detect less than a monolayer of displaced lattice atoms in a tungsten crystal. Similarly, the channeling behavior of 1-MeV helium

ions has been used to obtain quantitative information on the amount of lattice disorder in semiconductors following ion implantation (cf. Chapter 8). Precise energy analysis of the backscattered beam enables the lattice disorder to be studied as a function of depth, thereby providing (for example) information about the degree of perfection of the surface region compared to that of the underlying crystal.

Potentially, the most fruitful application of channeling in studying surface imperfections has not yet been exploited. It is based on the fact that no orientation dependence exists for the interaction with the *first* plane of atoms. Consequently, for a channeled beam, even in a perfectly clean, nonvibrating lattice, a prominent surface peak is observed in the energy spectrum of the backscattered yield, as has been demonstrated recently by Bøgh[8] in the case of tungsten. On the other hand, the presence of an adsorbed impurity layer, such as oxygen, on the crystal surface would affect this surface peak. If, ideally, the oxygen is adsorbed on a lattice site, then it would effectively "shadow" the first plane of tungsten atoms from the aligned beam, and the surface peak in the scattered spectrum from tungsten should disappear. Hence, by measuring the aligned spectra along various crystallographic directions, with and without absorbed impurities on the surface, it should be possible to identify the location of specific contaminants. Obviously, such information would be a powerful supplement to low-energy electron diffraction and to field-emission ion microscopy in the study of surface structures.

Location of Foreign Atoms

One of the most useful applications of proton and helium ion channeling to date is in determining the location of certain foreign atoms in crystals.[9,10] If the foreign atom is on a lattice site (i.e., substitutional), it will be unable to interact with the channeled beam, and hence a large attenuation in its interaction yield will occur. If, on the other hand, the foreign atom is interstitial, then along some of the major directions it will not lie within the forbidden region ($\sim$0.1 Å radius) around the atomic rows; consequently, the channeled beam can interact normally with it, and no attenuation in yield will be observed.

Hence, by investigating simultaneously the interaction of the beam with both the lattice and the foreign atoms, one obtains a quantitative measure of the distribution of foreign atoms between substitutional and specific interstitial positions.

Of course, to apply the method, it must be feasible to detect the interaction of the beam with a small concentration of foreign atoms in the

presence of the atoms of the most lattice. Fortunately, there are many different close-encounter processes available, and in the majority of cases a satisfactory one can be found, provided the atomic concentration of foreign atoms exceeds $\sim 10^{-4}$:

1. Whenever the foreign atom is heavier that the lattice atom, Rutherford scattering can be used to distinguish between them (see, for example, Figure 2b in reference 9).
2. If the foreign atom has an atomic number less than ~ 10, it can usually be detected by means of a specific nuclear reaction, such as (p,α), (p,γ), or (d,p), while Rutherford scattering can still be used to study the interaction with the lattice (see Figure 2 of reference 11).

Figure 40 illustrates the use of channeling in determining the location of various types of implanted *heavy* atoms (cf. Chapter 8) in three different silicon crystals, using method 1 above. In each case, for simplicity, only that portion of the energy spectrum that corresponds to scattering from the embedded heavy atoms has been given.

In the Au case, the interaction yield shows no orientation dependence in that the peaks observed when the beam is channeled along the ⟨111⟩ or ⟨110⟩ axes are indistinguishable from that for the random (i.e., *un-*

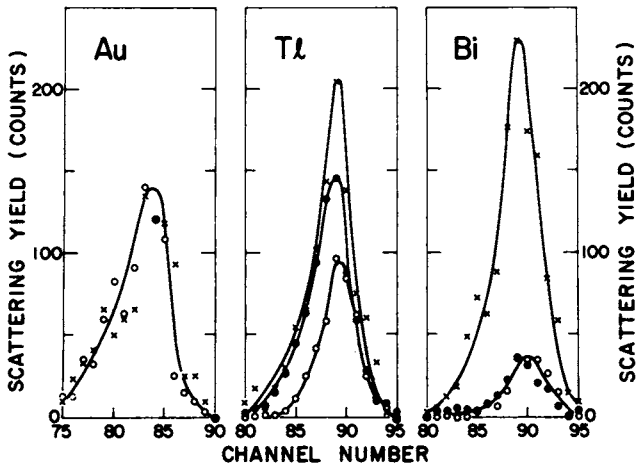

FIGURE 40. Orientation dependence of the backscattered spectra from heavy foreign ions implanted into silicon (taken from reference 12, Figure 3). Implant conditions: $\sim 10^{14}$ ions/cm^2 at 40 keV, 450°C. Spectra were obtained with the He$^+$ beam incident along: ○, a ⟨111⟩ axis; ●, a ⟨110⟩ axis; X, a random direction.

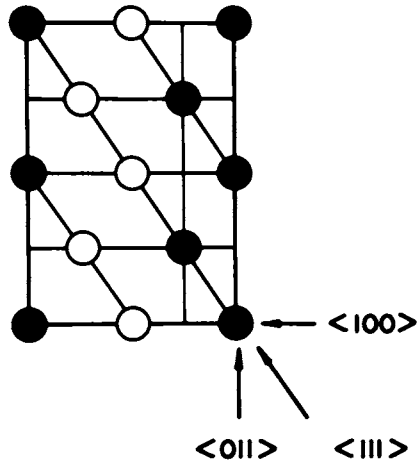

FIGURE 41. Atomic configurations in the {110} plane of a diamond-type lattice such as Si: ●, substitutional sites; ○, regular interstitial sites.

channeled) beam. Hence, the Au atoms must be in some sort of random positions located well away from the atomic rows.

The interaction with Bi, on the other hand, falls almost to zero along both the ⟨111⟩ and ⟨110⟩ axes, indicating that ~90 percent of the Bi atoms lie at the intersection of these two atomic rows. Inspection of the atomic configurations in a diamond-type lattice (Figure 41) shows that the Bi atoms must therefore be on substitutional sites.

The third case, Tl, is a particularly intriguing one in that the interaction is reduced by about twice as much for the beam incident in the ⟨111⟩ direction as in the ⟨110⟩ direction. This indicates that there are about twice as many Tl atoms located along the ⟨111⟩ rows as along the ⟨110⟩ rows. From this it can be concluded that, although some of the Tl atoms are on lattice sites, an approximately equal number are located in the regular interstitial holes along the ⟨111⟩.

These examples illustrate how channeling studies along two or more axes can be used to determine by *triangulation* the exact location of foreign atoms in a crystal. Currently, the most widespread application of this "atom location" technique is in studying the ion implantation of semiconductors (cf. Chapter 8). However, it has also been used in conjunction with studies of hyperfine interactions (Chapter 9), and of inert gas diffusion in solids,[13] since in both these fields it is of importance to know exactly where the foreign atoms are located within the unit cell.

REFERENCES

1. J. U. Andersen, J. A. Davies, K. O. Nielsen, and S. Andersen, Nucl. Instrum. Methods *38*, 207 (1965).
2. D. S. Gemmell and R. E. Holland, Phys. Lett. *14*, 945 (1965).
3. R. S. Nelson and D. F. Holloway, Phil. Mag. *15*, 845 (1967).
4. J. Lindhard, Kgl. Dan. Vidensk. Selsk. Mat. Fys. Medd. *34*, No. 14 (1965).
5. E. Bøgh and J. L. Whitton, Phys. Rev. Lett. *19*, 553 (1967).
6. G. R. Bellavance, N. Johansson, and D. Marsden (CRNL), private communication.
7. E. Bøgh, in *Proceedings of the Cairo Solid State Conference: Interaction of Radiation with Solids*, A. Bishay, ed. (Plenum Press, New York, 1966).
8. E. Bøgh, Can. J. Phys. *46*, 653 (1968).
9. J. A. Davies, J. Denhartog, L. Eriksson, and J. W. Mayer, Can. J. Phys. *45*, 4053 (1967).
10. W. M. Gibson, F. W. Martin, R. Stensgaard, F. Palmgren Jensen, N. I. Meyer, G. Galster, A. Johansen, and J. S. Olsen, Can. J. Phys. *46*, 675 (1968).
11. W. M. Gibson, J. U. Andersen, and E. Uggerhoj, paper presented at Conference on Radiation Effects in Semiconductor Components, Toulouse, France, March 1967.
12. L. Eriksson, J. A. Davies, N. Johansson, and J. W. Mayer, J. Appl. Phys. *40*, in press (Feb. 1969).
13. H. Matzke and J. A. Davies, J. Appl. Phys. *38*, 805 (1967).

CHAPTER 8

Ion Implantation

The introduction of atoms into a solid substrate by bombardment of the solid with ions in the keV to MeV energy range is known as ion implantation. Ion implantation has broad applicability to solid-state physics and to the fields of nuclear and atomic physics as well. For example, nuclear magnetic moments may be determined from studies of hyperfine interactions of atoms implanted into ferromagnetic materials. On the other hand, these same interactions with known nuclear magnetic moments may be used to investigate the electromagnetic fields in solids. Some of the interesting possibilities for this interplay are discussed in more detail in Chapter 9. The solid-state aspects of ion implantation are particularly broad because of the range of physical properties that are sensitive to the presence of foreign atoms in solid substrates. The mechanical, electrical, optical, magnetic, and superconducting properties of a solid are affected and indeed may be dominated by the properties of implanted layers. Implantation makes it possible to obtain impurity concentrations and distributions which are of particular interest and which are otherwise unattainable. In semiconductors, for example, higher impurity doping concentrations can be obtained than are available by conventional techniques.

Small accelerators can be used with great effectiveness in the field of ion implantation, both to produce and study the basic processes involved and to exploit the possibilities, scientific and technological, that ion implantation provides. Some of the most interesting areas for study are:

1. The interaction of ions in solids (Chapter 6).
2. Hyperfine interactions (Chapter 9).

3. Doping of semiconductors. This case is treated in more detail in the section beginning on page 144.

4. Radiation damage. The damage associated with ion implantation may well dominate the properties of an implanted layer and thus is an important subject for study. Some aspects of this problem for the case of silicon are discussed in the following section. Ion-implantation damage is also interesting as a simulation of damage created in fast-neutron irradiation.

5. Electrical transport in amorphous layers. Under certain conditions less than one tenth of a monolayer of energetic ions can form an amorphous layer in silicon and germanium. The conduction through and along this layer can be used to deduce the transport properties of amorphous layers.

6. Formation of thin magnetic films and thin superconducting layers. By implantation it is possible to add atoms to an appropriate solid substrate which should dominate the magnetic and superconducting properties of a thin layer near the surface. Alloys which are thermodynamically unstable at normal metallurgical preparation temperatures may be created in this way. There is almost no work yet in these areas.

As current work on ion sources proceeds, new low-power sources compatible with the terminal power available in low-energy accelerators will make an increasing variety of ions easily accessible. However, even now by using gaseous compounds containing an atom of interest, or by introducing solids into an rf discharge in helium or argon, a wide variety of beams may be produced with sufficient intensity for implantation purposes. It is almost essential that a mass-separating magnet be available to eliminate the unwanted species that often dominate the beam of interest. Beyond this requirement, however, the basic instrumentation can be extremely simple.

Because semiconductors have received a great deal of attention in recent ion-implantation work we will use them to illustrate both the radiation damage associated with implantation and some of the current results for the implantation of electrically active impurities in silicon. These examples are intended to emphasize the wide-open character of the field, where detailed physical understanding in most situations does not exist.

Radiation Damage—Lattice Disorder

An ion incident on a single crystal will lose energy in both electronic and nuclear collision processes as it slows down and comes to rest in the

crystal. Lindhard *et al.*,[1] have derived a comprehensive theoretical treatment of the partition of energy between electronic and nuclear processes. For the case of heavy ions of mass greater than silicon, a large part of the ion energy will be lost in nuclear collision processes even up to several hundred keV ion energies. These collisions are relatively violent, involving rather large energy transfers to atoms of the lattice, displacing them from their lattice sites. These atoms in turn displace others. The net result is the production of a disordered region along the path of the ion.

A quantitative determination of the number of silicon atoms displaced more than $\approx$0.2 Å from a lattice site has been made with helium ion backscattering measurements following implantations of 40-keV Sb ions at room temperature.[2,3] The lattice disorder produced by the Sb implantation is shown as a function of dose in Figure 42. The linear increase in damage with dose corresponds to displacement of about 3000 silicon atoms per incident ion. This result is about a factor of 2 larger than the value calculated by Sigmund.[4] This discrepancy implies either

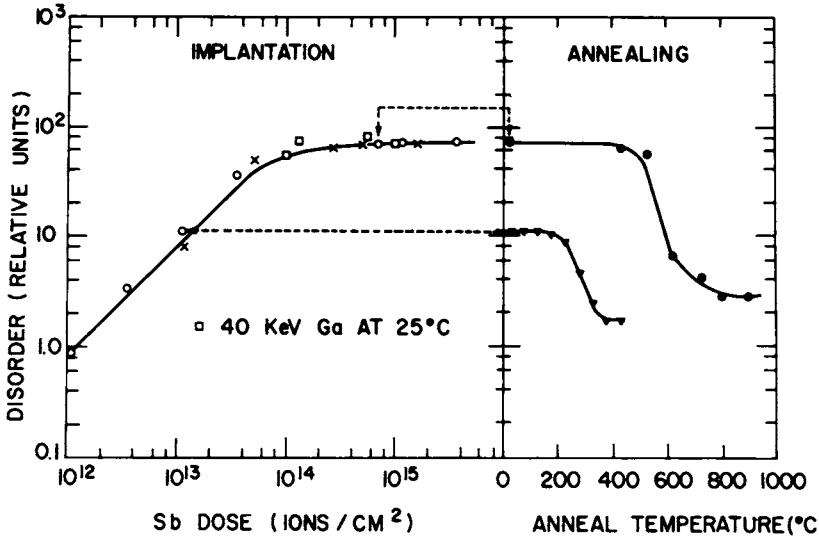

FIGURE 42. Left part: Dose dependence of the lattice disorder following 40-keV Sb implantations in Si at room temperature: ○ for incidence within 0.5° of the ⟨111⟩, X for incidence along a "random" direction, 8° away from the ⟨111⟩. Also shown (□) are points for 40-keV Ga implantations. Right part: Annealing characteristics of the lattice disorder: ● for a "saturation" Sb dose (7×10^{14}/cm²), ▼ for a "below saturation" Sb dose (10^{13}/cm²). (Taken from reference 3, Figure 3.)

that the displacement energy is not well defined in a heavily disordered region or that some of the "displaced" atoms are nearest neighbors surrounding a defect and are detected by the channeling technique because of lattice distortions greater than 0.2 Å. The actual discrepancy may be even somewhat larger than a factor of 2, because Sigmund's estimate does not consider the possibility of recombination of vacancies and displaced atoms that must occur at least to some extent.

As shown in Figure 42, the disorder approaches a saturation value as the ion dose is increased to approximately 10^{14} ions/cm^2. This corresponds to formation of an amorphous region as verified by electron diffraction measurements.[5] At low doses, the disordered regions around individual tracks are spatially separated; at high doses, they overlap and the disorder saturates.

Much of this lattice disorder can be restored by annealing. The data of Figure 42 indicate that the anneal temperature required to reorder the lattice is higher for the amorphous region than for the isolated clusters. Similar behavior has been noted in germanium. In both crystals, the anneal characteristics exhibit two well-defined regimes[6]:

1. At low doses, where the disordered regions are well separated from each other, reordering occurs at 180°C in Ge and at 260°C in Si.
2. At higher doses, where the disordered regions overlap sufficiently to form an amorphous layer, reordering occurs at 380°C in Ge and at 570°C in Si. These temperatures represent the midpoint in 10-min isochronal anneal curves. At very high doses ($>10^{15}$/cm^2 at 40 keV) where the concentration of implanted ions approaches 1 percent of the substrate, the reordering of the amorphous layer is not clearly defined and residual disorder is found even after anneals at 800°C.

By use of heated substrates (T>200°C in Ge and 300°C in Si), implantations can be performed to doses of 10^{14} to 10^{15} ions/cm^2 without producing large amounts of lattice disorder. In this case, the disorder around each track apparently anneals sufficiently rapidly so that each incident ion penetrates into essentially disorder-free material. Figure 43 shows the lattice disorder in silicon as a function of the substrate temperature for a 40-keV Sb implantation to dose levels of $\approx 2 \times 10^{14}$ ions/cm^2. In room-temperature implantations at this dose level, an amorphous layer is formed (100 percent lattice disorder in Figure 43). As the implantation temperature is increased above 150°C, there is a decrease in lattice disorder. At substrate temperatures above 300°C, the lattice disorder is below the detectable limit ($\approx 8 \times 10^{15}$ displaced atoms/cm^2. The temperature dependence of the lattice disorder is roughly consistent

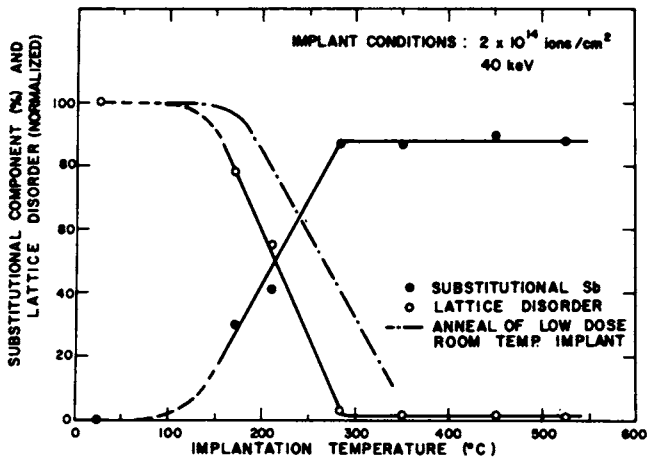

FIGURE 43. Influence of implantation temperature on the substitutional Sb component (●) and on the lattice disorder (○) in silicon. Implant conditions: 2×10^{14} Sb ions/cm^2 at 40 keV. The anneal behavior of a low dose ($\sim 10^{13}$ ions/cm^2) room temperature implant is also shown (------) for comparison. (Taken from reference 7, Figure 4.)

with the anneal characteristics (dashed line in Figure 43) of the isolated disordered regions.

The annealing of the displaced atoms in the isolated disordered regions closely resembles the anneal of divacancies[8] in fast-neutron-irradiated material. Much more work is required to clarify the physical nature of these regions and the disorder they contain.

THE CASE FOR SEMICONDUCTORS AND THE SEMICONDUCTOR CASE

There is a growing interest in the application of implantation in solid-state device technology. Although the technique is relevant to materials other than semiconductors, within the past five years the interest has centered on the use of ion implantation as a process for fabrication of semiconductor devices. Implantation techniques have been used to form P-N junction devices in silicon, germanium, gallium arsenide, cadmium telluride and silicon carbide.[9] In addition, bipolar and field-effect transistors, as well as other devices, have been fabricated. At present, it is by no means clear to what extent this technique will be utilized in commercial device processing. However, one can outline some of the reasons for interest in these techniques.

The successful application of transistors in electronic circuitry is based upon the control of the thermal diffusion of minute quantities of dopant elements into semiconductors, normally silicon. In the emitter of a bipolar transistor there are only approximately 10^{16} dopant atoms per cm^2 (about six monolayers). The electrical characteristics of the devices are determined by the concentration and distribution in depth of the dopant species. In thermal diffusion, the concentration is given by the equilibrium solubility at the process temperature and the distribution in depth is given by the diffusion constant and process time.

In ion implantation, on the other hand, the number of implanted ions is controlled by the external system rather than by the physical properties of the substrate. This has the advantage that dopant elements can be introduced in concentrations well above the equilibrium solubility at thermal diffusion temperatures.[2,7] Under certain conditions, nearly all these atoms are located on lattice sites. This will have important applications in compound semiconductors, particularly the II–VI compounds, where it is difficult to introduce dopants by diffusion without changing the substrate material.

The depth to which the ions penetrate depends primarily upon the incident energy and is typically between 100 and 10,000 Å.[10,11] The crystal lattice and the beam-to-substrate orientation influence the penetration depth and the distribution in depth. By careful choice of parameters it is possible to produce dopant distributions (and hence electrical characteristics) that cannot be achieved by conventional diffusion techniques. Another advantage is that geometrical control can be achieved in a simple manner by the use of metal masks, oxide layers, or photoresist.

ANALYSIS OF IMPLANTED LAYERS IN SILICON

In spite of the fact that implantation is a nonequilibrium process, it has been possible to deduce some of the process characteristics. There are many experimental techniques for evaluating implanted layers. Hall-effect and sheet-resistivity measurements indicate the number of carriers and their mobility.[12,13] The channeling technique (using MeV He^+ ions as a probe) has been used to determine the lattice location of the implanted dopant atoms (Chapter 7). The results of these two classes of experiments are presented briefly below.

LATTICE LOCATION

There are a number of factors that influence the lattice location of the implanted ion. Among these are ion dose, substrate temperature during

implantation, subsequent heat treatment, and the ion species. The channeling technique (Chapter 7) has been used to determine the lattice site location of the implanted atoms. In the silicon lattice, it is possible to specify the number of atoms on substitutional sites, on the regular interstitial site along the ⟨111⟩ axis, and on nonregular lattice positions (i.e., positions that are not aligned with any low index direction).

1. In room-temperature implantations of Bi and Tl at 40 keV, high substitutional components have been observed for doses less than 2×10^{13} ions/cm^2.[14] This is shown in Figure 44, which plots the percent substitutional and lattice disorder as a function of ion dose. At doses greater than $\approx10^{14}$ ions/cm^2, the lattice structure in the implanted layer is completely destroyed; under such conditions the substitutional Bi and Tl components are undefined. At present, the reason for the sharp decrease in substitutional level at a dose of $\approx3\times10^{13}$ ions/cm^2 is not understood.

2. As might be anticipated from the previous discussion, the substrate temperature during implantation has a marked influence on the number of atoms on lattice sites. As can be seen in Figure 43, there is a rapid increase in the substitutional content as the substrate temperature is increased above 200°C. Over the temperature range between 300°C and 550°C, the substitutional levels of Sb are near 90 percent for doses less than 10^{15} ions/cm^2. At higher doses, there is a decrease in the fraction substitutional that can be associated with an increase in lattice disorder.

3. One of the most striking aspects of ion implantation is that the

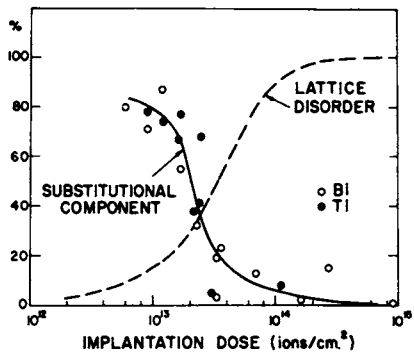

FIGURE 44. Dose dependence of the substitutional level (%) of unannealed Tl (●) and Bi (○) implants in silicon. Implant conditions: 40 keV at 25°C. The dotted line indicates the total amount of lattice disorder in the implanted region, expressed as the percentage of silicon atoms displaced more than 0.2 Å from their equilibrium lattice sites. (Taken from reference 14.)

lattice location of the implanted atoms depends on the particular ion species.[2,7] Although the Group V elements, As, Sb, and Bi, tend to be on substitutional lattice sites, the Group III elements, Ga, In, and Tl, are found in nearly equal numbers on both substitutional and the regular interstitial sites for hot substrate implantations at 350°C. Other elements, such as Au or Cd, have very small components on any regular lattice site under similar implantation conditions.[7]

4. Figure 45 shows the annealing behavior of a hot substrate (450°C) Tl implantation in silicon. After implantation, about 60 percent of the implanted atoms were found to be distributed equally between substitutional and interstitial sites. During annealing in the temperature range 525–575°C, the substitutional component decreases rapidly toward zero, and a corresponding increase is observed in the interstitial component. This indicates that the substitutional Tl atoms have moved to the regular interstitial sites. Upon further anneal, the interstitial component also decreases toward zero, indicating that Tl is either precipitating within the crystal or migrating out to the surface region. This behavior is confirmed in low dose ($\approx 10^{13}$ ions/cm^2) Tl implantations at room temperature. As shown in Figure 44, ≈80 percent of the implanted atoms are substitutional after implantation. Upon anneal to 575°C,

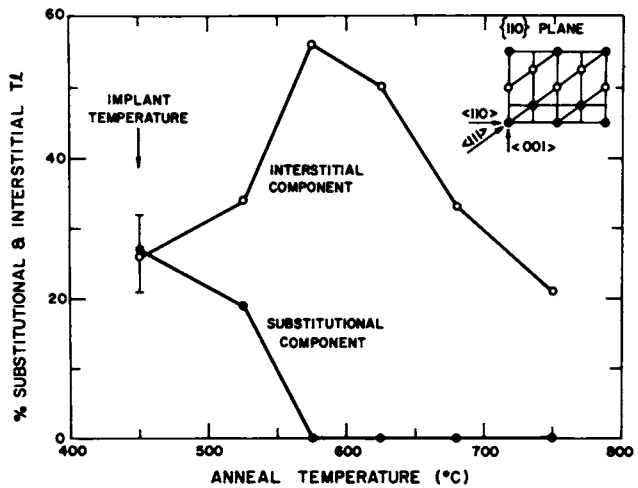

FIGURE 45. The lattice location of Tl ions implanted into silicon at 450°C as a function of subsequent annealing treatment. Implant conditions: 2×10^{14} ions/cm^2 at 40 keV. The location of the embedded Tl was determined at room temperature with 1.0-MeV helium ions. The insert shows the atomic configuration: lattice sites (●) versus interstitial holes (○) in a {110} plane of the Si lattice. (Taken from reference 15.)

these substitutional Tl atoms moved to regular interstitial sites. Under comparable implantation conditions, Bi maintains its high substitutional content out to 800°C anneal temperatures. This type of behavior is not understood and represents a fruitful area for further study. The lattice distortion associated with impurity atoms in either substitutional or interstitial positions or in the damaged region created by the ion as it is introduced is almost surely closely coupled with the electrical properties the atoms exhibit.

ELECTRICAL MEASUREMENTS

Ion-implanted layers can be readily adapted for evaluation of their electrical properties. Ions of a given dopant species are implanted into a substrate of opposite conductivity type to produce a P-N junction when properly annealed. The electrical isolation provided by the junction permits measurement of the characteristics of the implanted layer. Hall and sheet-resistivity measurements can be used to determine the number of carriers per cm^2 and their average mobility.[5,12,13] Some care must be taken when evaluating Hall measurements in implanted layers since the effective Hall mobility is weighted by the contribution of layers with higher mobility (i.e., the portion of the implanted layer with lower dopant and defect concentrations) in a different manner than the conductivity mobility.[13]

Interpretation of the anneal behavior of implanted layers is difficult because an increase in the number of carriers/cm^2 could be due to the dissociation of defects and/or the movement of the implanted species to substitutional sites. In spite of this difficulty, it has been possible to obtain some correlation of electrical measurements in silicon with data on lattice disorder and the lattice location of implanted atoms.[13]

1. The electrical characteristics of the different Group V elements show quite similar behavior. In room-temperature implantations to dose levels such that an amorphous layer is formed (10^{14} to 10^{15}/cm^2), there is a major anneal stage in the number of carriers/cm^2 at the temperature where the lattice reorders. For lower-dose implantations, the measured number of carriers/cm^2 is nearly equal to the number of implanted ions/cm^2 for anneal temperatures between 400 and 500°C.

2. In contrast to the behavior of the Group V elements, the anneal characteristics of the Group III elements are quite complex. Hall measurements on hot substrate Tl implantations have shown that a conversion from P- to N-type behavior occurs on annealing to approximately 575 to 600°C. Combined with the channeling data (see Figure 45), this

indicates that Group III dopants on interstitial sites can act as donors. This may be the reason that high-dose boron implantations exhibit reverse anneal behavior in the temperature range of 550 to 650°C.[16]

Future Developments

The application of ion implantation to the study of solids encompasses a wide range from development of contacts on semiconductors to investigation of atomic interactions. It is clear that further work is required to clarify the basic processes involved in implantation in semiconductors. The results may well lead to significant advances in the fabrication of semiconductor devices.

On the simplest level, implantation is a convenient way of introducing controlled amounts of elements into solid substrates. This provides a means of studying reactions not possible under the limitations set by conventional thermal techniques.

References

1. J. Lindhard, V. Nielsen, M. Scharff, and P. V. Thompson, Kgl. Dan. Vidensk. Selsk. Mat. Fys. Medd. *33*, No. 10 (1963); see also A.R. Sattler, in *Radiation Effects in Semiconductors*, F. L. Vook, ed. (Plenum Press, New York, 1968), p. 243.
2. J. A. Davies, J. Denhartog, L. Eriksson, and J. W. Mayer, Can. J. Phys. *45*, 4053 (1967).
3. L. Eriksson, J. A. Davies, and J. W. Mayer in *Radiation Effects in Semiconductors*, F. L. Vook, ed., (Plenum Press, New York, 1968), p. 398.
4. P. Sigmund, Argonne National Laboratory (private communication). This calculation is a more refined treatment of the Khinchin-Pease results.
5. L. N. Large and R. W. Bicknell, J. Mater. Sci. *2*, 589 (1967).
6. J. W. Mayer, L. Eriksson, S. T. Picraux, and J. A. Davies, Can. J. Phys. *46*, 663 (1968).
7. L. Eriksson, J. A. Davies, N. Johansson, and J. W. Mayer, J. Appl. Phys. *40*, in press (Feb. 1969).
8. L. J. Cheng and J. Lorii, Phys. Rev. *171*, 856 (1968).
9. See for example, J. W. Mayer and O. J. Marsh in *Applied Solid State Science, Volume 1*, C. J. Kressman and R. Wolfe, eds., (Academic Press Inc., New York, 1968).
10. J. Lindhard, M. Scharff, and H. E. Schiøtt, Kgl. Dan. Vidensk. Selsk. Mat. Fys. Medd. *33*, No. 14 (1963).
11. J. F. Gibbons, Proc. IEEE *56*, 295 (1968).
12. W. M. Gibson, F. W. Martin, R. Stensgaard, F. Palmgren-Jensen, N. I. Meyer, G. Galster, A. Johansen, and J. S. Olsen, Can. J. Phys. *46*, 675 (1968).

13. J. W. Mayer, O. J. Marsh, G. A. Shifrin, and R. Baron, Can. J. Phys. *45*, 4073 (1967).
14. L. Eriksson, G. R. Bellavance, and J. A. Davies, Rad. Effects *1*, in press (Jan. 1969).
15. J. A. Davies, L. Eriksson, and J. W. Mayer, Appl. Phys. Lett. *12*, 255 (1968).
16. A. H. Clark and K. E. Manchester, Trans. AIME (to be published).

CHAPTER 9

Interactions of Nuclear Moments with Solid-State Environments

The interaction of nuclear magnetic dipole and electric monopole and quadrupole moments with the electronic wave functions at the nucleus have been extensively used to give information concerning the environment of nuclei in a wide variety of solids. Mössbauer experiments and experiments measuring gamma-ray (and beta-ray) angular correlations have been of major importance in these studies in addition to experiments involving nuclear magnetic resonance and the hyperfine interactions visible in electron spin resonance. The majority of studies of this kind have been made using radioactive or stable nuclear isotopes introduced into solids during crystal growth or by thermal diffusion. Both the Mössbauer effect and gamma-ray angular correlation can, however, be studied using nuclei excited in nuclear reactions, such as Coulomb excitation, (α,α') inelastic scattering, and (α,p) reactions, and observed almost immediately thereafter (on the very short time scale of nuclear lifetimes). As a result of such a nuclear reaction, the nucleus will have recoiled in the solid lattice generally coming to rest before, but only very shortly before, the measurements are made.

The Mössbauer and gamma-ray angular correlation techniques as well as the resonance measurements can also be used to study the environment of nuclei implanted in solids using relatively high-energy (20 keV to 2 MeV) ions from accelerators. Such nuclei may be either radioactive or stable isotopes, and their environment may reflect, as in the case of nuclei recoiling following a nuclear reaction, the position of a nucleus in terms of the configuration of its near neighbors in the cascade of radiation damage that the ion has itself created. This area of study is ripe for active collaboration between solid-state and nuclear physicists. Two aspects of it are treated briefly in the sections that follow.

PERTURBED GAMMA-RAY ANGULAR CORRELATIONS

The probability for observing a gamma ray from an excited nuclear state in general depends on the angle between the nuclear spin axis and the direction of observation. If the nuclei emitting the gamma rays have their nuclear spins randomly oriented in space (unoriented), there is no preferred direction of emission, and the angular correlation is isotropic. An anisotropic angular correlation can only be observed from excited nuclei that are produced with some orientation of their spins. The study of gamma angular correlations is an important method in nuclear spectroscopy. The spins of nuclear levels can be determined, as well as the electromagnetic multipolarities involved in the various gamma transitions. Our interest here is in perturbed angular correlations (PAC) for gamma rays.

During the lifetime of an excited nuclear state, the nuclear spin orientation may be altered because of interactions between the nuclear magnetic dipole moment μ and extranuclear magnetic fields or between the nuclear quadrupole moment Q and electric field gradients. The observed angular correlation will be changed from that expected for the initial nuclear orientation if the interactions are sufficiently strong to change the nuclear orientation. PAC are, therefore, a measure of these interactions.

These electromagnetic interactions represent an interesting conjunction of nuclear and solid-state physics. With the aid of external fields and an understanding of the extranuclear fields in solids, numerous measurements of PAC have been performed to determine μ and Q for excited nuclear states. Likewise, the reverse is true, for if the nuclear properties μ, Q, and the mean life τ are known, PAC measurements become a tool for studying extranuclear electromagnetic fields for various atomic or solid-state environments.

Most of the previous PAC work has dealt with radioactive sources and generally with sources not dynamically introduced (implanted) into a solid. The present discussion of PAC will, however, be limited to applications involving low-energy nuclear particle accelerators in a dual role. First, the accelerated particles are used to induce nuclear reactions in a target, populating an excited state in the residual nuclei with a definite spin orientation. Second, the kinematics of the nuclear reaction cause these excited nuclei to recoil into a solid-state environment that is to be investigated. With low-energy accelerators or mass separators, the single role of the accelerator can also be utilized, implanting radioactive nuclei into a solid-state environment to be studied, but this case will not be considered here.

The most recent review article on angular correlations including

perturbations is by Frauenfelder and Steffen.[1] Articles by Devons and Goldfarb[2] and Biedenharn[3] are additional extensive reviews of the general subject of angular correlations. Heer and Hovey[4] have reviewed angular correlation studies from the point of view of solid-state physics. Proceedings from three recent conferences concerning PAC are also available.[5–7] The area of nuclear-reaction techniques directed to spin orientation and gamma correlations is discussed by Litherland and Ferguson.[8]

INITIAL NUCLEAR SPIN ORIENTATION AND ITS PERTURBATION

In order to have experimental sensitivity to PAC, it is important that the nuclear reaction produces as large an anisotropy as possible, that is, as large a spin orientation as possible. In general, the fewer magnetic substates $|m|$ of an excited nuclear state that are populated, the stronger the anisotropy of the gamma angular correlation. Litherland and Ferguson[8] have developed a technique which limits the magnetic substate population for a nuclear reaction $X(a,b)Y^*$ by detecting the outgoing particles b at either 0° or 180° relative to the incoming beam direction of the bombarding particles a.

The (α,n) and (α,p) reactions, as examples for this technique, populate only the magnetic substates $|m|=\frac{1}{2}$ for zero-spin targets, $S_X=0$, since the alpha particle has $S_a=0$ and the neutron and proton $S_b=\frac{1}{2}$. Inelastic scattering (α,α') on zero-spin targets limits $|m|=0$, while (p,p') limits $|m|=0$ and 1. This technique, of course, requires a coincidence of the gamma rays with outgoing particles b detected on the beam axis, in order to ensure axial symmetry. Since our interest is to recoil the residual nuclei into different solid materials, it is better to detect the outgoing particles at 180° rather than 0° because of the larger recoil momentum of the residual nuclei. The beam energy can be adjusted somewhat to obtain the kinematic recoil that is needed to get the residual nucleus out of the target and properly into the solid material to be investigated.

Coulomb excitation is another reaction that can be used with this technique. Since the reaction mechanism is electromagnetic in nature, the angular correlations can be calculated even in cases where several magnetic substates are populated.[9] Coulomb excitation with low-energy accelerators is, however, applicable only to low-energy excited states because the Coulomb-excitation cross section decreases rapidly with excitation energy. In fact, low-energy accelerators do not compete well in this case with tandem Van de Graaffs from which 50–60-MeV oxygen ions are easily obtainable.

A modification of this technique is to leave the outgoing particle b

undetected and rely on the reation mechanism to limit the magnetic substate population. Although usually the alignment and thus the anisotropy in the angular correlations are smaller than with the 180° geometry (and may be zero), it has the advantage that only a singles measurement of the gamma rays is required instead of coincidences.

Another technique[8,10] that has been used following accelerator excitation of nuclei is to select an ensemble of oriented nuclei by detecting, at some angle, cascade gamma rays populating the state of interest in coincidence with the de-excitation gamma rays. Because triple coincidence measurements are difficult, this gamma-gamma technique is usually performed without detecting the outgoing particles. In this case, the alignment is usually not so large as in the 180° geometry, and thus the technique will not be emphasized. The advantages are that only gamma detectors outside the reaction chamber are needed, and in some situations thicker targets can be used.

During the lifetime of an excited nuclear state, interactions with electromagnetic fields may alter the initial nuclear alignment and, thus, perturb the angular correlation from what it would have been in a field-free environment. In a semiclassical description, the torque from these interactions causes a precession of the nuclei around some axis which changes their spin orientation. In a quantum-mechanical description, these interactions cause transitions between the magnetic substates as a function of time which change the initial magnetic substate population. The resulting perturbation of the angular correlation provides information about these interactions and in turn about the extranuclear fields which produced them.

EXPERIMENTAL TECHNIQUES IN PAC

To perform solid-state studies by measurements of PAC, it is important to choose an excited nuclear state with properties that will show sensitivity to the specific effect of interest. This choice may be limited to isotopes of a certain atom because of an interest in a specific electron configuration. Depending on whether the study is directed to magnetic fields or electric field gradients, μ or Q of the state should be large. It should be remembered that states with $J<1$ have no quadrupole moments and states with $J=0$, no magnetic moments. The mean lifetime τ of the state is often important for the study of time-dependent solid-state effects; τ also determines the type of experimental technique to be used for the PAC measurements. As discussed above, it is necessary that the nuclear state be populated with significant spin orientation to give a strong anisotropy in the gamma angular correlation. In addition, the

kinematics of the nuclear reaction and the stopping power[11] of the target must be consistent with recoiling the residual nucleus into the desired solid-state environment.

There are two methods of observing PAC: time differential and time integral. These require quite different experimental techniques. The time-differential approach requires a measurement of the number of gamma rays at a given angle as a function of the time delay between the formation of the aligned state and its subsequent decay. It is basically a time measurement with the gamma rays detected at one or perhaps two angles. The time-integral method consists of detecting the number of gamma rays decaying from the aligned state only as a function of angle. This then is the experimental time integral of the PAC over the nuclear lifetime.

For the time-differential measurements, it is necessary that the time resolution of the experimental apparatus is small in comparison to the perturbation times and to the mean life τ of the nuclear state. With present experimental limitations of 200–300 psec on nuclear time difference measurements, the time-differential method is only applicable for nuclear states with τ greater than about 1 nsec. (Details of nuclear timing have been recently reviewed by Schwarzschild and Warburton.[12]) In the time-differential method, a timing signal which corresponds to the formation of the aligned nuclear state is required together with a timing signal from the gamma detector which marks the decay of a state at a given angle. The time difference is measured in a TAC (time-to-amplitude converter). The start time signal may be derived in several ways. For the axially symmetric 180° geometry, the outgoing particles b from the reaction $X(a,b)Y^*$ are usually detected in an annular solid-state detector through which the incident beam passes. In the event that the outgoing particles are to be undetected, a start signal can be obtained by beam pulsing of the accelerator. Pulsing techniques have been well developed for neutron time-of-flight measurements.[13] For the gamma-gamma cascade method, the start signals would come from the first gamma ray.

The kinds of detectors and the associated electronics to be used depend on the desired time resolution. For resolutions (FWHM) greater than 10 nsec, NaI scintillators can be employed for the gamma detection despite the 250 nsec decay time. The large photopeak efficiency of NaI is important for energy resolution. A schematic diagram of the timing apparatus is shown in Figure 46. Normal photomultiplier tubes and electronics are adequate. Rise times of most silicon solid-state detectors are sufficient in this case.

For time resolutions of less than 10 nsec, fast electronics becomes

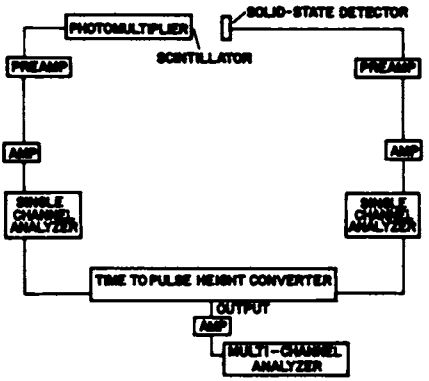

FIGURE 46. A schematic diagram of the timing apparatus used in time-differential measurements where the lifetime τ of the nuclear state is greater than about 10 nsec. For nuclear states with shorter lifetimes, fast electronics described in reference 14 is required.

necessary together with plastic scintillators and solid-state detectors with 1–2-nsec collection times. Plastic scintillators have improved timing properties but have the disadvantage of almost no photopeak efficiency and hence poor energy resolution because of their dependence on the Compton process. The fast–slow coincidence technique has been discussed in detail.[14] The timing is done with the fast electronics, while slow electronics is used to improve energy resolution.

A typical experimental geometry for time-differential measurements is shown in Figure 47. The detectors must be positioned at distances such that the angular resolution, as well as the time resolution, is sufficient to resolve the time-dependent anisotropies of the perturbed correla-

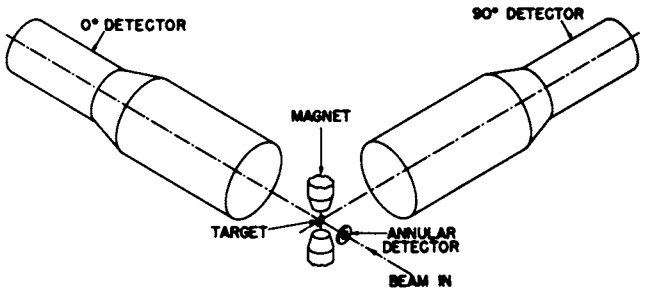

FIGURE 47. A typical experimental geometry for PAC studies with an accelerator. Detection of the outgoing particles at 180° in an annular solid-state detector produces, in general, strong anisotropic gamma-ray angular correlations.

tion. The positioning of two gamma detectors 90° apart as shown in the figure allows a convenient extraction of the precession frequency of the nuclear alignment in a perturbing magnetic field. Data from a time-differential measurement are shown in Figure 48.

The time-integral measurements are usually performed when the perturbation times or lifetimes τ are less than the time resolutions that can be achieved in the time-differential method. The time-integral mea-

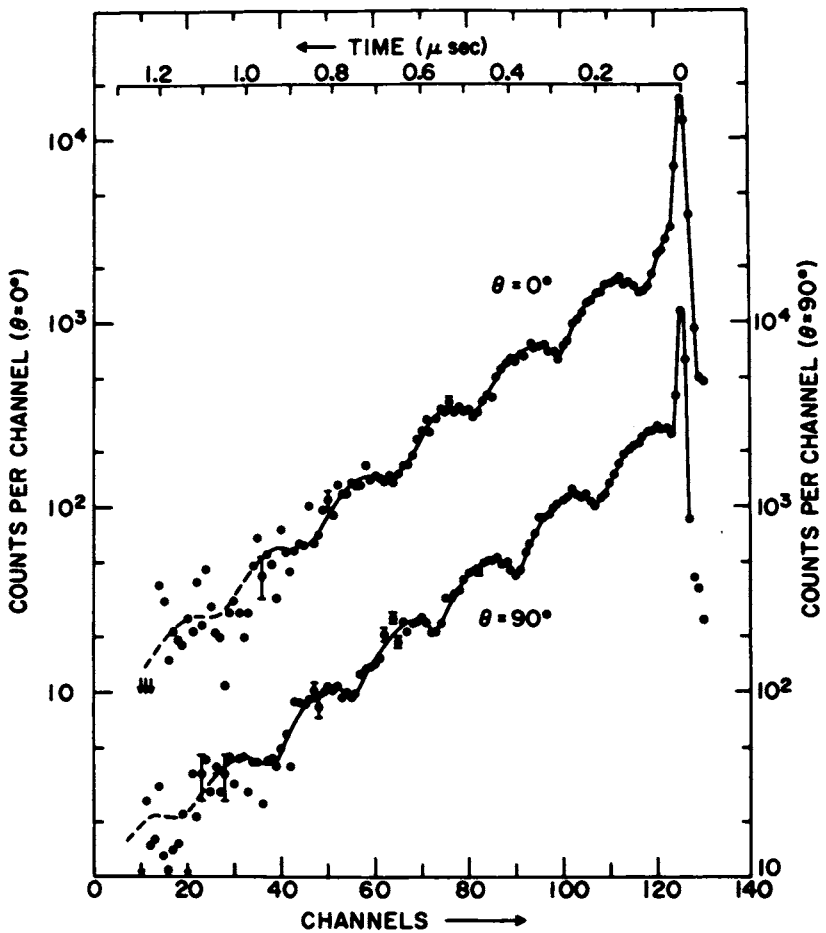

FIGURE 48. Data from a time-differential measurement of PAC produced by a static magnetic field. These results are for an excited state of ^{18}F in copper, which was aligned by the $^{16}O(^3He,p)^{18}F$ reaction in the 180° geometry.[15] The modulations on the decay curves correspond to a Larmor precession of the gamma-ray correlation.

surements have the disadvantage that the characteristic time dependence of a given interaction is absent, so in the event that both electric and magnetic interactions occur, it is difficult to separate their effects. In general, the precision of this method is less than that of the time-differential method. The time-integral method has a powerful advantage in that by varying τ (by choice of suitably different nuclear states), transient effects down to a few psec can be observed. The experimental geometry for time-integral measurements is similar to that in Figure 47, except that either one gamma detector should move as a function of angle or several gamma detectors should be positioned at various angles. NaI detectors are usually used for the gamma rays. For static external magnetic fields, as for example in ferromagnetic studies, the measurements are often made with field up and field down relative to the plane defined by the gamma detectors, so that the sense of the rotation of the angular correlation is reversed to double the observable effect. Data from a time-integral measurement are shown in Figure 49. Measurements in the 180° geometry require a coincidence between pulses from the gamma detectors and those from the solid-state detector. The re-

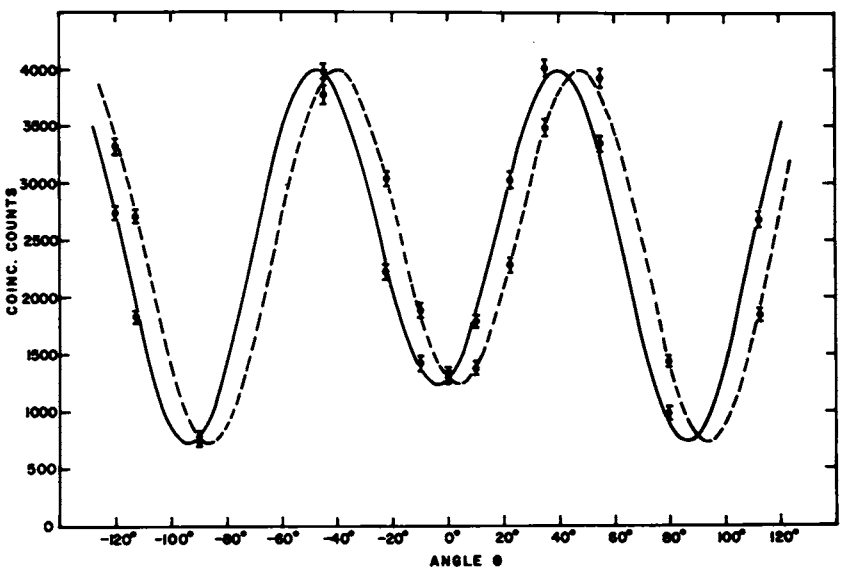

FIGURE 49. Data from a time-integral measurement of PAC produced by ferromagnetic hyperfine fields. The results were obtained with Coulomb excitation in the 180° geometry.[16] The solid data points correspond to the angular correlation with field up, while the open data points correspond to the angular correlation with field down.

solving time of the coincidence circuit must be larger than the lifetime of the state to give the proper time integration. In the event that the outgoing particles are to remain undetected, the time-integral experiments become very simple because they reduce to a singles measurement of gamma rays as a function of angle. A single measurement allows one to use Ge(Li) solid-state detectors for the gamma rays. The energy resolution and the signal-to-background ratio are greatly improved for these detectors as compared with NaI detectors. These two features give one considerably greater choice in the nuclear states that can be used.

It is clear that the experimental measurement of PAC requires more sophisticated experimental technique than in the solid-state applications of accelerators discussed in earlier sections. In some situations, a rather large amount of very fast and complex electronic gear is practically a necessity.

SOLID-STATE PROBLEMS OF CURRENT INTEREST FOR PAC

The application of PAC to solid-state physics as indicated earlier is rather straightforward. For a nuclear state of known properties, the observed perturbations in various materials can be directly interpreted in terms of the magnetic fields or electric field gradients of the solid-state environment. From a knowledge of such electromagnetic fields, one can proceed to a better understanding of the atomic structure that produces them. There are a large number of solid-state problems to which PAC can provide information. We will indicate here a few of these.

PAC experiments with no magnetic interactions have been performed to investigate electric field gradients of different materials for both single crystals and polycrystals.[1] The case of fluorine in copper is particularly simple. Copper has a cubic lattice so that electric field gradients should be small at lattice sites. The relaxation of ^{18}F alignment in Cu has been observed[15] to be very long (>750 nsec) indicating the weakness of the perturbation effect and verifying the cubic symmetry of the ^{18}F site. The PAC technique also allows studies of time-dependent quadrupole interactions such as those arising from lattice vibrations in solids or with liquids of different viscosity.

PAC have recently been extensively used for the study of magnetic fields in solids. Internal hyperfine fields have been examined for various atoms in ferromagnetic materials. In addition to the theoretical interest in these hyperfine fields, their precise values are important as a tool for nuclear magnetic-moment studies. Time-integral measurements[16] have been made for a number of large-A nuclei with considerable concentration on the rare-earth nuclei from $150 < A < 190$ where the low-lying

collective levels have lifetimes ranging from a few psec to nsec. Most of these measurements have been performed via Coulomb excitation using high-energy oxygen beams from tandem accelerators. These measurements revealed transient effects in PAC. In the time the recoiling nuclei are slowing down, typically a fraction of a psec, the nuclei may see high electric field gradients, or large magnetic fields due to certain excited atomic states. Time-integral measurements in ferromagnetic materials showed interactions occurring in a time less than 5 psec, which were consistent with transient fields arising from the pickup of polarized electrons.[17]

Recently, time-differential studies[18] have attacked the same problem of hyperfine fields at the nuclear site in ferromagnetic materials. Most of these measurements were done with a pulsed beam and the $^{19}F(p,p')$ reaction using the 198-keV first excited state which has a lifetime of $\tau = 128$ nsec. The results showed several nonequivalent Larmor precession frequencies indicating that the ^{19}F recoil nuclei were stopping at several nonequivalent locations having different magnetic fields. Theoretical calculations[19] have been made regarding the ratio of recoils that substitutionally find lattice sites, to those stopping at interstitial positions, but there is only a limited understanding with regard to different atoms recoiling in a given material. The above experiments[18] show that a significant fraction of ^{19}F atoms stop in interstitial positions. Mössbauer studies[20] and several PAC experiments[16] show for heavier nuclei that a significant fraction of recoils find lattice sites. More experimental information is needed in this area.

The magnetic hyperfine fields produced at the nucleus due to surrounding atomic electrons can be enormous for certain unpaired electrons. Little experimental information is available concerning these paramagnetic fields for random directions or with partial ordering as a function of external magnetic fields. Goldring and Scharenberg have observed large paramagnetic field contributions for rare-earth atoms.[21]

In the process of recoiling nuclei into solids, it is possible to cause various excitations in the atomic electron shells; the excitations may be paramagnetic.[4] It is known that the lifetimes of these atomic excitations vary with the solid-state environment. In metals the lifetimes are of the order of a psec, while in some insulators the lifetimes are as long as seconds. These time-dependent paramagnetic effects can be studied with time-differential PAC unless the atomic lifetimes are smaller than achievable time resolutions, in which case time integral measurements for nuclear states of small τ would allow a lifetime determination of the atomic excitation.

PAC can be applied to the study of magnetic fields in superconductors

as, for example, penetration[22] and quantized fluxoids.[23] In the latter study, time-differential PAC measurements were made as a function of temperature using radioactive nuclei diffused into Type II superconducting niobium. The results were consistent with singly quantized fluxoids predicted by theory, although the data were not sensitive enough to distinguish a square or triangular lattice for the equilibrium fluxoid configuration. In studies such as these, recoiled aligned nuclei, just as the diffused radioactivity, become microscopic probes of the somewhat more macroscopic magnetic phenomena.

Properties of excited electron states for free atoms can also be studied with PAC following a nuclear reaction by recoiling the aligned residual nuclei along with their atomic environment into a vacuum rather then into a solid. The excited atomic states may be multiply ionized depending on the atom and the available energy and will have different lifetimes and different hyperfine magnetic fields. The resulting magnetic interaction at the nucleus is thus time-dependent and random. Time-integral PAC studies for different τ can yield information on the average hyperfine fields. A modification of such experiments is to vary the vacuum recoil distance with a stopper like Cu which would maintain the remaining nuclear alignment. The interaction times can then be varied for one convenient lifetime τ. Often for such interactions, the nuclear alignment is relaxed in less than 10 psec.

Another approach to the study of hyperfine fields of free atoms has been discussed by Goldring.[24] The hyperfine fields are forced to change direction after a given time interval by recoiling the aligned nuclei into gas. The magnetic field at a nucleus changes in a collision, so that by varying the gas pressure, and thereby the collision time, different PAC are induced. For small collision times, the magnetic fields essentially average to zero, while for long intervals significant perturbations result. Time-integral measurements of these PAC as a function of pressure yield information on the magnitude of these hyperfine fields. In turn, the exceedingly high fields become a useful tool for measuring nuclear magnetic moments.

Range and range straggling for heavy recoil ions can be measured in a straightforward manner using PAC.[25] The stopping material of a given thickness is sandwiched between a thin target and a ferromagnetic backing. The forward recoil velocity for the 180° geometry can conveniently be varied by changing the bombarding particle energy. The fraction of recoil nuclei that reach the ferromagnetic backing will show strong PAC, while the correlations of the nuclei that do not will be unaffected. Assumptions employed in stopping theory[11] have not all been experimentally tested. Outside of their intrinsic interest, these results are very

important for the widely used Doppler shift-attenuation method of measuring nuclear lifetimes.

In summary, PAC methods can be used as a microscopic probe of electromagnetic fields. These methods have several advantages over nuclear magnetic resonance techniques which, in general, are more precise. PAC measurements require a very small number of impurity atoms and do not require the penetration of radio-frequency fields. PAC can also be used in the study of transient effects which cannot be seen in NMR experiments. As compared to PAC measurements with radioactive sources, either diffused or implanted, nuclear reaction studies have the advantage of large nuclear alignments and a greater selection in excited states.

MÖSSBAUER STUDIES

The Mössbauer effect is another area like perturbed angular correlations for which a strong interdependence exists between nuclear and solid-state physics. Whereas PAC are an indirect manifestation of the interactions between nuclear moments and the electromagnetic fields of the environment, the Mössbauer effect directly observes the energy changes in the magnetic substates resulting from these interactions. These energies can be measured with small, variable Doppler shifts because of the recoil-free gamma emission and resonant absorption of the Mössbauer effect; they are related to the same interactions between the nuclear magnetic-dipole moment and the extranuclear magnetic field and between the nuclear quadrupole moment and electric-field gradients that are obtainable from PAC. In addition, the Mössbauer effect gives information about the electron charge density surrounding the nucleus from isomer shifts and about the lattice from the recoil-free fraction f.

A particle accelerator plays a slightly different role in the Mössbauer studies than in PAC. The nuclear reaction excites a nuclear state and recoils the excited residual nucleus into the solid material; however, no particular spin orientation is required, at least for the majority of the Mössbauer studies. One advantage of accelerator experiments is that a larger choice of Mössbauer states can be excited than nature allows for with radioactivity. A severe disadvantage is that the background radiation always associated with accelerator beams makes the Mössbauer measurements very difficult. Alternatively, of course, a particle accelerator used as a mass separator can be used to introduce radioactive Mössbauer nuclei into solid-state environments.

There are many good review articles and books on the Mössbauer

effect.[26] In addition, there are several review articles directly related to Mössbauer studies with particle accelerators, namely, those by Walker and Lee,[27] Obenshain,[28] and Kalvius *et al.*[29] The first of these is aimed only at low-energy Van de Graaff accelerators.

EXPERIMENTAL TECHNIQUES USING ACCELERATORS

The Mössbauer effect has been observed following (d,p) and Coulomb-excitation reactions. The great technical difficulty is to overcome the background of bremsstrahlung and Compton-scattered gamma rays resulting from the accelerated particle beam. This has been handled in several ways. A coincidence with either an outgoing particle or a cascade gamma ray following the reaction isolates the Mössbauer gamma ray from background. For the ^{56}Fe(d,p)^{57}Fe reaction there is the convenient 122-keV gamma ray that decays to the 14.4-keV level. In Coulomb-excitation Mössbauer experiments, there is the inelastically scattered particle which can be detected with an annular solid-state detector in the 180° geometry. Such Mössbauer measurements generally require long accelerator runs to achieve statistical accuracy at beam levels and coincidence rates that are consistent with maximum detector counting rates. Reduction in the background is thus quite important.

A technique[29] that has been very successful in reducing background is to recoil the excited nuclei through vacuum to a solid backing which is beyond a shielded beam catcher. This also eliminates beam damage and heating of the solid being studied. Beam-pulsing techniques[30] have been used with the ^{56}Fe(d,p) ^{57}Fe reaction where the beam is actually off during the counting time.

The development[31] of a resonant detector allows for considerable improvement in the signal-to-background ratio for ^{57}Fe studies. The resonant detector is an electron measuring device which takes advantage of the large conversion coefficient, $\alpha = 9.7$, of the Mössbauer level. With an ^{57}Fe enriched cathode, this detector is very sensitive to resonance absorption because of the high probability for conversion-electron decay. It can be made with a low efficiency for nonresonant gamma rays, thus giving a large signal-to-background ratio.

LOW-ENERGY ACCELERATOR EXPERIMENTS

Mössbauer experiments can yield information regarding the magnetic field, electric field gradients, and the electron charge density of the extranuclear environment, as well as information about lattice excitations. Here, only the types of Mössbauer experiments that are unique to particle accelerators will be mentioned.

Coulomb-excitation reactions[27,28] have expanded Mössbauer studies to a number of levels that could not conveniently be used with radioactive sources. Since Mössbauer measurements are restricted to excited states below about 150 keV, the Coulomb-excitation process has sufficient cross section for exciting these levels with low-energy accelerators. The low-lying collective levels of the deformed rare-earth region $150<A<190$, as for example the Yb isotopes, are good candidates for this purpose because of their large Coulomb-excitation cross sections. These new Mössbauer levels allow the study of solid-state environments with different nuclear properties, that is, with different magnetic and quadrupole moments, lifetimes, and energies. Also, the atomic system of the implanted ion can be varied. The studies may be extended to a variety of host materials by the recoil technique, although the technique is less flexible to use with low-energy accelerators than with tandem Van de Graaffs.

The interesting problem of where the recoil ion stops can be investigated with the Mössbauer effect following a nuclear reaction. The electromagnetic fields are different for lattice sites and interstitial positions. It may thus be possible to measure the relative populations of lattice sites and interstitial positions for different host materials with several recoil ions. In addition, the time-dependence of these populations can be observed using Mössbauer levels of different lifetimes or using a time-differential measuring technique. A large fraction of implanted ^{57}Fe atoms following Coluomb excitation find lattice sites in iron in a time less than the 100 nsec half-life of the 14.4-keV level.[32]

Electron and lattice excitations of the solid material induced by the recoiling ion (radiation damage) can in principal be studied by the Mössbauer effect. The flexibility of adjusting the recoil velocity and range by changing the reaction kinematics may aid such studies.

In general, the Mössbauer studies with accelerators yield information that is similar to that from PAC studies. These Mössbauer measurements are often more sensitive to the extranuclear environment but are also more difficult to perform than the PAC measurements. If a particular Mössbauer measurement can be made with radioactive sources, the nuclear-reaction-induced measurements do not compete well because of the background difficulties.

REFERENCES

1. H. Frauenfelder and R. M. Steffen, *Angular Correlations in Alpha-, Beta- and Gamma-Ray Spectroscopy II*, K. Siegbahn, ed. (North-Holland Publishing Co., Amsterdam, 1965), p. 997.

2. S. Devons and L. J. B. Goldfarb, "Angular Correlations," in *Encyclopedia of Physics,* S. Flugge, ed. (Springer, Berlin, 1957), Vol. 42, p. 362.
3. L. C. Biedenharn, "Angular Corrtlations in Nuclear Spectroscopy," in *Nuclear Spectroscopy, Part B,* F. Ajzenberg-Selove, ed. (Academic Press, Inc. New York, 1960), p. 732.
4. E. Heer and T. B. Hovey, in *Solid State Physics,* F. Seitz and D. Turnbull, eds. (Academic Press, Inc., New York, 1959), Vol 9.
5. E. Karlsson, E. Matthias, K. Siegbahn, eds., *Perturbed Angular Correlations* (North-Holland Publishing Co., Amsterdam, 1964).
6. A. J. Freeman and R. B. Frankel, eds., *Hyperfine Interactions in Matter* (Academic Press, Inc., New York, 1967).
7. E. Matthias and D. A. Shirley, eds., *Proceedings of International Conference on Hyperfine Interactions Detected by Nuclear Radiation* (North-Holland Publishing Co., Amsterdam, 1968).
8. A. E. Litherland and A. J. Ferguson, Can. J. Phys. *39,* 788 (1961); A. J. Ferguson, *Angular Correlation Methods in Gamma-Ray Spectroscopy* (North-Holland Publishing Co., Amsterdam, 1965).
9. K. Alder, A. Bohr, T. Huus, B. Mottelson, and A. Winther, Rev. Mod. Phys. *28,* 432 (1956).
10. E. K. Warburton and H. J. Rose, Phys. Rev. *109,* 1199 (1958).
11. J. Lindhard, M. Scharff, and H. E. Schiott, Kgl. Dan. Vidensk. Selsk. Mat. Fys. Medd. *33,* No. 14 (1963).
12. A. Z. Schwarzschild and E. K. Warburton, *Annual Review of Nuclear Science* (to be published, 1969).
13. J. B. Marion and J. L. Fowler, eds., *Fast Neutron Physics I* (Interscience Publishers, New York, 1963).
14. A. Z. Schwarzschild, *Nucl. Instrum. Methods 21,* 1 (1963).
15. A. R. Poletti and D. B. Fossan, Phys. Rev. *160,* 883 (1967).
16. L. Grodzins, R. R. Borchers, and G. B. Hagemann, Phys. Lett. *21,* 214 (1966); F. Boehm, G. B. Hagemann, and A. Winther, Phys. Lett. *21,* 217 (1966); L. Grodzins, reference 7, page 607.
17. R. R. Borchers, B. Herskind, J. D. Bronson, L. Grodzins, R. Kalish, and D. E. Murnick, Phys. Rev. Lett. *20,* 424 (1968).
18. J. Braunsfurth, J. Morganstern, H. Schmidt, and H. J. Korner, Z. Phys. *202,* 321 (1967); R. G. Stokstad, R. A. Moline, C. A. Barnes, F. Boehm, and A. Winther, reference 7, page 699; and O. Klepper and H. Spehl (to be published).
19. C. Erginsoy, G. H. Vineyard, and A. Shimizu, Phys. Rev. *A118,* 139 (1965).
20. G. D. Sprouse, G. M. Kalvius, and S. S. Hanna, Phys. Rev. Lett. *18,* 1041 (1967).
21. G. Goldring and R. P. Scharenberg, Phys. Rev. *110,* 701 (1958).
22. H. R. Lewis, Jr., Thesis, University of Illinois, 1958.
23. J. R. Alonso, Thesis, MIT, 1967.
24. G. Goldring, reference 7, page 640.
25. O. Klepper, L. Lehmann, and H. Spehl, reference 7, page 767.
26. R. L. Mössbauer, "Recoilless Nuclear Resonance Absorption," Ann. Rev. Nucl. Sci. *12,* 123 (1962); H. Frauenfelder, *The Mössbauer Effect* (W. A. Benjamin, New York, 1962); and Gunther K. Wertheim, *Mössbauer Effect: Principles and Applications* (Academic Press, Inc., New York, 1964).
27. J. C. Walker and Y. K. Lee, *Nuclear Research with Low Energy Accelerators* (Academic Press, Inc., New York, 1967).

28. F. E. Obenshain, reference 7, page 655.
29. G. M. Kalvius, G. D. Sprouse, and S. S. Hanna, reference 7, page 686.
30. J. Christiansen, E. Recknagel, and G. Weyer, Phys. Lett. *20*, 46 (1966).
31. J. Christiansen, P. Hindennach, U. Morfeld, E. Recknagel, D. Riegel, and G. Weyer, Nucl. Phys. *A99*, 345 (1967).
32. G. D. Sprouse, G. M. Kalvius, and S. S. Hanna, Phys. Rev. Lett. *18*, 1041 (1967).

CHAPTER 10

Research in Materials Analysis

Many interesting research opportunities exist for using small accelerators and nuclear techniques to analyze the elemental composition of materials and to study various physical processes, particularly where trace quantities of chemical elements must be measured. Research is needed not only to discover new techniques and to measure and improve the ultimate sensitivities of presently known techniques but also to determine, for specific problems, whether nuclear techniques have advantages over other methods of analysis. The latter objective seems especially promising in that it implies collaboration between disciplines. Other chapters of this report attest to the fact that an interdisciplinary approach to a problem has often proven most important not only for solving a given problem but also for opening up entire new areas of research.

Analysis for constituent chemical elements with a small accelerator in general consists of irradiating a given material with a beam of charged nuclear particles or neutrons produced by the accelerator and detecting the resulting characteristic gamma rays or charged particles. Except for the case of small accelerators which are used for generating fast neutrons, the accelerator beam should be magnetically analyzed so that only a single species of nuclear particle is incident on the target. Emitted radiations may be detected with scintillation or solid-state detectors, the pulses from these detectors being analyzed with a multichannel pulse-height analyzer. The spectrum of pulse heights so produced will be characteristic of the nuclear reactions induced by the incident beam in the constituent target elements.

An extensive published literature and many excellent texts exist in the field of materials analysis. The reader may, however, find references 1–6 useful in that they emphasize areas of current research interest.

It is convenient to divide the measurement techniques into two categories: activation analysis and analysis of prompt radiations. Of these two, the analysis of prompt radiations is much less highly developed and, therefore, a more promising area for research with small accelerators. Even in activation analysis, however, much basic data are still needed, and new applications to problems in other fields may confidently be expected.

The use of charged nuclear-particle beams for analyzing materials and for studying physical processes which occur at surfaces requires much more thorough investigation. The richness of the techniques, perhaps especially where prompt analysis of radiation is used, is such that collaboration between small accelerator groups and groups in other research fields should be most rewarding.

Activation Analysis

In this method, a stable element present in a sample is detected through the radioactivity produced as a result of nuclear reactions between that element and the irradiating beam. After irradiation, the sample containing the activated elements is placed in a low-background detector and the emitted radiations, usually gamma or beta rays, are measured. The sensitivity of the measurement is such that it is most commonly used for measuring elements which are present only in trace quantities. The trace elements which are to be measured may be present in the sample as extraneous impurities or they may be purposely introduced. The latter situation occurs, for example, when stable isotopes are used as tracers. This latter technique is important since it can be used in many cases where the use of radioactive materials is precluded prior to analysis.

An important advantage of activation analysis is that it is often nondestructive. It is true, however, that in many cases increased sensitivity can be obtained through chemical separation of the specific element of interest. Both the spectrum of gamma rays and the half-life for decay of activity are characteristic of the radioactive isotope that has been produced. In certain cases, background can be reduced, and as a consequence, very high sensitivity can be obtained by detecting the radiation in a coincidence arrangement.

The type of radiation which is used for activation will depend on the trace elements that are being measured and on the material in which they are present. Most commonly, the sample to be analyzed is placed in the high-intensity thermal neutron flux which is present in a nuclear reactor. It is also possible, however, to produce a desired radioactivity

by bombarding the sample with high-energy electrons, bremsstrahlung, fast neutrons, or charged nuclear particles. Research in activation analysis, with accelerators reaching energies of 6.0 MeV or less, is judged to be most promising for charged nuclear-particle beams and to a lesser degree for fast neutrons. Therefore, only these two types of irradiations will be discussed in the present report.

FAST NEUTRON ACTIVATION

Activation analyses for some elements are more simply performed with fast neutrons from a small accelerator source than with thermal or fast neutrons from a nuclear reactor. A compact discussion of accelerator neutron sources including operating characteristics, costs, and detection sensitivities is given by Strain.[7] For the elements N, O, F, Al, Si, P, Cr, Mn, Cu, Y, Mo, and Nb, the lower limits of detection, based on a 14-MeV neutron irradiation for 10 min or less at 10^8 neutrons/cm^2/sec, range from 40 to 400 μg. Fast neutron activation analysis has proven particularly important for oxygen analysis and is used by many laboratories and testing facilities for routine and often large-scale automated analyses for this element.[5] A useful compilation of sensitivities and gamma-ray spectra for 14-MeV neutron irradiations has been prepared by Cuypers and Cuypers.[8] CAUTION: Since 14-MeV neutrons are produced through the T(d,n)^{4}He reaction, a tritium target is required in the accelerator. Tritium, however, is a radioactive gas with a 12-year half-life and can be a health hazard if not handled properly. Adequate provision must, therefore, be made for handling the targets safely and for ensuring that no tritium escapes from its prescribed containers.

A number of interesting examples of fast neutron activation analyses may be found in reference 1. While the choice between fast neutron activation analysis and other methods must be carefully made for a specific problem, it is clear that a small accelerator used as a neutron source can provide an important tool for studying many problems in materials preparation and characterization.

CHARGED-PARTICLE ACTIVATION

Interest in charged-particle activation analysis has increased in the past few years to the point where conferences on this subject alone were held in 1965 and 1967 in Grenoble, France, and Liége, Belgium, respectively.[2,6] Although Coulomb barrier effects on reaction cross sections, and consequently on detection sensitivities, will limit small accelerators to activation of the light elements, there are still many opportunities for

research in this region. Some of the references and examples given here include work performed at higher energies than can be achieved with small accelerators. In many cases, the higher energies are needed in order to achieve the highest possible detection sensitivity; the sensitivity that may be achieved with a small accelerator may be quite adequate for a particular problem of interest.

The bombarding particles of greatest interest are protons, deuterons, and ^{3}He particles; for low-energy alpha particles on light nuclei, only the $^{10}B(\alpha,n)^{13}N$ reaction produces a useful radionuclide. An excellent discussion and a list of references for charged-particle activation analysis has been given by Tilbury.[3] Much interest has centered on ^{3}He particles since their advantages for activating the light elements were pointed out by Markowitz and Mahony.[9] Other useful reports on ^{3}He activation analysis may be found in references 10–14.

A major difference between nuclear charged particles and other radiations used to produce radioactivation is that charged particles can penetrate only relatively short distances into matter. (A 2-MeV proton has a range of just under 50 μm in silicon.) While this short penetration prevents bulk analysis of materials, it can be an important advantage for the analysis of surfaces. The following examples illustrate some of the ways in which charged-particle activation analysis can be used.

1. The oxide layers formed on P-type silicon during etching and quenching and the oxidation rate of etched silicon on subsequent exposure to oxygen have been measured using the $^{18}O(p,n)^{18}F$ reaction; after irradiation with protons, the radioactivity corresponding to ^{18}F was measured. The oxidation rate as a function of time for the etched silicon was measured by exposing the silicon to an atmosphere which was enriched to contain 20 percent of molecular ^{18}O. For a proton bombarding energy of 4.2 MeV, the sensitivity of the method was such that oxide layers as thin as 0.01 monolayer were measurable.[15]

2. The microscopic distribution of oxygen and carbon in metals has been observed by bombardment of metallographically polished samples with 6.5-MeV ^{3}He ions and autoradiography of the activated areas. Positional resolution of 13 μm has been obtained in samples having bulk carbon concentrations of about 250 ppm.[16]

3. Oxygen diffusion in beryllium has been studied by etching surface layers away between irradiations and using the ^{16}N radioactivity produced by the $^{18}O(d,\alpha)^{16}N$ reaction to measure the amount of oxygen in a thin surface layer of the sample.[17]

4. The amount of carbon in silicon has been measured at the 5–10 ppm level using 3.0-MeV deuterons and the $^{12}C(d,n)^{13}N$ reaction.

By etching successive surface layers away between irradiations as in the previous example, it was found that sawing and lapping operations introduced carbon into the samples down to depths of between 100 and 200 μm.[18]

Analysis of Prompt Radiations

In this method, the target is irradiated with a beam from an accelerator as in activation analysis, but the emitted radiations, which may be charged particles, neutrons, or gamma rays, are detected instantaneously after a reaction has occurred. Some measurements of this type have been performed for neutron resonance capture and for fast neutron irradiations, but the most interesting possibilities for small accelerators attend to irradiations with charged nuclear particles. In principle, excellent sensitivities and specificities can be achieved because of the variety of available choices from which the optimum reaction can be selected. In addition, with prompt analysis, advantage can be taken of the fact that some nuclear reactions possess sharp energy resonances. Prompt analysis of radiation also makes possible measurements in which a small beam spot is scanned across the target.

A few of many examples that can be given are the following:

1. The use of charged particles from a 2-MV accelerator for surface analyses has been studied; for both thick and thin targets, elastically scattered protons and alpha particles, and protons from deuteron-induced reactions, were found to be useful for both qualitative and quantitative analyses of surface constituents.[19]

2. Gamma rays from low-energy proton resonance reactions have been used for the analysis of carbon, oxygen, boron, and fluorine in the same sample. For fluorine, the 1373-keV resonance in the $^{19}F(p,\alpha\gamma)^{16}O$ reaction was used and a sensitivity of 10 parts per billion was easily obtained.[20] A considerable simplification of the gamma-ray spectra can often be obtained by irradiating a sample at energies just *above* and just *below* a resonance to the same integrated charge and then subtracting one run from the other.[21]

3. Beams of 100- to 200-μm diameter have been used successfully for the microexamination of surfaces. As a test, sandwich stacks of thin foils of aluminum and copper were scanned end-on and reaction gamma rays were measured.[22]

4. The ion transport mechanism in the growth of oxide films during anodic oxidation of aluminum has been studied by using ^{18}O as a stable

tracer.[23] The position of the ^{18}O and Al atoms was determined by measurements near sharp resonances for the $^{18}O(p,\alpha)^{15}N$ and $^{27}Al(p,\gamma)^{28}Si$ nuclear reactions. Because the incident beam begins to lose energy as soon as it enters the target, resonances can be used to measure the amount of a given isotope as a function of depth below the surface of the material, consistent, of course, with penetration range and effects due to energy loss straggling. In further studies of the $^{18}O(p,\alpha)^{15}N$ reaction, an ultimate sensitivity of 10^{-12} g of ^{18}O has been estimated.[24]

5. The $^{32}S(d,p)^{33}S$ reaction has been used to measure the amount of sulfur in a thin film on a copper–nickel alloy. A sulfur surface density of 10^{-7} g/cm^2 was easily measured. Since the area bombarded was 0.5 mm^2, the actual weight of sulfur needed for the test was 2×10^{-10} g.[25]

References

1. V. P. Guinn, ed., *Proceedings of the International Conference on Modern Trends in Activation Analysis, College Station, Texas, April 19–22, 1965* (Texas A & M U., College Station, Tex., 1965).
2. *Proceedings of the First Conference on Practical Aspects of Activation Analysis with Charged Particles, Grenoble, France, June 23, 1965* (Euratom, EUR 2957 d-f-e).
3. R. S. Tilbury, *Activation Analysis with Charged Particles,* Nat. Acad. Sci.–Nat. Res. Council Nucl. Sci. Series, NAS-NS 3110 (Clearinghouse for Federal Sci. and Tech. Info., Springfield, Va., 1966).
4. A. A. Smales, "Radioactivity Techniques in Trace Characterization," p. 307, in *Trace Characterization, Chemical and Physical,* W. W. Meinke and B. F. Scribner, eds., Nat. Bur. Stand. Monograph 100 (U.S. Govt. Printing Office, Washington, D.C., 1967).
5. V. P. Guinn, "Nuclear Methods," p. 337, in *Trace Characterization, Chemical and Physical,* W. W. Meinke and B. F. Scribner, eds., Nat. Bur. Stand. Monograph 100 (U.S. Govt. Printing Office, Washington, D.C., 1967).
6. H. G. Ebert, ed., *Proceedings of the 2nd Conference on Practical Aspects of Activation Analysis with Charged Particles, Liége, Belgium, September 21–22, 1967* (Euratom, EUR 3896 d-f-e).
7. J. E. Strain, "Non-Reactor Neutron Sources," p. 33, in *Guide to Activation Analysis,* W. S. Lyon, Jr., ed. (D. Van Nostrand Co., Inc., New York, 1964).
8. M. Cuypers and J. Cuypers, *Gamma-Ray Spectra and Sensitivities for 14-MeV Neutron Activation Analysis* (Texas A & M U., College Station, Tex., April 12, 1966).
9. S. S. Markowitz and J. D. Mahony, Anal. Chem. *34,* 329 (1962).
10. J. D. Mahony, "Reactions of He^3 with Light Elements: Applications to Activation Analysis," Lawrence Radiation Lab Rep. UCRL 11780 (1965).
11. E. L. Steele, "Helium-3 Charged Particles in Activation Analysis," General Atomic Rep. GA-6568 (1965).
12. E. Ricci and R. L. Hahn, Anal. Chem. *37,* 742 (1965).
13. E. Ricci, R. L. Hahn, J. E. Strain, and F. F. Dyer, "He^3 Activation Analysis," in *Proceedings of the International Conference on Modern Trends in Activa-*

tion Analysis, College Station, Texas, April 19-22, 1965, J. P. Guinn, ed. (Texas A & M U., College Station, Tex., 1965), p. 200.
14. E. Ricci and R. L. Hahn, Anal. Chem. *39,* 794 (1967).
15. J. D. Ritter, M. N. Robinson, B. J. Faraday, and J. I. Hoover, J. Phys. Chem. Solids *26,* 721 (1965).
16. D. M. Holm, J. A. Basmajian, and W. M. Sanders, "Observations of the Microscopic Distribution of Oxygen and Carbon in Metals by He^3 Activation," Los Alamos Scientific Laboratory Rep. LA-3515 (1966).
17. I. L. Morgan, report in *Proceedings of the First Conference on Practical Aspects of Activation Analysis with Charged Particles, Grenoble, France, June 23, 1965* (Euratom, EUR 2957 d-f-e), p. 132.
18. E. Shuster and K. Wohlleben, "Nondestructive Determination of Carbon in Silicon through the $C^{12}(d,n)N^{13}$ Reaction," p. 45, in *Proceedings of the 2nd Conference on Practical Aspects of Activation Analysis with Charged Particles, Liége, Belgium, September 21–22, 1967,* H. G. Ebert, ed. (Euratom, EUR 3896 d-f-e).
19. O. U. Anders, Anal. Chem. *38,* 1442 (1966).
20. I. L. Morgan, *op. cit.,* p. 149.
21. T. B. Pierce, report in *Proceedings of the First Conference on Practical Aspects of Activation Analysis with Charged Particles, Grenoble, France, June 23, 1965* (Euratom EUR 2957 d-f-e), p. 174.
22. T. B. Pierce, "The Examination of Surfaces by Scanning with Charged Particles," p. 389, in *Proceedings of the 2nd Conference on Practical Aspects of Activation Analysis with Charged Particles, Liége, Belgium, September 21–22, 1967,* H. G. Ebert, ed., (Euratom, EUR 3896 d-f-e).
23. G. Amsel and D. J. Samuel, J. Phys. Chem. Solids *23,* 1707 (1962).
24. G. Amsel and D. J. Samuel, Anal. Chem. *39,* 1689 (1967).
25. E. A. Wolicki and A. R. Knudson, Int. J. Appl. Rad. Isotopes *18,* 429 (1967).